Modeling and Optimal Control of Human Walking for Motion Understanding and Usage in Lower-Limb Exoskeletons

by

Mennatallah Rihan

A thesis
presented to the University of Waterloo
in fulfillment of the
thesis requirement for the degree of
Master of Applied Science
in
Mechanical and Mechatronics Engineering

Waterloo, Ontario, Canada, 2023

Author's Declaration

I hereby declare that I am the sole author of this thesis. This is a true copy of the thesis, including any required final revisions, as accepted by my examiners.

I understand that my thesis may be made electronically available to the public.

Abstract

Wearable robotics, also known as exoskeletons, are devices typically worn over the human limbs to provide support and help with movement. Either by assisting the user to increase their capabilities, to help them regain movement abilities like in rehabilitation or to be used as an everyday device for restoring mobility. Exoskeletons have shown promising results in helping individuals regain their mobility by assisting them in walking tasks. However, there are still some challenges we need to overcome in order for the exoskeletons to be a significant part of the daily life. These challenges include but are not limited to: improving the control strategies to provide a better, more comfortable walking motion and to be able to adapt to different walking styles based on the individual needs and reject any perturbations to the motion. Exoskeletons have the potential to change the lives of millions of people suffering from mobility impairments around the world.

The current problem with exoskeleton control in gait is mainly based on the idea of using pre-defined trajectories to control the motion, this causes the system to be rigidly imposing motion on the user which is uncomfortable and feels unnatural. This thesis aimed to implement a modified version of the Geyer/Song model to create a more flexible trajectory generation method and add optimal control as a method to control the model gait parameters. The model was verified against the original model from [1]. Given the lack of dependency on any libraries to model the neuromuscular system, the model is compatible with C++ based libraries for the dynamics. A simplified mechanical walking problem was implemented with optimal control to serve as a skeleton problem and allow for the addition of the muscle and reflex systems.

A comparison was done on the muscle and joint layers of the modified model. The results have shown that the modified model follows the referenced model behaviour in terms of the motion generated despite some modifications and software differences. The optimal control problem for mechanical walking converged with an objective function of torque minimization and angular momentum minimization and gave a cyclic solution successfully. The results from the torque minimization showed greater promise since they were smoother and close to the expected human walking motion. The muscle-based optimal control walking was formulated but did not converge and thus the further complexity of the reflex system was not added in this thesis.

To test the new trajectories, a mechanical frame was designed to hold the TWIN exoskeleton and allow the testing of any modifications with minimum human interaction. The frame is able to hold the exoskeleton and motion is played on it in two positions, one with the exoskeleton hanging with sufficient ground clearance to avoid any ground contact

and two with the exoskeleton able to make ground contact and push off to move forward stably.

An experiment was designed to evaluate how individuals feel and react to the different exoskeleton trajectories and modes of operation. Initial results showed that the overall EMG signals from the lower limb were lower in the use of the exoskeleton and that the difference between grip forces and loads on crutches showed up the most in periods of instability. These results can help us identify how comfortable the person feels with the motion being imposed on them.

Acknowledgements

I would like to express my deepest gratitude to my supervisor Katja Mombaur for providing me with this amazing opportunity to work on a topic I was passionate about and introducing me to a new passion; the field of optimal control.

I could not have undertaken this journey without the support of Jonathan Lin who has helped push me forward, advised me, and more commonly listened to me complain about things not working.

Many thanks to Francisco Andrade Chavez and Jonas Grosse Sundrup for their continuous support.

I would like to express my appreciation to my readers: Arash Arami and Richard Nuckols for taking the time to read my thesis and for their precious feedback.

Special thanks to my parents: Sabry and Wafaa for instilling the confidence in me to undertake this journey. My siblings: Rehab, Eman and Yasser for pushing me to pursue my dreams and believing in me.

Thank you, Jan, Mahsa, Pranav, Kareem, Anas, Will, and Christian for all the help with the courses and experiments. For all the late nights spent working together.

Thank you to my second family abroad, my friends: Philopatear, Marian, and Michael. You made a lonely road so much less lonely.

Dedication

To my father, who has always put my education first. His unwavering belief in my abilities and his encouragement to pursue my dreams have been invaluable. This accomplishment is as much his as it is mine. Thank you, Dad.

Table of Contents

List of Figures

List of Tables

Quote

"The most effective debugging tool is still careful thought, coupled with judiciously placed print statements"

– Brian W. Kernighan

Chapter 1

Introduction

The introduction of robotics in our daily lives has greatly increased in recent years, robots are created to do many actions that humans perform ranging from industrial occupations to household tasks such as cooking and cleaning. A flourishing area of interest is the use of wearable robotics as assistive mobility devices called exoskeletons. The very first exoskeleton created was the Hardiman exoskeleton in 1961 [2], it was a robotic wearable device that was meant to enhance the user's strength, helping humans lift over 1500 pounds easily. Exoskeletons have come a long way since then, they are divided into two big categories, passive and active. Passive exoskeletons are generally used to support the user as they do their occupational tasks and to prevent injuries. The active exoskeletons are generally used to enhance human capabilities, assist in motion or compensate for the loss of specific motions.

Aside from increasing human capabilities, exoskeletons are also meant to help restore missing functionalities. The greatest example of that is using lower-limb exoskeletons to help spinal cord injury (SCI) patients regain their mobility. However, the majority of existing exoskeletons created to date have a few drawbacks that hinder their assistance. Most safe-to-use exoskeletons such as ReWalk, REX etc. are meant to be used with crutches and are bulky making them hard to use.

An area that still needs further development is the method that the exoskeletons use to move about, it becomes the motivation to understand human motion better in order to further develop exoskeleton motion to help individuals regain their natural motions. The human body performs a series of complex underlying mechanisms just to take a step forwards, and although sounding simple the walking task is far from it. If we consider doing the same motions with robots it becomes a much harder problem to solve. Robots

need specific instructions in order to perform any motion. Taking a step is not a challenge to the regular human but it creates a significant challenge to robotic systems.

There are several methods implemented when it comes to walking with exoskeletons. Most exoskeletons use a set of predefined trajectories collected from healthy subjects without an exoskeleton or while wearing it in a passive mode. The problem with this method is it assumes each person walks the exact same way and does not provide any customization. This thesis aims to use an existing model in the literature [1] that represents a simplified version of the human neuromuscular system along with optimal control to create a natural walking motion. After the creation of the human model, we would lump the exoskeleton model into the existing human model and generate the trajectories which would then be transferred for use with the lower-limb exoskeleton and tested. The trajectories will be tested on the TWIN exoskeleton while being attached to the mechanical frame to prevent the need for human wearers. After thorough testing without humans, the exoskeleton would then be tested with a human wearer and the human comfort would be analyzed to determine if this trajectory is in fact good.

1.1 Motivation

Yearly, between 250,000 and 500,000 people worldwide suffer a spinal cord injury (SCI) the majority coming from vehicular accidents and falls [3] and in Canada the estimates say over 86,000 people are living with spinal cord injury, and the number is projected to increase over the coming decades [4] [5].

A spinal cord injury is any damage to the spinal cord itself or nerves at the end of the spinal canal [6] that disrupts the communication pathway between the brain and the nerves controlling the limbs. This type of injury is usually either caused by trauma to the spine (traumatic SCI) or due to inflammation or tumour (non-traumatic SCI). This often leads to permanent damage, mainly affecting the mobility of specific limbs and thus causing paralysis from the point of injury downwards. The injury is considered complete when all the motor control and feeling below the injury place are lost, and incomplete when some residual motor control or feeling is retained.

One of the biggest challenges faced after spinal cord injuries is the loss of the ability to move, the affected individuals lose their sense of independence and mobility. Furthermore, when the affected individuals are unable to perform daily tasks that involve them moving around on their own, other problems arise. The problems include but are not limited to muscular atrophy, osteoporosis and pressure sores.

That is where the exoskeleton technology comes in, to aid humans, by potentially helping the affected people walk again alleviating some of the problems they experience. Active lower-limb exoskeletons attach to the user from the trunk downwards and mainly provide power to the hip and knee joints to help the individual perform certain motions. This technology has the ability to improve the lives of many individuals and is not limited to spinal cord injuries, it can help in the rehabilitation process of many injuries such as strokes. The lower-limb exoskeletons currently being used have some limitations that need to be explored. The main areas of concern reported by individuals with SCI were the ease of use, being compact and custom, safety and affordability [7].

1.2 Thesis contribution

This thesis aims to provide better insight into human walking motion and consequently provide more human-like trajectory generation for a lower limb exoskeleton. In addition, this thesis aims to validate trajectories on a lower-limb exoskeleton against human data to estimate human comfort.

In order to achieve this goal, we had to go through several development phases. First, the neuromuscular model was created from Geyer's model [8] with the higher control system from [1] using pure C++ and interfacing with Rigid Body Dynamics Library (RBDL) [9]. The development in C++ allowed the flexibility for integration with C++-based libraries. After testing and debugging the model, it was compared against the original model from [1] and validated. The second phase was the addition of optimal control to replace the higher controller of the model, firstly, a skeleton problem for mechanical walking was created and the complexity of the model was attempted gradually from muscles to reflexes. Several optimal control libraries such as casAdi [10] and Bioptim [11] were tested for the muscle layer due to compatibility issues. In the end, MUSCOD-II [12] was chosen since it did not result in a compatibility issue but the problem did not converge to a solution. The third part of this thesis focused on the testing of the lower-limb exoskeleton and proposing a method to estimate human comfort which uses a combination of sensors; grip sensors for crutches and EMG for muscle activations.

Summary of contributions:

- Implementation of the Geyer model [1] in C++ with some differences
- Optimal control of a purely mechanical model for walking
- Formulation of an optimal control problem for muscle-based walking

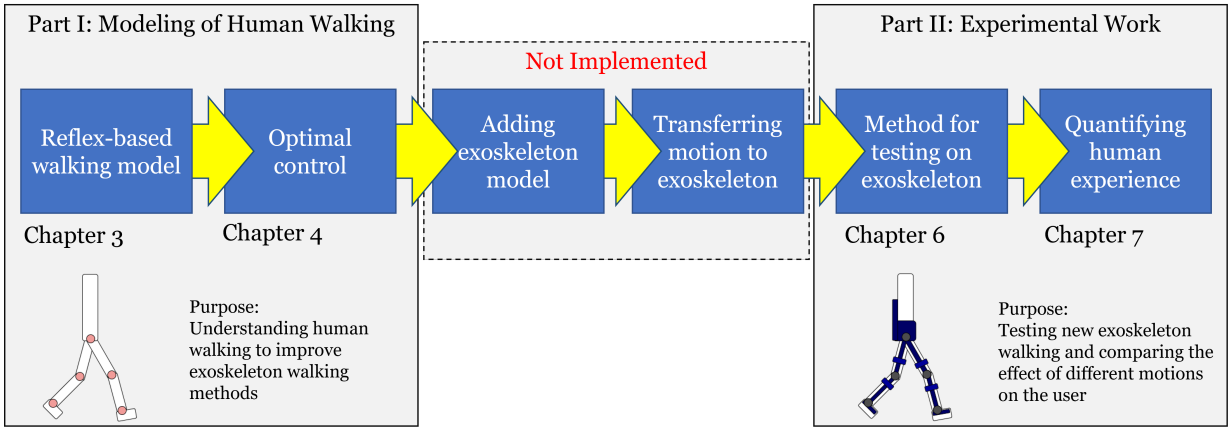

Figure 1.1: Thesis Flow

- Design and manufacturing of test bench for the TWIN exoskeleton
- Exploratory experiment to examine the human response to different exoskeleton trajectories or modes

1.3 Thesis outline

This thesis is divided into two fundamental parts, in part I: Modelling of Human Walking, Chapter 2 discusses the basics of human locomotion and methods used in modelling along with some basic existing human models. Chapter 3 discusses the reflex-based walking model from Geyer/Song [1] and a modified implementation using C++. Chapter 4 explains the formulation of walking as an optimal control problem and discusses the results of different objective functions. Part II: Experimental Work, Chapter 5 provides a background on the current exoskeleton technology, control methods used and a brief description of the TWIN exoskeleton used in this thesis. Chapter 6 shows the design and creation of a test-bench setup for the TWIN exoskeleton. Chapter 7 explores a method to quantify the human experience during walking with the exoskeleton through the use of EMG and grip sensors. Chapter 8 presents the conclusion, and limitations and explores potential future work.

Part I

Modelling of Human Walking

Chapter 2

Human Locomotion

To create better exoskeletons that mimic human motion, it is essential to understand human motion and the underlying mechanisms that govern it. This chapter will go through some basics of human motion, the first section will describe some main anatomic terms that are used to describe the motion and the different phases of walking that make up the gait cycle. The second section will cover preliminaries of modelling and optimal control. The third section will go through some popular models of human walking motion.

2.1 Biomechanics of Human Movement

2.1.1 Human anatomic planes and terms

Before we start describing how humans walk or perform any motion, it is needed to elaborate on a few common terms used in biomechanics to describe the human joints and the planes of motion. The planes of human motion can be seen in Fig 2.1 [13]. The sagittal plane divides the body into left and right halves. The transverse plane crosses the body parallel to the ground and divides the body into superior and inferior parts. The coronal plane splits the body into the front (anterior) and back (posterior) halves. Similarly, there are three axes of rotation in the human body. The sagittal axis, which passes from the front to the back, is defined by the intersection of the sagittal and transverse planes. The frontal axis passes from left to right and is defined by the intersection of the frontal and transverse planes. The longitudinal axis goes from the ground to the head and is defined by the intersection of the sagittal and frontal planes.

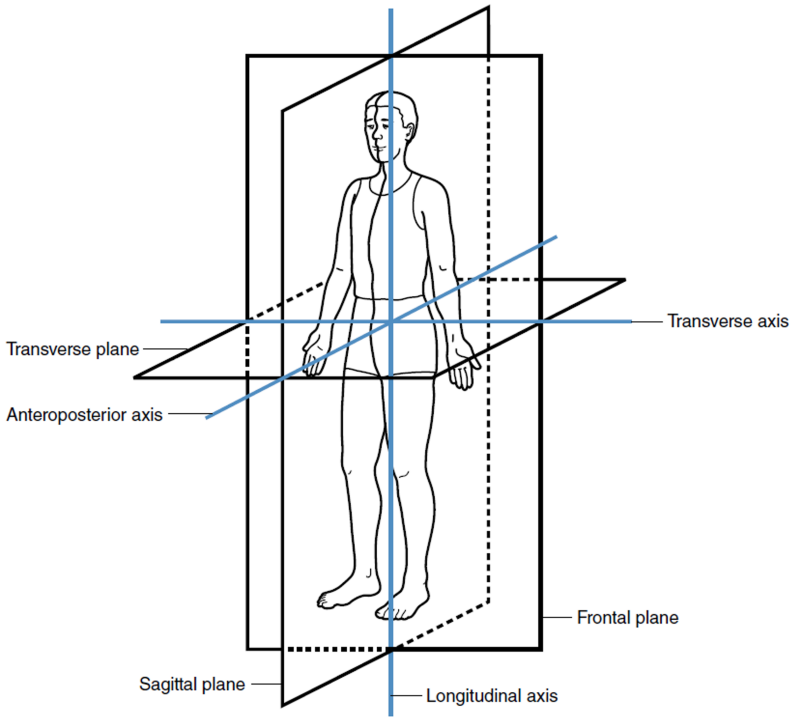

Figure 2.1: Human planes from [13], the human limb motion can be defined by separation into three planes; sagittal, frontal and transverse plane.

The movement of the human joints is described by the planes and axes. The rotations about the sagittal plane about the frontal axis are called flexion and extension Fig . Rotations about the frontal plane about the sagittal axis are called abduction/adduction, side flexion, inversion/eversion. Rotations about the transverse plane about the longitudinal axis are called internal/external rotations, horizontal flexion/extension and supination/pronation.

2.1.2 The Human Gait Cycle

Walking is an essential motion that occurs in our day-to-day life, most healthy people do not spend much of their time consciously thinking about how to walk as it slowly becomes an unconscious action. The human walking motion can be classified as a cycle that occurs simultaneously in each leg known as the gait cycle shown in [14, Fig 2.3].

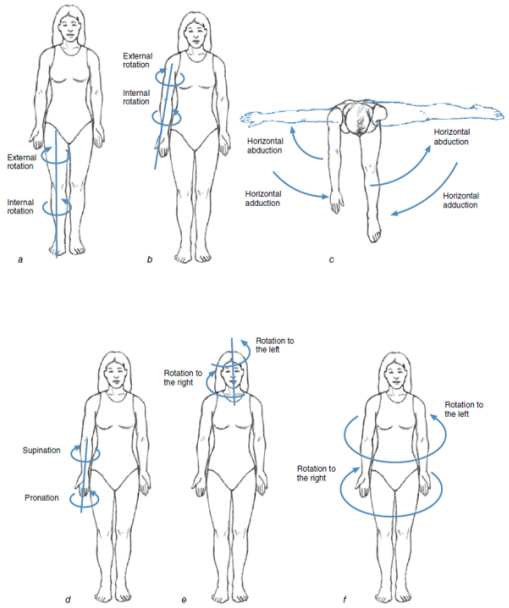

(a) Movements in the transverse plane

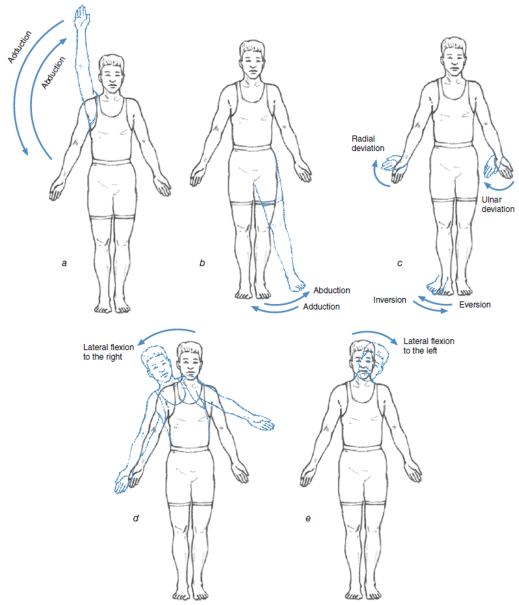

(b) Movements in the frontal plane

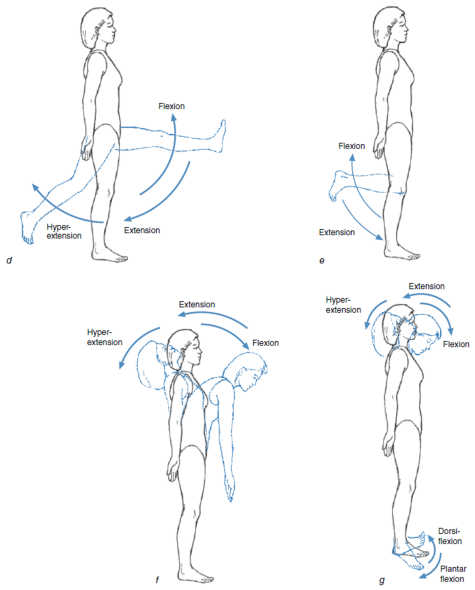

(c) Movements in the sagittal plane

Figure 2.2: Movements in planes from [13]

Each step taken involves going through the gait cycle, which consists of two main phases per foot: the swing phase and the stance/support phase [15]. The word support refers to the foot being in contact with the ground, during these contact phases also known as the stance phase the human foot moves through several sub-phases: Heel-strike, foot-flat, heel-off and toe-off. The swing phase refers to the foot swinging in the air from the moment of loss of contact in toe-off to regaining contact in heel strike. There is a phase while both legs are doing their own gait cycles that result in both feet having contact with the ground, that phase is known as double support. Most literature considers the start of the gait cycle at the moment contact is made. In that case, the leg goes through the phases in the order shown in Fig 2.3.

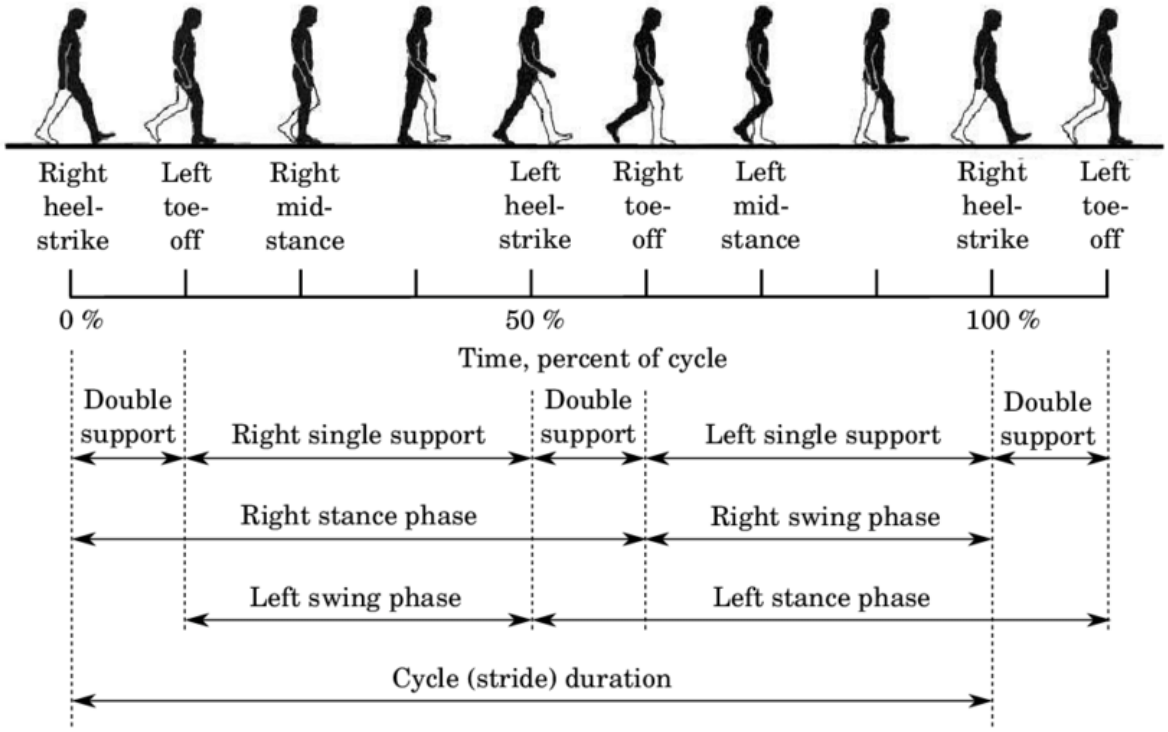

Figure 2.3: Human walking phases from [14], the figure shows two steps making up a complete cycle.

1. Heel Strike defines the initial point of the foot contact, namely when the heel "strikes" the ground for the first instance, it is categorized by an impact in ground reaction

forces.

2. Toe Strike is the second contact point that occurs when the toe/ball of the foot hits the ground after the heel strike.

3. Heel Off is the first point in this cycle that is a release of contact, it occurs when the heel lifts off from the ground.

4. Toe Off defines the end of the contact cycle, it occurs when the toe loses contact with the ground.

Another method of dividing the human gait cycle is using single support and double support phases, The word support reflects the ground contact points, with single being a single foot in contact and double meaning both feet are on the floor. The double support phase begins when the toe of one foot is in contact and the other foot heel makes ground contact and usually lasts about 20 % of the single step Fig 2.3

Sagittal plane motion

The main joints concerned with locomotion are the hip, knee and ankle joints. In extra simplification, we can assume the contribution to only be in the sagittal plane through the flexion/extension of the hip, knee and ankle Fig 2.4 [16].

During the gait cycle, the hip swings forward reaching the maximum flexion angle near the end of the swing phase right before the touchdown of the foot around 90% of the gait cycle. After the contact, the leg is in the stance phase and the hip starts to extend reaching maximum extension at approximately 50% of the gait cycle, around when the other foot strikes.

The knee joint is minimally flexed when the heel strike occurs, then some knee flexion occurs in the first phase of the motion reaching the first peak around 17% of the gait cycle to absorb the loading. The knee then slowly extends to almost full extension at 40% of the gait cycle. Then the knee enters flexion again then the heel of the foot loses contact and then the toe. It reaches maximum flexion around 73% of the gait cycle to help in ground clearance during the swing phase. The knee then starts extending again to prepare for the landing.

The ankle joint motion is vital to the gait cycle as it absorbs the shock at the heel-strike position and allows the propulsion of the foot off the ground in takeoff. The motion starts with the ankle in a neutral position as heel-strike occurs then proceeds in plantar flexion

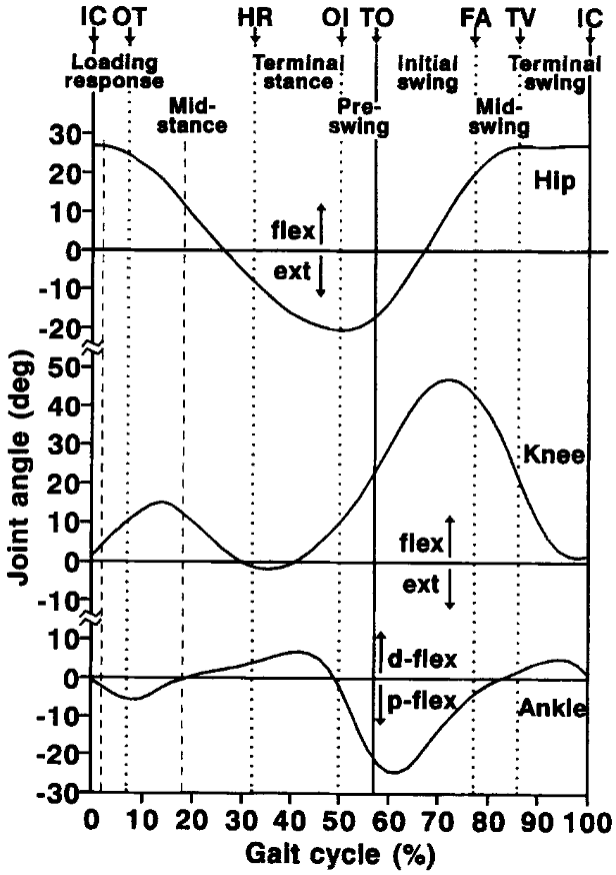

Figure 2.4: Leg joint angles in gait cycle from [16]

until the foot is flat. After foot flat the ankle then dorsiflexes to move the shank forward. The ankle begins plantar flexion in the heel-off phase to propel the heel off the ground and then push the toes off the ground as well. In the swing phase, the ankle dorsiflexes to allow for foot clearance off the ground.

Forces

The highest ground reaction forces through the gait cycle occur in the vertical axis. A typical vertical ground reaction force for a single foot in contact can be seen in [17, Fig 2.5]. The first peak (F1) in the force happens in the loading response following the impact in the heel-strike phase and decreases to reach (F2) which happens in the mid-stance phase

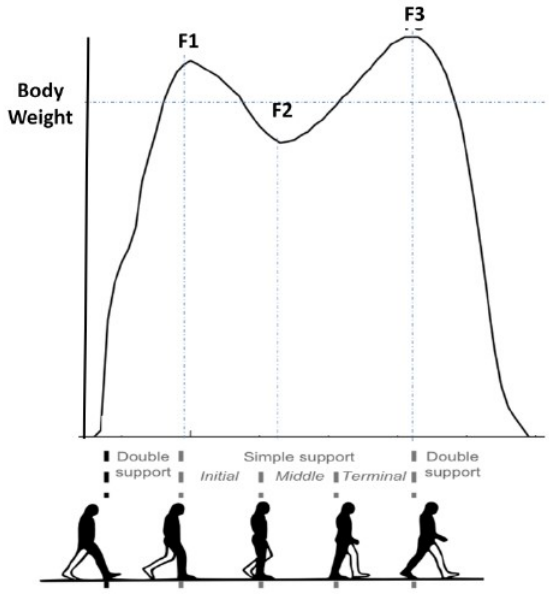

Figure 2.5: Vertical ground reaction forces during gait cycle from [17]

as the other leg moves through the swing phase. The last peak (F3) occurs after the heel loses contact (heel-off) when all the force is at the toe. Finally, the force decreases again to reach zero at toe-off.

2.2 Methods and theory

2.2.1 Rigid Body Dynamics

For the scope of this thesis, we use rigid body dynamics through the Rigid Body Dynamics Library (RBDL) so it becomes essential to understand the equations that govern the system. Rigid bodies refer to any body that is not deformed by forces acting on it, and rigid bodies can be connected together through joints to create a rigid body system as shown in Fig 2.6. Joints impose a constraint between the bodies to connect their motion and provide a degree of freedom (DOF) between the bodies, that degree of freedom can be a rotational one like the figure or a translation. The resulting motion of the system is defined using its position, velocity, acceleration, forces and torques.

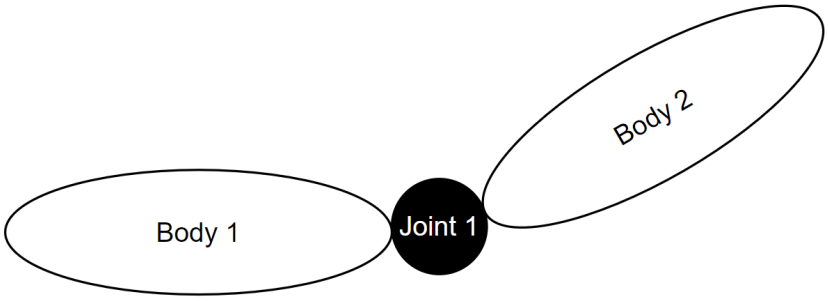

Figure 2.6: Simple rigid body system consisting of two bodies and a single joint connecting them

There are two types of rigid-body systems, one that is connected to a fixed base to the ground and only has the degrees of freedom of the added joints and the other is a floating base system which has additional degrees of freedom that represent their position and orientation in space. The addition of those degrees of freedom causes the system to have redundant coordinates since the actuated degrees of freedom are less than the total degrees of freedom of the system. In this thesis, both the human system and the human-exoskeleton system are considered a floating base.

For interaction with the environment, there are contact points considered that constrain the dynamics of the system and deal with the redundancy that occurs from the floating base dynamics. Since we are dealing with walking, the dynamics are subject to change with each change of phase of motion. Additional contact points are added or removed accordingly. The addition of contact points occurs when the rigid body system collides with the floor which causes an impact. These impacts are assumed to be inelastic and occur instantaneously.

$$\mathbf{H}(q)\ddot{q} + \mathbf{C}(q,\dot{q})\dot{q} = \tau \tag{2.1}$$

The dynamics of rigid bodies can be described using the generalized equation of motion 2.1 where $\mathbf{q}$ is a vector of generalized coordinates that describe the configuration of the system, $\dot{\mathbf{q}}$ and $\ddot{\mathbf{q}}$ are the first and second-time derivatives of $\mathbf{q}$, respectively, $\mathbf{H}$ is the generalized inertia matrix, $\mathbf{C}$ is the generalized nonlinear force matrix, and τ is the vector of external forces and torques acting on the system.

The forward dynamics formulation 2.2 is used to calculate the resultant acceleration of the system based on the input torque τ and the current configuration of the system.

$$\ddot{q} = FD(q, \dot{q}, \tau) \tag{2.2}$$

The inverse dynamics formulation is used to calculate the torques τ required to move the system according to the input generalized accelerations $\ddot{q}$.

$$\tau = ID(q, \dot{q}, \ddot{q}) \tag{2.3}$$

The generalized coordinates or degrees of freedom of the rigid-body system q used contains additional degrees of freedom to represent the floating base idea. This means the addition of 6 degrees of freedom for a full 3-dimensional model or the addition of 3 degrees of freedom for a simplified 2D model. The 3D model has three translations and rotations XYZ, while the 2D model used has 2 translations YZ and 1 rotation X. The additional degrees of freedom are not actuated which means that the first 3 terms τ are considered zero.

Given that the motion of concern is walking, it goes through a series of phases where the system dynamics change. The change is caused by the changes in contact points in each phase. The contacts added to the system can be described as constraints that act on the points of contact to force the position of that point to be zero 2.4.

$$g(q) = 0 \tag{2.4}$$

The addition of constraints changes the dynamics equation of the system to be Eq 2.5 where $\mathbf{G}$ is the constraints Jacobian $G = \partial g / \partial q$ and λ the Lagrangian representing the force in the constraint

$$\mathbf{H}(q)\ddot{q} + \mathbf{C}(q, \dot{q})\dot{q} = \tau + \mathbf{G}^T\lambda \tag{2.5}$$

by differentiating the positional constraint twice the resulting equation is 2.6

$$G(q)\ddot{q} + \dot{G}(q)\dot{q} = 0 \tag{2.6}$$

Using eq 2.6 in eq 2.5 we get a resulting system of equations 2.7

$$\begin{gathered} \dot{q} = v \\ \dot{v} = a \\ H(q)a + C(q, v) = \tau(q, v) + G(q)^T\lambda \\ G(q)a + \dot{G}(q)v = 0 \end{gathered} \tag{2.7}$$

or a linear system as follows:

$$\begin{pmatrix} H(q,p) & G(q,p)^T \\ G(q,p) & 0 \end{pmatrix} \begin{pmatrix} \ddot{q} \\ -\lambda \end{pmatrix} = \begin{pmatrix} \tau - C(q,\dot{q}) \\ -\gamma(q,\dot{q}) \end{pmatrix} \tag{2.8}$$

where $\gamma = \dot{G}(q)\dot{q}$

Since the impact is inelastic and instantaneous, the constraint must force the velocity after the impact (v_+) to remain zero in order to satisfy the positional contact constraint. The velocity right before v_- and right after v_+ are different and can be computed through Eq 2.9. where Λ represents the contact impulse that occurs.

$$\begin{pmatrix} M(q,p) & G(q,p)^T \\ G(q,p) & 0 \end{pmatrix} \begin{pmatrix} v_+ \\ \Lambda \end{pmatrix} = \begin{pmatrix} M(q,p)v_- \\ \gamma(q,v,p) \end{pmatrix} \tag{2.9}$$

2.2.2 Muscle model (Hill-type)

Human motion is controlled through the contraction of muscles, the human body has over 650 muscles that get activated for specific motions. In the case of walking, our concern is with the leg muscles since they provide motion and stabilization.

There are three different types of muscles in the human body; skeletal, cardiac and smooth. Given that our concern is motion, we are concerned with the skeletal muscles that cause the skeleton to move by exerting forces on it.

The skeletal muscles range in size, shape and arrangement of fibres. The muscles are generally made up of many motor units that consist of muscle fibres innervated by motor neurons [18]. The active contractile part of the muscle comes from the Sarcomere. The Sarcomere consists of two protein filaments Actin and Myosin which are the active structures that cause muscle contraction.

The most popular muscle model used to date is the hill-type muscle model derived by physiologist Archibald Vivian Hill. The model consists of three elements to represent the muscle as a mechanical system and is explained in detail in [19]. The contractile element (CE), the parallel element (PE) and the series element (SE). as shown in Fig 2.7. There are several variations of this model used, in this section we will discuss some of the most popular equations and models used.

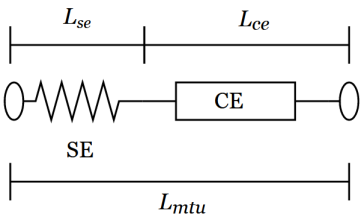

Figure 2.7: Hill type muscle model

The force in the muscle comes from the contraction of the contractile element, through the Actin-Myosin cross-bridges formed on the Sarcomere level and the stretching of the spring elements. The parallel and series elements are modelled as two non-linear springs. The parallel element represents the connective tissue that surrounds the muscle like the fascia, epimysium etc. The series element represents the tendon attached to the muscle and the elastic part of the muscle fibres. The final force exerted by the muscle is a combination of the forces from the active (CE) element and the passive (PE, SE) ones. The simplest model consists of only a series element and a contractile element, and the resulting force can be simply calculated through Eq 2.10.

$$F_{CE} = F_{SE} \tag{2.10}$$

For the length relationship, L_{mtu} represents the entire length of the muscle-tendon unit

$$L_{mtu} = L_{CE} + L_{SE} \tag{2.11}$$

Series elastic element

The series elastic element behaves as a non-linear spring according to a force-length relationship in Eq 2.19 where force is only applied if the length of the series element L_{SE} passes a threshold of L_u which is the unloaded length. K_1 is a constant representing $K_1 = F_o/(U_o L_u)^2$ where F_o is the maximum isometric force and U_o is the strain of the SE when loaded with F_o, usually assumed as $U_o = 0.04$.

$$F_{SE} = \begin{cases} K_1(L_{SE} - L_u)^2, & L_{SE} > Lu \\ 0, & L_{SE} \leq Lu \end{cases} \tag{2.12}$$

Contractile element

The contractile component is activated based on an input signal called muscle activation α. For the hill model, the muscles get a time-varying signal ranging $[0, 1]$ called excitation u that translates into muscle activation α with a first-order delay τ. An example of how this is implemented in Eq 2.13

$$\dot{\alpha} = \frac{(u - \alpha)}{\tau(\alpha, u)} \tag{2.13}$$

The resulting force in the contractile element can be expressed as Eq 2.14, the force is a simple multiplication of the max force F_o, the force-velocity factor F_V and the force-length factor F_L.

$$F_{CE} = F_o \alpha F_L F_V \tag{2.14}$$

The force-length relationship represents the change in force output based on the current muscle length, the maximum force produced by the muscle F_o is at the point of length L_o, this relationship has been modelled through several equations in the literature; a parabolic function Eq 2.15, Gaussian-based Eq 2.16 and an exponential sine Eq 2.17 with constants modified to fit real data. A comparison of the parabolic and Gaussian relationship models can be seen in [19, Fig 2.8]

$$F_L = max(-\frac{1}{W_1^2}(\frac{L_{CE}}{L_o} - 1)^2 + 1, 0) \tag{2.15}$$

$$F_L = exp(-\frac{1}{W_1^2}(\frac{L_{CE}}{L_o} - 1)^2) \tag{2.16}$$

$$F_L = 0.32 + 0.71exp(-1.112(\frac{L_{CE}}{L_o} - 1)^2)sin(3.722(\frac{L_{CE}}{L_o} - 0.656)) \tag{2.17}$$

The force-velocity relationship represents the change in force output based on the current velocity of the muscle contracting. The relationship consists of both an eccentric and concentric part modelled in Eq 2.18 can be seen [19, Fig 2.9]

$$FV = \begin{cases} \frac{b + a\dot{L}_{CE}/L_o}{b - \dot{L}_{CE}/L_o}, & \dot{L}_{CE}/L_o \leq 0 \\ \frac{C_{ecc}\dot{L}_{CE}/L_o + v_1}{\dot{L}_{CE}/L_o + v_1}, & 0 < \dot{L}_{CE}/L_o \leq \delta v_1 \\ v_3 + v_2\dot{L}_{CE}/L_o, & \dot{L}_{CE}/L_o > \delta v_1 \end{cases} \tag{2.18}$$

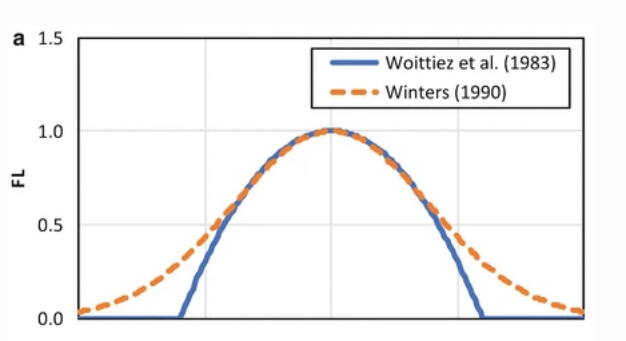

Figure 2.8: Different force-length relationship models against relative contractile element length normalized against optimum length. Figure from [19]

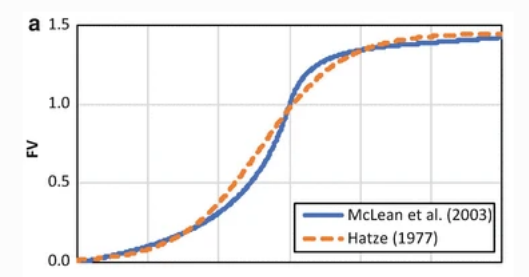

Figure 2.9: Different force-velocity relationship against relative contractile element velocity normalized against optimum length. Figure from [19]

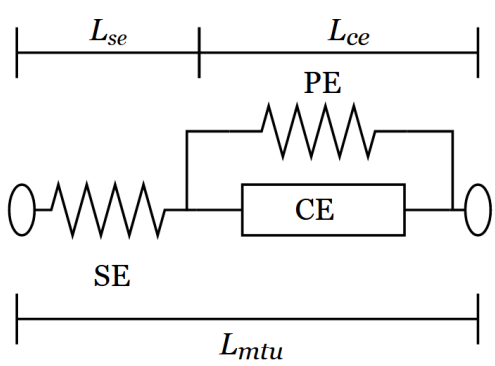

(a) Hill-type model when parallel element is only parallel to the contractile element

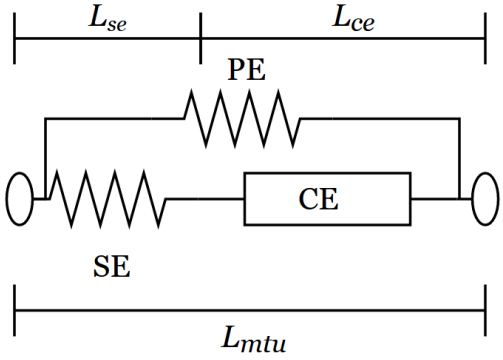

(b) Hill-type model when parallel element is parallel to the entire model

Figure 2.10: variations of parallel element placement in hill-type models

Parallel elastic element

The parallel element can either be parallel to the entire muscle in Fig 2.10b or only parallel to the contractile element as seen in Fig 2.10a. The force of the parallel elastic element is a function of its length similar to that of the contractile element. When the parallel element is only parallel to the contractile element the force is expressed in Eq 2.19. When placed parallel to the entire muscle, the force is expressed in Eq 2.20

$$(F_{CE} + F_{PE})cos\theta = F_{SE} \tag{2.19}$$

$$F_m = F_{PE} + F_{SE} = F_{PE} + F_{CE}cos(\theta) \tag{2.20}$$

2.2.3 Optimal Control Methods

Optimal control theory is a branch of mathematics created to find the optimal/best way to control a dynamic process that is described by differential equations, it's a method that works to find the most suitable control signal to minimize a specific performance index or cost function [20].

Problem formulation

The problem formulation in optimal control uses a mathematical model to describe the dynamics of the system which is contained within the equations of motion represented in the state vector $x(t)$. This model takes into account the dynamics that govern the behaviour of the system, as well as the effects of the control inputs $u(t)$. The optimal control problem involves finding the control inputs that minimize the cost function Φ subject to constraints g, r_{eq}, r_{ineq} on the system dynamics and the control inputs. The general formulation is shown in Eq 2.21

$$\begin{aligned} \min_{x(\cdot),u(\cdot),p,T} \quad & \int_0^T \phi_L(x(t),u(t),p)dt + \phi_M(T,x(T),p) \\ \text{s. t.} \quad & \dot{x}(t) = f(t,x(t),u(t),p) \\ & g(t,x(t),u(t),p) \geq 0 \\ & r_{eq}(x(0),..,x(T),p) = 0 \\ & r_{\text{ineq}}(x(0),..,x(T),p) \geq 0 \end{aligned} \tag{2.21}$$

The right-hand side part $f(t,x(t),u(t),p)$ carries the information of the model, which is a set of ordinary differential equations that describe the dynamics of the system as described previously in 2.2.1. The constraints acting on the system come in three types; $g(t,x(t),u(t),p)$ which represent the path constraints, boundary constraints: r_{eq} for equality and r_{ineq} for inequality constraints.

Since the previous equation covers a single-phase optimization problem, a modification had to be made resulting in Eq 2.22 where j represents the number of the phase of motion, n_{ph} represents the total number of phases. The objective function, system dynamics and constraints are different for each phase.

$$\begin{aligned} \min_{x(\cdot),u(\cdot),p,s_j,s_j+1,..,s_{nph}} \quad & \sum_{j=0}^{n_{ph}-1} \int_{s_j}^{s_j+1} \phi_L(x(t),u(t),p)dt + \phi_M(s_j+1,x(s_j+1),p) \\ \text{s. t.} \quad & \dot{x}(t) = f_j(t,x(t),u(t),p) \\ & t \in [s_j, s_j+1] \\ & j = 0,...,n_{ph}-1 \\ & g_j(t,x(t),u(t),p) \geq 0 \\ & r_{eq}(x(0),..,x(T),p) = 0 \\ & r_{\text{ineq}}(x(0),..,x(T),p) \geq 0 \end{aligned} \tag{2.22}$$

For the purpose of this thesis, since walking is a motion in which there is always contact, the dynamics equations used for the phases all follow Eq 2.5.

The optimal control problems within this thesis are solved with the direct multiple shooting method through the software packages Bioptim [11] and MUSCOD-II [12].

Direct multiple shooting method

The given problem is solved using the direct multiple shooting method, which is an adaptation of the single shooting method that is used to solve boundary value problems. The problem starts from an initial value and integrates to reach the final value iteratively changing the initial guess using a root finding method such as Newton's method until it is able to satisfy the boundary conditions [21]. Multiple shooting employs the same methods as single shooting with the addition of dividing the entire time interval into equal parts named shooting intervals, then each interval is treated like a single shooting node with the addition of continuity constraints imposed to ensure the continuity between each interval and the next.

Direct multiple shooting method was created in [22] to solve constrained optimal control problems. To discretize the controls, the time grid is created:

$$t_0 < t_1 < ... < tm - 1 < t_m = t_f \tag{2.23}$$

The control signal 2.24 is approximated for each sub-interval by a basis function ϕ_j and parameters q_j. The base function can be a piece-wise constant, piece-wise linear or cubic. The chosen method in this thesis is piecewise linear.

$$\begin{gathered} u(t) \approx \phi_j(t, q_j) \\ t \in I_j[t_j, t_{j+1}] \qquad for \quad j = 1, ..., m \end{gathered} \tag{2.24}$$

Multiple shooting method involves splitting the time interval $[t_o, t_{end}]$ into m sub-intervals deemed multiple shooting intervals (ms-intervals), each interval is treated as an initial value problem and starts from an initial guess for the states $[s_o, ..., s_m]$ resulting in m initial value problems

$$\begin{gathered} x = f(t, x, \phi_j(t, q_j)) \\ x(t_j) = s_j, \quad t \in I_j \end{gathered} \tag{2.25}$$

Then integrations (shots) are performed from these initial points. Since each interval is calculated independently, additional constraints on the continuity between the endpoint of a ms-interval and the start point of the next are added in Eq 2.26.

$$x(t_{j+1}, s_j, q_j) - s_{j+1} = 0 \tag{2.26}$$

All the constraints are evaluated at each shooting node.

Multi-phase problems and transitions

Multiple shooting method allows us to formulate problems that consist of multiple phases, where the dynamics (right hand side) equations change in each phase. To deal with the transition between these phases can either maintain continuity in Eq 2.26 or allow for a discontinuity between the phases using a transition function $J_j(x(s_j^-), p)$ in $x(s_j^+) = x(s_j^-) + J_j(x(s_j^-), p)$ where s_j^- is the time before the transition and s_j^+ the time after the transition.

Discretized optimal control problem

This discretization allows us to get a large nonlinear programming problem (NLP). Using a vector y to represent all the discretized OCP variables (states, controls, phase durations) the OCP can be re-written as

$$\begin{aligned} \min \quad & \Phi(y) \\ \text{s. t:} \quad & \\ & G(y) = 0 \\ & R(y) \geq 0 \end{aligned} \tag{2.27}$$

where $R(y)$ represents the inequality constraints, $G(y)$ represents the equality constraints and Φ represents the discretized objective function.

The problem is solved using Sequential Quadratic Programming (SQP) methods in MUSCOD-II, which solves NLP problems iteratively by solving a Quadratic Programming (QP) problem at each iteration. Then the solution determines the next iteration Eq 2.28. Where α_k is the step length and Δy_k is the step direction.

$$y_{k+1} = y_k + \alpha_k \Delta y_k \tag{2.28}$$

The quadratic problem solved Eq 2.29 results in the step direction Δy_k

$$\begin{aligned} \min_{\Delta y_k} \quad & \nabla \Phi(y_k)^T \Delta y_k + \tfrac{1}{2} \Delta_k^T H_k \Delta w_k \\ \text{s. t:} \quad & \\ & G(y_k) + \nabla G(y_k)^T \Delta y_k = 0 \\ & R(y_k) + \nabla R(y_k)^T \Delta y_k \geq 0 \end{aligned} \tag{2.29}$$

2.3 Existing Human Models

In this section, we will explore some commonly used models to represent human movement, specifically walking. The models that exist in the literature range from the simplest

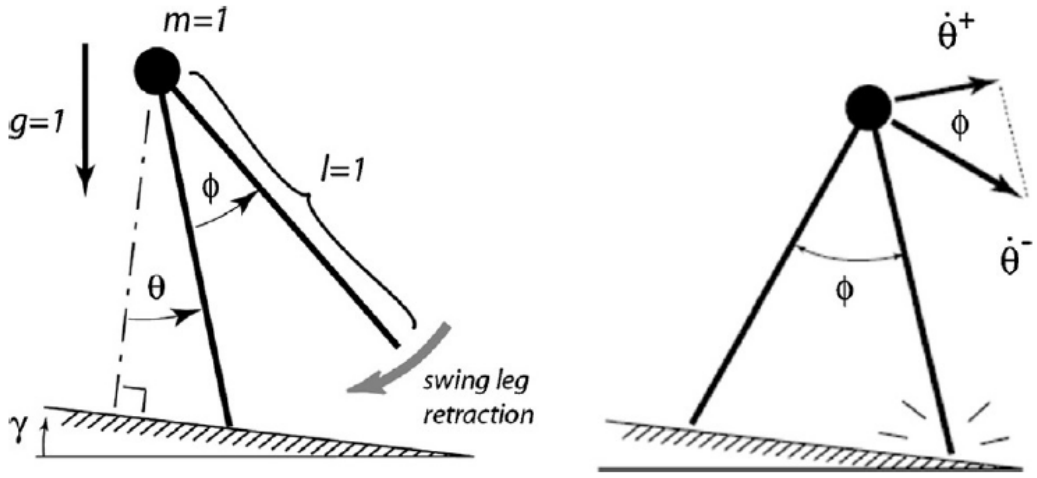

Figure 2.11: Bipedal pendulum model from [23]

template models of a single linear inverted and increase in complexity to reach full human models that contain both muscle and bone data.

This section will briefly describe the double linear inverted pendulum model. Then we will cover humans as a multi-body system model and the complex muscle and skeleton models commonly used in OpenSim.

2.3.1 Inverted pendulum model

Human walking has been compared to the movement of an inverted pendulum in the literature. There are numerous similarities between the two, specifically when one leg is placed on the ground, causing the body to swing like an inverted pendulum around the point of contact. By alternating between left and right legs, human walking can be described using the model of an inverted pendulum. The linear inverted pendulum (LIP) model has often been used to describe the human walking motion, it is based on the previous assumption that the center of mass of the human swings about the point of contact created by the foot on the ground. The simplest bipedal inverted pendulum model created in 1998 [24] consists of a point mass representing the human's center of mass and two rigid segments that represent the legs connected by a frictionless hinge at the hip joint. The model moves on a rigid ramp. A further simplification of this model in [23] includes the negligence of the swing leg mass, the assumption that the swing leg is controlled to

strike the ground with a specific angle and velocity and that the time spent in double support is very small in comparison to the total length of step.

By applying the Euler-Lagrange equation to the system's energy in [23, Fig 2.11] we can formulate the Lagrangian L through 2.30 where T is kinetic energy, V is potential energy, θ is the angle of rotation of the system and γ is the slope, mass m, length l and gravity g are assumed to be equal to one. By applying the Euler-Lagrange equation of mechanics to the system, it results in the differential equation of motion for the system 2.31. This equation represents the motion of the inverted pendulum during the stance phase.

$$L = T - V = \frac{1}{2}ml^2\dot{\theta}^2 - mglcos(\theta - \gamma) \tag{2.30}$$

$$\ddot{\theta} = gl^{-1}sin(\theta - \gamma) \tag{2.31}$$

The moment that the foot loses contact with the ground, it enters the swing phase. By ignoring the existence of the double support phase in walking, we can assume that the moment one leg enters the stance phase by foot contact, the other leg must be losing contact and thus starting the swing phase. By assuming a predefined controlled motion for the swing leg, the swing leg swings forward and then retracts to land in the specified position.

2.3.2 Multi-body system model

Another method of modelling human walking can be done by the creation of a multi-body system that represents the human as simplified rigid-body segments. An example of this can be seen in [25].

In [25] Fig 2.12 a 3-dimensional simulation model of human walking was created. The model consisted of eight rigid bodies: the trunk was split into two segments and it contained the properties of the head and arms as well. The lower body had two thighs, shanks and feet segments. All the dimensions and inertial properties of the segments were taken from statistical data. The segments were all connected with rotational degrees of freedom. The lower and upper trunk was connected with 1 degree of freedom, the hip was modelled as a spherical joint resulting in 3 degrees of freedom and the knee and ankle were given 2 degrees of freedom each. The total number of degrees of freedom in the model is 21 degrees.

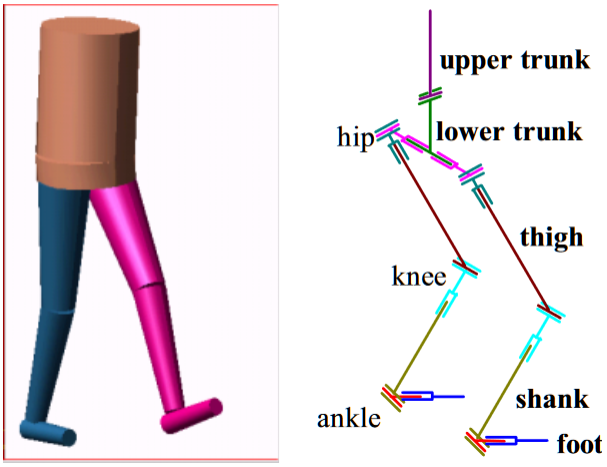

Figure 2.12: Multi-body model from [25]

Another example can be seen in [26], where the authors created a rigid body system consisting of 12 bodies: head, arms, 3-part trunk and legs. With 31 degrees of freedom seen in [26, Fig 2.13], the mechanical parameters of this model are taken after an adult human. This model uses point feet so each foot has one contact point, and thus this simplifies the model further and reduces the phases of motion. Each foot has two conditions, either in contact or not in contact. The dynamics of the system can be represented by Eq 2.8. Impacts with the ground can be computed through Eq 2.9.

This model has been used with optimal control formulation of human walking. The human walking was modelled as a two-phase optimal problem with single and double support based on the contact points. The objective function used was the minimization of the actuated joint torques and the motion of the head. The authors were able to generate a valid gait motion through the optimal control problem formulation, which shows that optimal control is able to generate a natural gait without the need for any motion capture data. A drawback of relying on this method purely is that the results are heavily influenced by the objective function selected. i.e selecting various objective functions can result in different gait motions.

2.3.3 More complex musculoskeletal models

The OpenSim software [27] is created to enable the creation of musculoskeletal models, visualizing their motion and interacting with the models. The software has several models

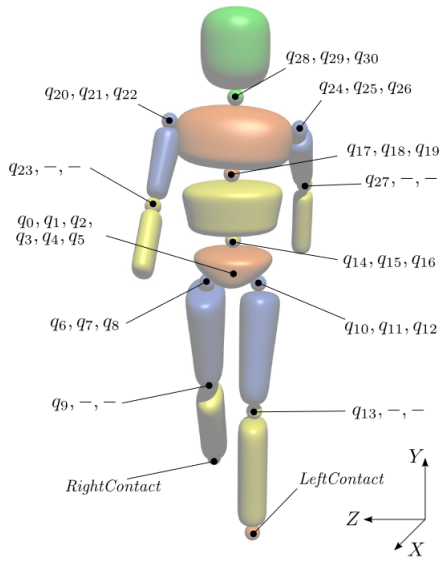

Figure 2.13: Degrees of freedom of model from [26]

of the human body, with complex models containing muscles and bones with their geometry and muscle insertion points. These models were used to simulate the human gait.

This model [28] which was created in 1990 for computer simulations and contains 18 muscle-tendon actuators and provides actuation for the hip, knee and ankle in the sagittal plane.

The mechanical part of the model used four rigid bodies; trunk, thigh, shank and foot. The segments were connected together with ideal revolute joints. Muscle-tendon unit lengths and moment arms were computed from the system's geometry. Similar to the Hill-type muscle models described earlier the change in muscle length l^{MT} was calculated based on the change in joint angle θ_k and the moment arm r_k Eq 2.32

$$dl^{MT} = r_k d\theta_k \tag{2.32}$$

Fig 2.14 adapted from [28] shows the muscle-tendon unit model used, it contains a contractile element CE and a series elastic element with stiffness K^T. Force in the tendon F^T is equal to the force in the contractile element $F^M cos(\alpha)$ where α is the pennation angle of the muscle. The muscle-tendon unit length L^{MT} is the sum of L^T and $L^M cos(\alpha)$. The expression for the force-length relationship is as follows in Eq 2.33 where the variables are

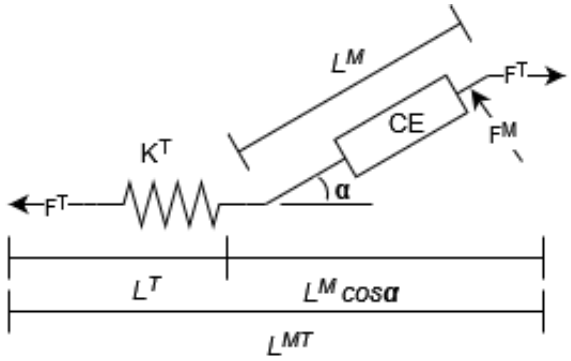

Figure 2.14: Simple hill-type model

normalized.

$$\bar{F^T} = \bar{F^M}\bar{l^M}cos(\alpha) = \bar{F^M}\bar{l^M}\sqrt{1 - (\frac{sin(\alpha_o)}{\bar{l^M}})^2} \tag{2.33}$$

The force in tendon F^T is both a function of normalized muscle length $\bar{L^M}$ in Eq 2.33 and normalized tendon length $\bar{L^T}$ in Eq 2.34, the normalized force $\bar{F^T}$ can be calculated by satisfying both equations.

$$\bar{F^T} = \frac{37.5}{\bar{l_S^T}}(\bar{l^{MT}} - \bar{l^M}\sqrt{1 - (\frac{sin(\alpha_o)}{\bar{l^M}})^2} - \bar{l_S^T} \tag{2.34}$$

This model only deals with the static properties of the muscles and tendons since it does not account for the force-velocity relationship of the muscles.

Another model developed was [29], The model contains the bone geometry and muscle data for the human lower extremity. The bones' surfaces are created with a mesh of polygons. 43 muscle-tendon actuators were added and connected to the bones. Some muscles were directly attached in a line like the Soleus muscle, but for more complicated attachments they represented the muscle wrapping with via points. The moment arms and muscle-tendon lengths were calculated through the geometry of the model.

The lower extremity model contains seven rigid segments: pelvis, femur, patella, tibia/fibula, talus, foot and toes. The hip joint was modelled as a ball and socket joint giving it three degrees of freedom. The knee was given a revolute joint with one degree of freedom in the sagittal plane. The ankle, subtalar and metatarsophalangeal joints were also modelled as revolute joints.

In order to calculate the muscle force as a result of the muscle-tendon length, the following model was formulated, this model accounts for the static properties of the muscles

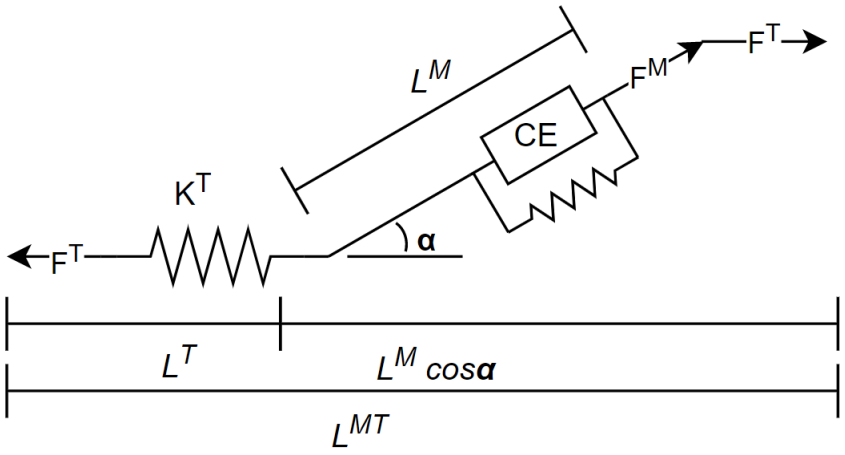

Figure 2.15: Opensim hill-type model

and tendons. The generic model is shown in Fig 2.15. For each muscle-tendon unit, the model is scaled by the muscle parameters. The equations are the same ones used in the previous model [28]

In [30] newer model was created to simulate the human musculoskeletal system for the control of gait. The model is made up of 22 rigid bodies representing the lower and upper body of a human model, the lower body contained: the pelvis, femur, patella, tibia/fibula, talus, calcaneus and toes. The upper body: combined head and torso, humerus, ulna, radius and hand.

The segments are connected by a total of 37 degrees of freedom, 20 in the lower body and 17 in the upper body. The hip joint has three degrees of freedom as a ball and socket joint, the knee has one degree of freedom for flexion/extension and the ankle, subtalar and metatarsophalangeal joints were each given one degree of freedom.

The model contained 80 muscle-tendon units in the lower limbs and 17 torque actuators in the upper limbs. The muscle-tendon units were modelled after the hill-type model shown in Fig 2.15. The force-length and force-velocity relationships in [30, Fig 2.16] for each muscle-tendon unit were scaled by the optimal fibre length, maximum isometric force, maximum shortening velocity, pennation angle at optimal fibre length and tendon slack length 2.16.

Such models, while providing higher accuracy than rigid body models or pendulum models, are computationally expensive and complex. Furthermore, due to the many

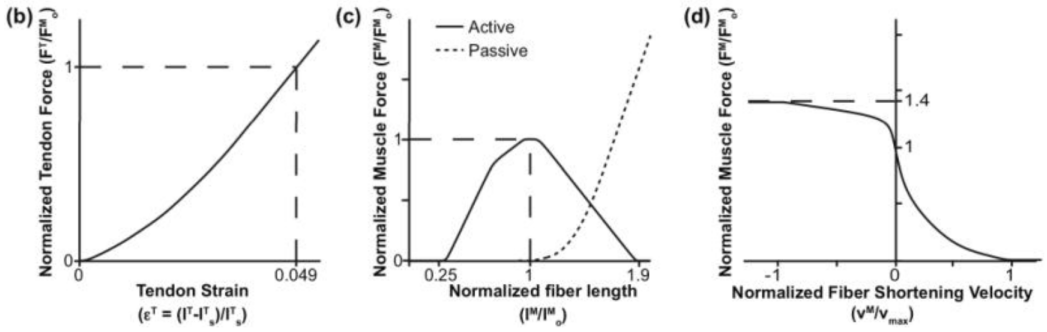

Figure 2.16: Generic curves of muscle force-length, force-velocity relationship and normalized tendon force

anatomical parts, these models require sufficient validation to ensure they accurately represent human anatomy and physiology. They might be more suitable to study human motion than generating patterns for motion to be used in other applications such as exoskeletons.

Chapter 3

Reflex Based Walking Model

In this chapter, we will explore the original model created in [8] and the creation of the walking model used in this thesis. Most of the model equations for the muscles and spinal reflexes stay the same. However, there are some changes to be noted in the method of implementation of the layers. The starting point for this model implementation originated from the reflex-based muscle model created by Hartmut Geyer and Hugh Herr in 2010[8] and the subsequent work added to it in 2015 by S . Song and H . Geyer in [1]. This model is explained in detail in the first section of this chapter, the second section describes the implementation created in this thesis and the third section is a comparison of the results of both models.

3.1 Model Equations and Parameters

The Neuromuscular model proposed by [8] is a bio-model created to represent human gait as a set of reflex signals sent to leg muscles, the muscles then act on each joint with a given torque to move them. The original model consists of 7 model muscles per leg for a purely sagittal motion, the muscles are the Glutei (GLU), Hip flexors (HFL), Hamstrings (HAM), Vasti (VAS), Gastrocnemius (GAS), Soleus(SOL), Tibialis anterior (TA). In [1] (2015) the hip adductors (HAD) and abductors (HAB) were added for an additional hip degree of freedom, Rectus Femoris (RF) and Biceps Femoris (BFSH) muscles were also added for the sagittal plane actuation.

The 2015[1] model consisted of 4 layers which can be seen in Fig 3.1, biomechanics layer, muscle-tendon unit (MTU) layer, reflex layer and supra-spinal control layer.

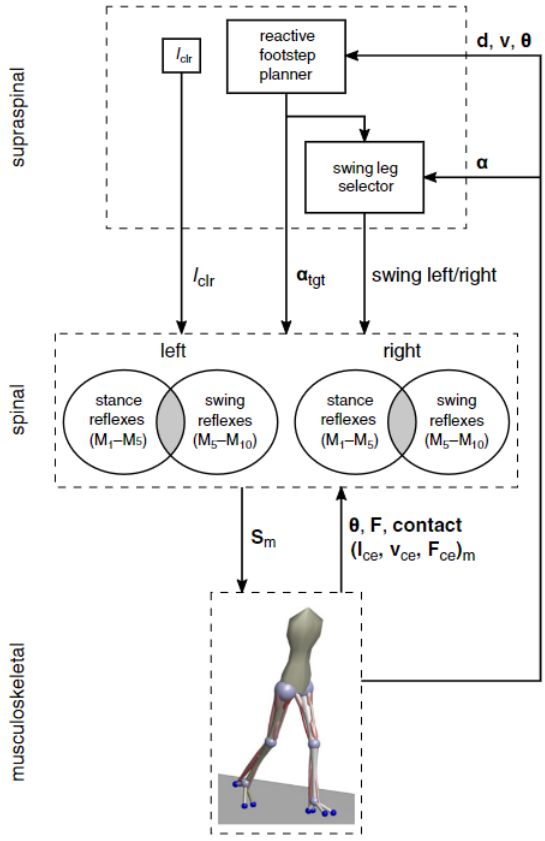

Figure 3.1: Neuromuscular model from [1]

1. Biomechanics layer: represents the model tree and contains the mechanical details of each segment and produces moment arms.

2. MTU layer: contains the muscle models for the 9 individual muscles in each leg, producing muscle forces.

3. Reflex layer: containing the reflex modules that calculate the individual muscle activation.

4. Supra-spinal control layer: responsible for calculating foot placement parameters, essentially controlling the behaviour of the previous systems.

In [1] the model has been implemented using MATLAB Simulink (R2013a) and is able to produce satisfactory results for walking, walking on slopes, turning, running and stair

ascent. The model is optimized for each motion type with 82 control parameters (7 for the reactive foot placement, 40 for stance reflexes, 31 for swing reflexes, and 4 for the modulation in the control transition) and each optimization run takes approximately 1 day [1]. This model has been used to implement neuromuscular controllers that can be used to control exoskeletons. This model provides certain advantages to the control by being torque based and by adapting to perturbation in motion. The model also has a few limitations that are concerned with the number of parameters it needs to run, and the fact that it cannot initiate the motion from standing.

This model and variations of it have been widely used in exoskeleton control earlier and has been chosen since it comes at a compromise in complexity because it only models the muscles and represents the human control as spinal reflexes while keeping the mechanical part simple with rigid bodies. Our assumption was using a bio-inspired model helps us reach a motion that feels much more natural and is even closer to real human walking motion.

In this thesis, we want to explore this model and re-create it using C++ and basic dynamics libraries to maximize compatibility with other C++ libraries. Then edit the control structure by adding optimal control to replace the supra-spinal control layer to modify walking parameters like step length or speed while maintaining the human-like motion generated by this model. Furthermore, as will be discussed in Chapter 4 we can use optimal control to find an optimal trajectory to get the model to start from standing. The hypothesis is, we can use optimal control to change the way the model walks in terms of step length and speed and optimize it to work with the additional weight and parameters of the lower-limb exoskeleton.

3.1.1 Biomechanics layer

The biomechanical layer serves as an interface between the torque output from the muscles to an actual motion performed by the system through the use of forward dynamics. Table 3.1 represents the segment mechanical and inertial values used in the creation of the model from [1], it should be noted that the joint position and the Centre of mass (COM) position in the table is referenced from the distal end of the respective segment. The model consists of seven segments: the combined head, trunk and arms (HAT) and for each leg: a thigh, a shank and a foot segment.

	Trunk	Thigh	Shank	Foot
Height (m)	0.80	0.46	0.46	0.08
Width (m)	0.4	0.1	0.1	0.1
Length (m)	0.1	0.1	0.1	0.2
Mass (kg)	53.5	8.5	3.5	1.25
Joint position	0.20 (w)	0.46 (h)	0.46 (h)	0.16 (l) 0.08 (l)
COM position	0.35 (h)	0.28 (h)	0.28 (h)	0.14 (l) 0.07(h)
I_{xx}	2.5	0.15	0.05	0.005
I_{yy}	1	0.03	0.003	0.005
I_{zz}	4.0	0.15	0.05	0.0007

Table 3.1: Segment parameters from [1]

3.1.2 Muscle layer

This layer contains the muscles in each leg and is connected to the previous layer with a torque interface at each joint. Each muscle or muscle group is modelled as a Hill-type muscle-tendon unit (MTU). Each MTU is composed of a contractile element (CE), a parallel (PE) and a series element (SE). In addition to the standard hill-type model, a buffer elasticity is added to prevent the collapse of the muscle [8]. The force coming from each MTU is dependent on the current muscle length (L_{CE}), activation (Act), maximum isometric force (F_{max}), and the force-velocity and force-length relationships.

The force in the muscle F_{mtu} is equal to the force in the series elastic element F_{se} Fig. 3.2 and is calculated from [31, eq. 3.1] where ϵ represents the tendon strain $\epsilon = (l_{se} - l_{rest})/l_{rest}$ where l_{rest} is the tendon resting length and $\epsilon_{ref} = 1$.

$$F_{mtu} = F_{se} = \begin{cases} if\ \epsilon > 0 & \dfrac{\epsilon}{\epsilon_{ref}^2} \\ if\ \epsilon \leq 0 & 0 \end{cases} \tag{3.1}$$

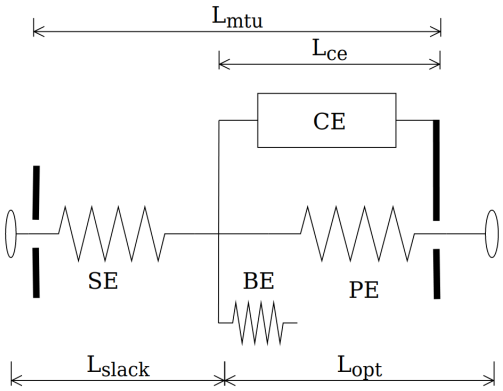

Figure 3.2: Hill type muscle used

Eq. 3.2 represents the force in the contractile element F_{ce} where $f_l(l_{ce})$ 3.3 is the force-length relationship and $f_v(v_{ce})$ 3.5 is the force-velocity relationship for the muscle.

$$F_{ce} = Act_m F_{max} f_l(l_{ce}) f_v(v_{ce}) \tag{3.2}$$

$$f_l(l_{ce}) = \exp c|\frac{l_{ce} - l_{opt}}{l_{opt} w}|^3 \tag{3.3}$$

The resulting force from 3.4 is used in the inverse of the force-velocity relationship in 3.5 to calculate the resulting contractile element velocity v_{ce} which translates into muscle velocity.

$$f_v(v_{ce}) = \frac{F_{se} + F_{be}}{F_{pe} + f_l(l_{ce}) Act} \tag{3.4}$$

$$f_v(v_{ce}) = \begin{cases} if\ v_{ce} < 0 & \frac{v_{max} - v_{ce}}{v_{max} + K v_{ce}} \\ if\ v_{ce} \geq 0 & N + (N-1)\frac{v_{max} + v_{max}}{7.56 K v_{ce} - v_{ce}} \end{cases} \tag{3.5}$$

The resulting velocity is used to calculate the new contractile element length for the next time step 3.6

$$l_{ce} = \int v_{ce} dt = \int [f_v(v_{ce})]^{-1} dt \tag{3.6}$$

3.1.3 Reflex layer

The reflex layer is categorized as 10 reflex modules for each leg, from M_1 to M_{10} based on whether the leg is in the stance (M_1 to M_5) or swing (M_5 to M_{10}) phase of the walking. Each of these modules act on different muscles, thus the total muscle activation results from a sum of those reflex modules and differs across muscles as presented in 3.7 through 3.15.

$$Stim_{GLU} = \begin{cases} M_1 + M_3 + M_4 & if\ Stance \\ M_6 + M_{10} & if\ Swing \end{cases} \tag{3.7}$$

$$Stim_{HFL} = \begin{cases} M_3 + M_4 & if\ Stance \\ M_6 + M_{10} & if\ Swing \end{cases} \tag{3.8}$$

$$Stim_{HAM} = \begin{cases} M_2 + M_3 + M_4 & if\ Stance \\ M_9 & if\ Swing \end{cases} \tag{3.9}$$

$$Stim_{RF} = \begin{cases} 0 & if\ Stance \\ M_8 & if\ Swing \end{cases} \tag{3.10}$$

$$Stim_{VAS} = \begin{cases} M_1 + M_2 & if\ Stance \\ M_{10} & if\ Swing \end{cases} \tag{3.11}$$

$$Stim_{BFSH} = \begin{cases} M_2 & if\ Stance \\ M_7 + M_8 + M_9 & if\ Swing \end{cases} \tag{3.12}$$

$$Stim_{GAS} = \begin{cases} M_2 & if\ Stance \\ M_9 & if\ Swing \end{cases} \tag{3.13}$$

$$Stim_{SOL} = \begin{cases} M_1 & if\ Stance \\ 0 & if\ Swing \end{cases} \tag{3.14}$$

$$Stim_{TA} = M_5 \tag{3.15}$$

For each individual reflex module, the stimulations are calculated based on the equations shown in 3.16 to 3.25. Where G represents a constant gain, with the subscript representing the muscle name and related parameter. The reflex parameters used are all from [8] [1]

As mentioned, the reflex modules contained in the stance phase are M_1 to M_5. Reflex module M_1 3.16 uses force feedback of the muscles (GLU, VAS and SOL) to introduce compliant leg action. Module M_2 3.17 prevents knee hyper-extension using force feedback from HAM and GAS, and length feedback from VAS and BFSH to inhibit the first and excite the latter muscle if the knee gets close to hyper-extension.

Module M_3 3.18 relates to maintaining the balance of the trunk by activating HFL,GLU and HAM muscles based on trunk angle θ_{HAT}, the intensity of this module is modulated by the force in the thigh and is the reason why the model was created with two thigh segments (upper and lower). Module M_4 3.19 activates HFL,GLU and HAM muscles to compensate for the moment created by the swing leg. The last stance module M_5 3.20 is also active in the swing phase, it uses the length of TA to prevent ankle hyper-extension in the stance phase and to provide adequate foot clearance in the swing phase.

$$M_1 = \begin{cases} GLU & F_{GLU}G^{st}_{GLU} \\ SOL & F_{SOL}G^{st}_{SOL} \\ VAS & F_{VAS}G^{st}_{VAS} \end{cases} \tag{3.16}$$

$$M_2 = \begin{cases} HAM & F_{HAM}G^{st}_{HAM} \\ VAS & -(\frac{l_{ce,BFSH}}{l_{opt,BFSH}} - l_{off,VAS-BFSH})^{+ve}G^{st}_{BFSH-VAS} \\ BFSH & (\frac{l_{ce,BFSH}}{l_{opt,BFSH}} - l_{off,BFSH})^{+ve}G^{st}_{BFSH} \\ GAS & F_{GAS}G^{st}_{GAS} \end{cases} \tag{3.17}$$

$$M_3 = \begin{cases} HFL & ((\theta^{tgt}_{HAT} - \theta_{HAT})G^{st}_{HFL} - \dot{\theta}_{HAT}G^{st}_{HFL})^{+ve} \\ GLU & ((\theta_{HAT} - \theta^{tgt}_{HAT})G^{st}_{GLU} - \dot{\theta}_{HAT}G^{st}_{GLU})^{+ve} \\ HAM & ((\theta_{HAT} - \theta^{tgt}_{HAT})G^{st}_{GLU} - \dot{\theta}_{HAT}G^{st}_{GLU})G^{st}_{GLU-HAM} \end{cases} \tag{3.18}$$

$$M_4 = \begin{cases} HFL & G^{st}_{GLU-HFL}S_{GLU} + G^{st}_{HAM-HFL}S_{HAM} \\ GLU & G^{st}_{HFL-GLU}S_{HFL} + G^{st}_{RF-GLU}S_{RF} \\ HAM & (G^{st}_{HFL-GLU}S_{HFL} + G^{st}_{RF-GLU}S_{RF})G^{st}_{GLU-HAM} \end{cases} \tag{3.19}$$

$$M_5 = \begin{cases} Stance & (\frac{l^{ce,TA}}{l^{opt,TA}} - l_{off,TA})^{+ve}G^{st}_{TA} - F_{mtu,SOL}G^{st}_{SOL-TA} \\ Swing & (\frac{l_{ce,TA}}{l_{opt,TA}} - l_{off,TA})^{+ve}G_{l,TA} \end{cases} \tag{3.20}$$

The swing modules are M_5 to M_{10}, and the purpose of the swing phase is to provide enough ground clearance and to place the foot at the desired angle. Module M_6 3.21 works on activating the muscles HFL and GLU based on the feedback of leg angle error which can be estimated from RF and HAM muscle angles. Module M_7 3.22 activates BFSH muscle based on the velocity of RF muscle. Module M_8 3.23 stops M_7 and uses the velocity of RF, BFSH and VAS to activate BFSH and RF. Module M_9 3.24 uses the length of HAM to activate HAM, BFSH and GAS to slow down the leg. The last module M_{10} 3.25 activates HFL, GLU and VAS to extend the leg and reach the target angle α_{tgt}.

$$M_6 = \begin{cases} HFL & (\frac{l_{ce,RF}}{l_{opt,RF}} - 1 - (\alpha_{tgt} - \alpha^{sw}_{ref-RF})^{+ve} C_{RF}) G^{sw}_{l,RF-HFL} \\ & + \frac{v_{ce,RF}}{l_{opt,RF}}{}^{-ve} G^{sw}_{v,RF-HFL} \\ GLU & (\frac{l_{ce,HAM}}{l_{opt,HAM}} - (1 - (\alpha_{tgt} - \alpha^{sw}_{ref-HAM})^{+ve} C_{HAM}) G^{sw}_{HAM-GLU} \\ & + \frac{v_{ce,HAM}}{l_{opt,HAM}}{}^{-ve} G^{sw}_{v,HAM-GLU} \end{cases} \tag{3.21}$$

$$M_{7-BFSH} = -\frac{v_{ce,RF}}{l_{opt,RF}}{}^{-ve} G_{v,RF-BFSH} \tag{3.22}$$

$$M_8 = \begin{cases} BFSH & (\frac{v_{ce,BFSH}}{l_{opt,BFSH} G_{lopt,BFSH}} + \frac{v_{ce,RF}}{l_{op,RF} G_{lopt,RF}})^{+ve} * \\ & (\frac{l_{ce,RF}}{l_{opt,RF}} - \frac{(G_{lopt,RF}(\alpha_{tgt} - \alpha^{sw}_{ref-RF}) + 1)}{G_{lopt,RF}}) * \\ & \frac{v_{ce,BFSH}}{l_{opt,BFSH}} G^{sw}_{v,BFSH} \\ RF & \frac{v_{ce,VAS}}{l_{opt,VAS} G_{lopt,BFSH}}{}^{+ve} G_{v,VAS-RF} \end{cases} \tag{3.23}$$

$$M_9 = \begin{cases} HAM & (\frac{l_{ce,HAM}}{l_{opt,HAM}} - (1 - G_{lopt,HAM}(\alpha_{tgt} - \alpha^{sw}_{ref-HAM}))^{+ve} G_{l,HAM} \\ BFSH & (M_{9HAM} - S_{thr,HAM})^{+ve} G_{S,HAM-BFSH} \\ GAS & (M_{9HAM} - S_{thr,HAM})^{+ve} G_{S,HAM-GAS} \end{cases} \tag{3.24}$$

$$M_{10} = \begin{cases} HFL & \frac{l_{ce,HFL}}{l_{opt,HFL}} - (1 + (\alpha_{tgt} + \frac{\pi}{2} - \alpha^{sw}_{ref-HFL})G_{lopt,HFL})^{ve} G^{sw}_{l,HFL} \\ GLU & \frac{l_{ce,GLU}}{l_{opt,GLU}} - (1 + (\alpha_{tgt} + \frac{\pi}{2} - \alpha^{sw}_{ref-GLU})G_{lopt,GLU})^{ve} G^{sw}_{l,GLU} \\ VAS & (\frac{l_{ce,VAS}}{l_{opt,VAS}} - l_{off,VAS})G^{sw}_{l,VAS} \end{cases} \tag{3.25}$$

Due to a change in the swing reflex equations, the swing phase is additionally divided into 4 subphases namely Sw_1, Sw_2, Sw_3 and Sw_4. The first switch occurs based on the contractile element length of BFSH muscle and enters Sw_1 which causes the knee to dampen by activating M_8, the second switch depends on the contractile element length of HAM muscle and enters Sw_2 which causes the knee to decelerate by activating M_9, the third switch depends on the contractile element length of RF and enters Sw_3 which stops the M_8 reflex, and the fourth depends on the velocity of the contractile element in HAM and enters Sw_4 which causes the knee to extend again by activating M_{10}.

3.1.4 Supra-spinal control layer/ Higher control

This layer was specifically implemented in the 2015 paper [1] and it decides which leg should be performing the swing phase along with the foot placements. Using the approach from [32] and presented in 3.26 where $\alpha^{w,s}_{tgt,L}$ represents the angle that the left hip-knee-ankle line (sagittal) makes with the ground/world (horizontal plane), d^s_L and v^s_L are the position and the velocity of the COM with reference to the other ankle (right)

$$\alpha^{w,s}_{tgt,L} = \alpha^s_0 - c^s_d d^s_L - c^s_v v^s_L \tag{3.26}$$

3.2 Model Implementation

This section will explain the current implementation of the model that was done using C++ and RBDL [9], while the original model presented in [8] was created in MATLAB/Simulink. An overview of the system can be seen in Fig 3.3. The model still uses most of the equations as [1] which were explained in the previous section except for differences in the method of implementation. The differences can be summarised in software used, ground contact modelling, omittance of the neural delay and the addition of a finite state machine for gait phases. The system is able to start from an initial configuration shown in Fig 3.4 and with a starting forward velocity of 1.442 m/s.

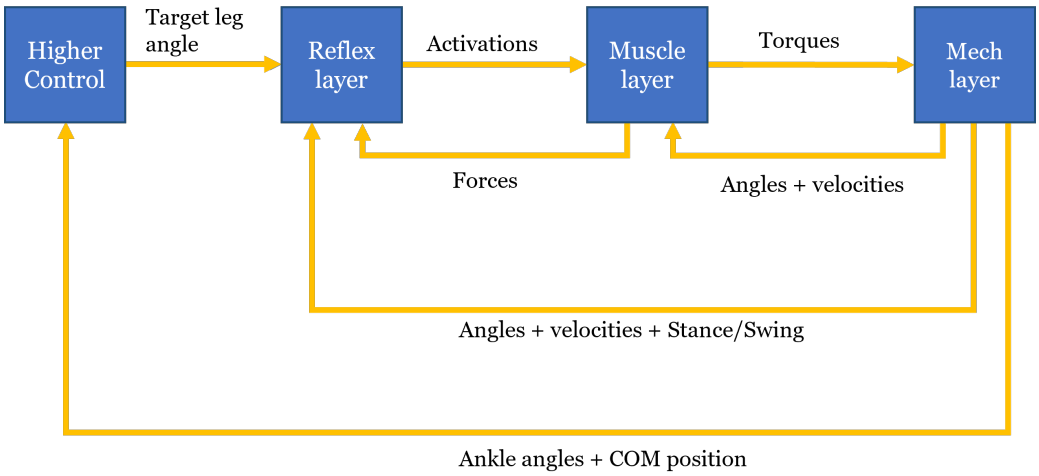

Figure 3.3: System overview

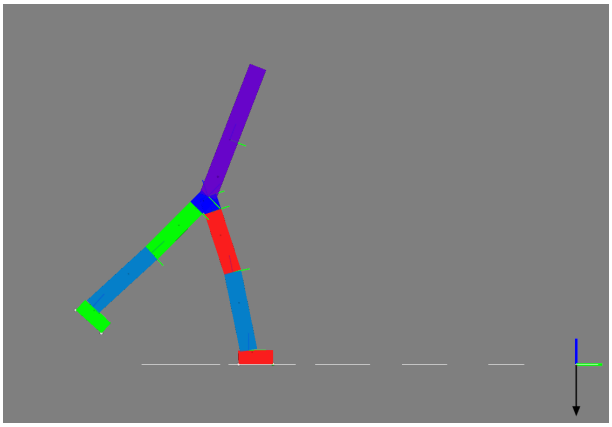

Figure 3.4: Starting configuration

3.2.1 Mechanical model

A seven-segment model was created based on the estimated human segment parameters from [1] and is available in table 3.1. This simplified model combines the Head, Arm and Trunk segments into one segment (HAT), with an attached thigh, shank and foot segment per leg. For the purpose of this work, this model shown in Fig 3.5 has been created using a LUA file to be used with a C++-based rigid body dynamics library (RBDL) [9], later for the addition of optimal control the model has been converted to a bioMod file [33].

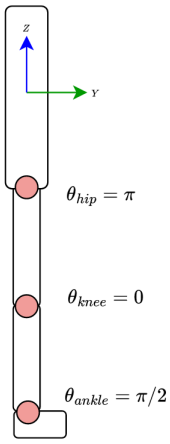

Figure 3.5: Seven-segment model

3.2.2 Ground contact modelling

In the original text [8] the foot had contact points at the toe and heel, and the ground was formulated as a spring-damper system. The resulting ground reaction force from the contact was calculated according to equation 3.27 given that $\Delta y_{cp} > 0$ and $\Delta \dot{y}*_{cp} > -1$ where k_y is the vertical contact stiffness, Δy_{cp} ground penetration, and $\Delta \dot{y}*_{cp}$ is the velocity normalized to v_{max}. The change in this modelling method compared to what was implemented in our model is what we assume caused the difference in behaviour upon the first contact engaging.

$$F_y = k_y \Delta y_{cp}(1 + \Delta \dot{y}*_{cp}) \tag{3.27}$$

In our implementation, two contact points on each foot were selected, one on the heel and the other toe as seen in Fig 3.6. The model starts from a set state that follows the same start as the referenced model, with the left foot (Red) fully in contact as seen in Fig

3.4. The type of contact used in the model is a constraint-based rigid contact model with fully inelastic impacts. This type of contact constraint is implemented on the acceleration level and works by maintaining the acceleration of the contact point at zero.

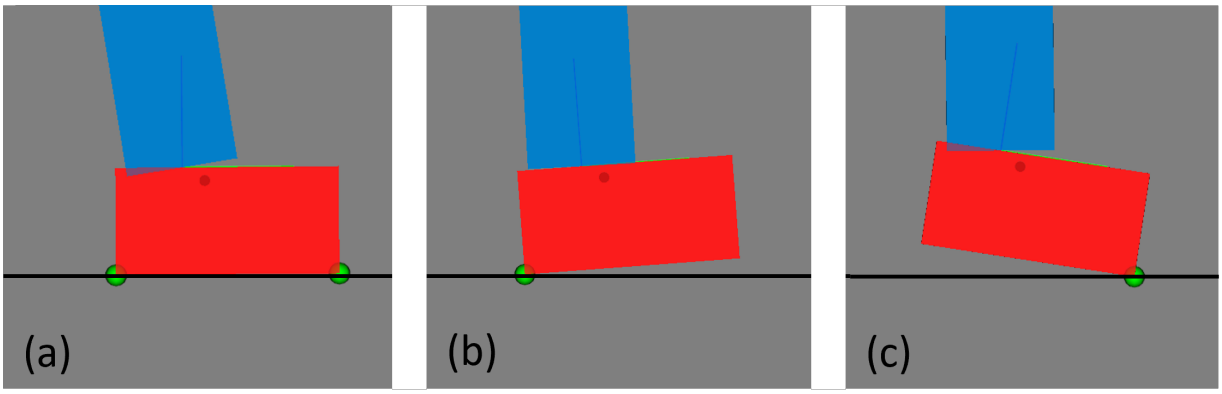

Figure 3.6: Foot contact points, (a) representing heel only contact, (b) heel and toe contact, (c) toe only contact.

Similar to [23], the equations of motion of the system can be expressed as in Eq 3.28, where M represents the mass/inertia matrix, G is the Jacobian matrix, γ is the corresponding hessian matrix, N the non-linear effects and F external forces (gravity, joint torques u, etc.) the λ is the Lagrangian multiplier, which is equivalent to the contact force caused by the constraints.

$$\begin{pmatrix} M(q,p) & -G(q,p)^T \\ G(q,p) & 0 \end{pmatrix} \begin{pmatrix} \ddot{q} \\ \lambda \end{pmatrix} = \begin{pmatrix} N(q,\dot{q}) + F(q,v,p,u) \\ \gamma(q,v,p) \end{pmatrix} \tag{3.28}$$

The constraint is unilateral and hence only disengages when the foot is about to pull away from the floor instead of pushing on it, which can be detected from a switch of signs in the contact forces present in the Lagrangian term λ of the dynamics equation of the model 3.28, Fig 3.7 shows the contact forces in the vertical direction in the first step of the motion, where it starts with the two points of the left foot in contact for less than 0.05 seconds denoted by the two lines. The starting value for the forces is quite low (around 100 N) which is only around 12.5% of the total model weight. The dip in the forces around t=0.05s does not happen in the natural human ground reaction forces measured when walking, this part is due to the model used. It occurs in the implemented model when the stance knee (left) reaches full extension activating the over-extension torque model,

this same spike can be seen in the torque in Fig 4.12. The force then shows a decrease around t=0.3s which corresponds to the midstance phase. The following shift in phases occurs when heel contact is released, then left toe force increases as the right leg swings forward, the spike seen at 0.6 seconds in the left toe force occurs when the right leg makes ground contact. Then the toe force decreases gradually until reaching zero, which is when the switch is detected right before a switch of signs for the forces occurs.

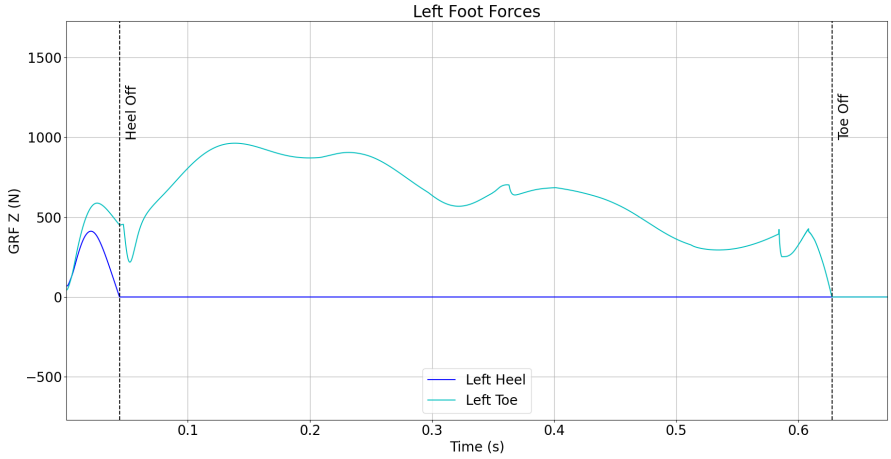

Figure 3.7: Left foot vertical ground reaction forces distributed on heel and toe contact points to show a decrease of forces to zero before constraints disengage

The constraints come into effect when the contact points' height reaches zero, also detected by a switch of signs in the kinematics of the system. The zero height implies the foot has hit the floor, causing the contact constraint to engage and since this is an inelastic contact it creates an impact. Upon the addition of a contact point, the dynamics equation changes and the velocities after the impact need to be recomputed to maintain the constraints and handle the discontinuity between the previous velocities and the next. The velocities after the impact can be computed through 3.29 where M represents the mass/inertia matrix, G represents the Jacobian, v_- is the velocity before the impact and v_+ is the velocity after the impact.

$$\begin{pmatrix} M(q,p) & G(q,p)^T \\ G(q,p) & 0 \end{pmatrix} \begin{pmatrix} v_+ \\ \Lambda \end{pmatrix} = \begin{pmatrix} M(q,p)v_- \\ \gamma(q,v,p) \end{pmatrix} \tag{3.29}$$

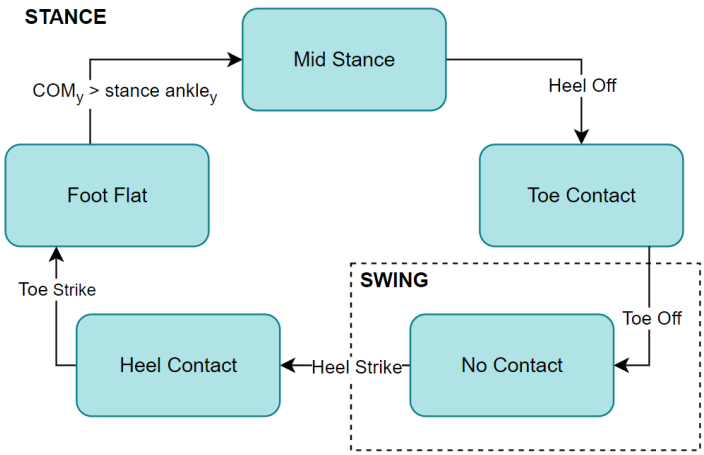

Figure 3.8: Finite state machine diagram

3.2.3 Finite state machine

Another key difference in the implemented model was in the switching between the different phases of the motion. The system was not left free to decide the swing and stance legs based on foot position like in [1] explained in subsection 3.1.4 instead, the system was forced into a finite state machine (FSM) that represented all the walking phases for each foot shown in Fig 3.8.

The first point of contact comes when the heel of the foot strikes the ground and the system enters the Heel Contact phase, the next transition comes from the toe striking the ground and entering the Foot Flat phase. The next phase Mid stance depends on the location of the total Centre of mass (COM) of the body, it has to cross the location of the stance ankle joint to move on to the lift-off of the heel which leaves only Toe Contact ending with the last phase where there is no contact and the leg is in the swing phase.

3.2.4 Simulation

The mechanical system was created using a BioMod file [33], the file contained all the technical parameters such as mass, inertia matrices and the model tree. The reflex-muscle layers were written purely using C++. The entire system was solved using RBDL [9] for forward dynamics and integrated through the implementation of the classic Runge-kutta method and then visualized in BioViz [34].

3.3 Results and discussion

In order to verify the results, initially the motion was played on BioViz visualizer [34] created for Biorbd [33] to visually verify that the model is able to walk continuously. The total simulation time tested was 6 seconds and the model was successfully able to walk without falling as seen in Fig. 3.9

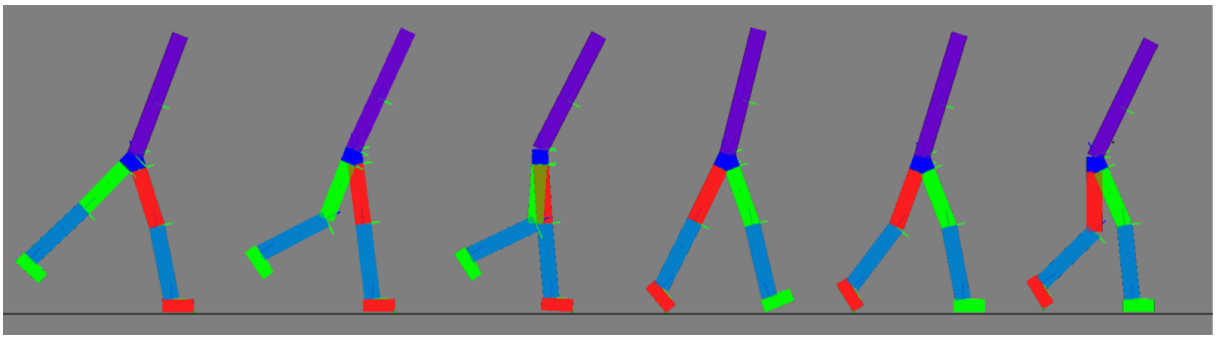

Figure 3.9: Resulting step motion

3.3.1 Switching data

After confirming that the model runs, the phase switching sequence was collected and compared against the referenced model from [1]. It can be seen in Fig 3.10 that both models successfully switch between the stance and swing phases. However, the implemented model only switches phases according to the FSM explained in 3.2.3 while the reference model does not have the same restriction and switches back and forth between the phases around $t = 1.3s$ in Fig 3.11 This could be due to the modelling of the ground reaction force that has an added elasticity.

Another point of comparison between the models is the variation in stride time, which is represented in Fig 3.12. It was calculated through 10 seconds of motion in both models. This resulted in the reference model taking 7 steps and the implemented model taking 9 steps. In the first 7 steps of both models, the standard deviation in stride time was calculated, which shows that there is a greater variation of stride time in the implemented model of approximately 19 ms vs only 9 ms in the referenced model.

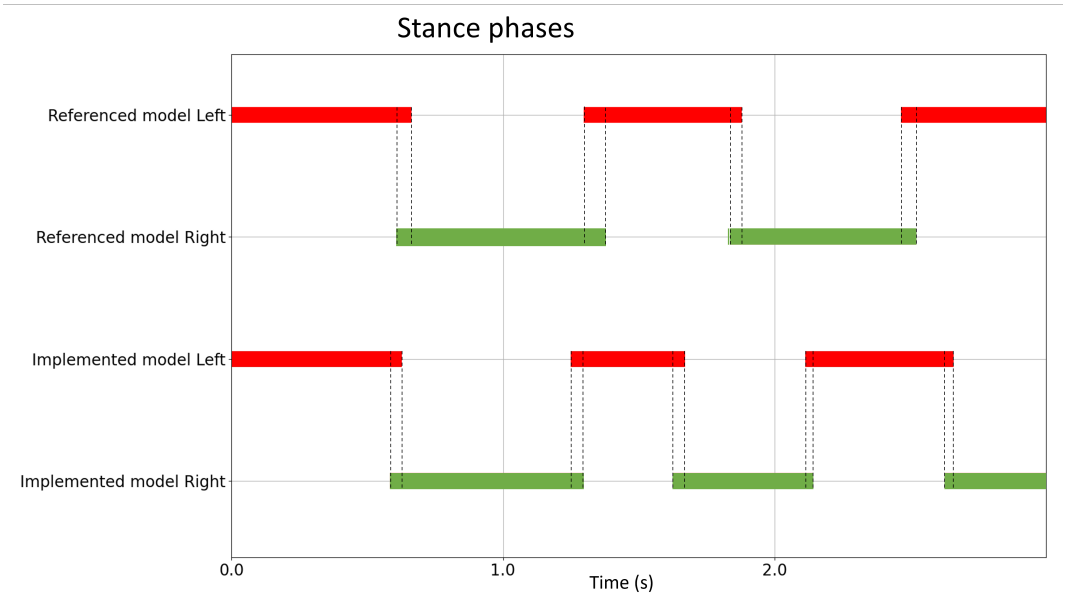

Figure 3.10: Stance of both legs in the referenced and the implemented mode, dashed line represents double support time

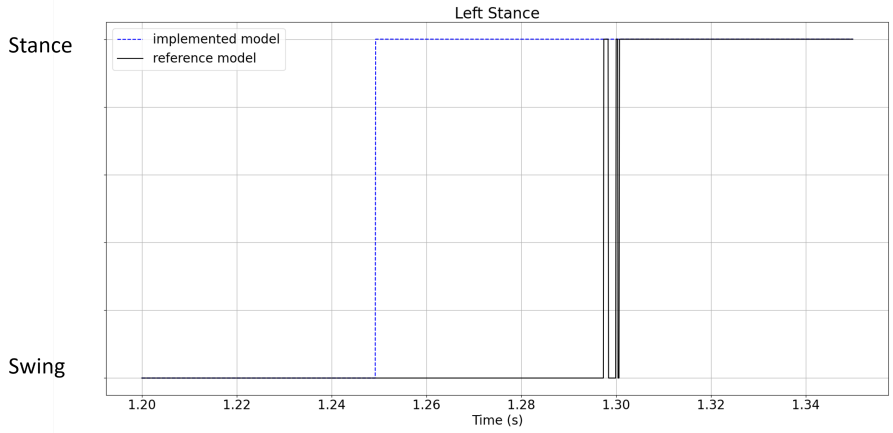

Figure 3.11: Left leg switching between stance and swing

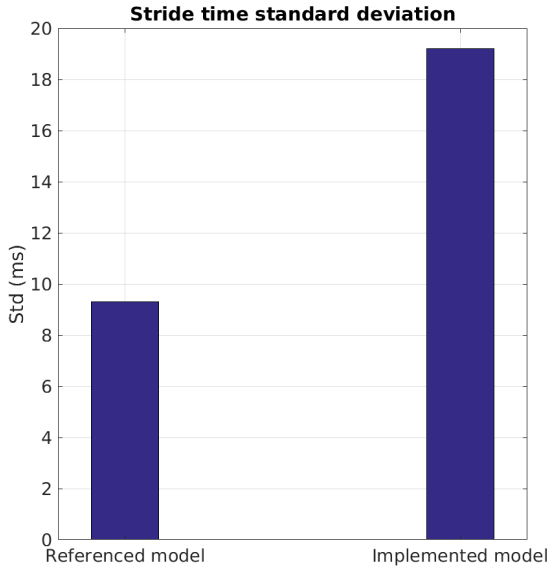

Figure 3.12: Stride time standard deviation

3.3.2 Joint angle data

Next, the joint angle data were extracted and compared against the results of the original model from [1] for a simulation time of 3 seconds which can be seen in Fig 4.7.

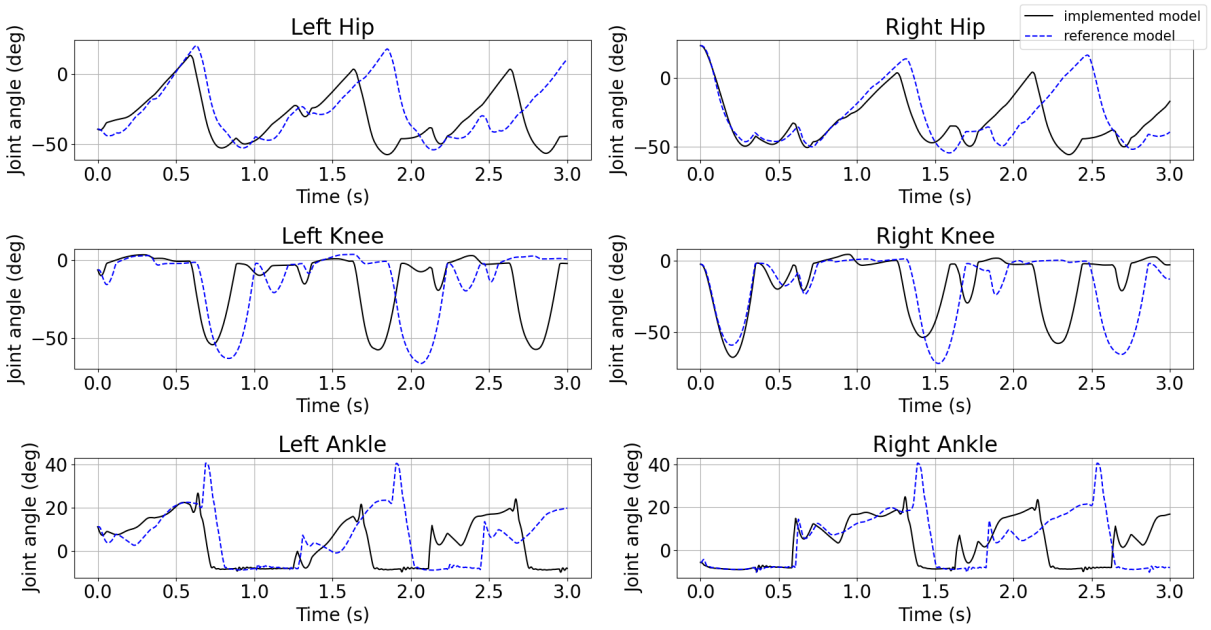

Figure 3.13: Comparison of joint angles of the reference model [1] against implemented model for 3 seconds. The referenced zero angle corresponds the standing straight configuration with maximum hip and knee extension and a 90 °ankle

The implemented model starts from the same position as the reference model, and should theoretically follow the exact trajectories. However, as can be seen in the plots, there are deviations in amplitude and timing. The deviations in timing are assumed to have happened due to the different switching methods implemented as FSM and due to the omittance of the neural delays implemented in [1]. The amplitudes for the ankle specifically seem to be lower in the implemented model where it is less than 30 °while the referenced model reaches 40 °, this is probably due to the difference in ground contact modelling where the reference model allowed the foot to go through the floor with a spring-like effect and the implemented model used an inelastic impact to represent the ground contact. The same reason might have affected the other joints as well, especially given that the greatest effect is seen in the ankle which is the closest to the ground and the effect of impact would be felt most at the ankle joint and decreases as you go back up to the knee and hip.

3.3.3 Joint torques data

The joint torques from the model were collected and compared visually against those of the referenced model in Fig 3.14. The joint torques show more difference against the referenced model. For the left knee in the implemented model, the torques show more spikes than in the referenced model. The first spike at $t = 0.8s$ is due to the activation of the torques that are applied to prevent the over-extension of the knee, they become active when the knee angle crosses the set threshold of 174 °extension The same over-extension prevention torque is activated at different times which causes the spikes in both the implemented and the referenced model. The second spike at $t = 1.3s$ happens at the left foot contact and could be due to the impact that occurs at that point in time. In case of the right knee, the spike occurring at $t = 1.6s$ happens when the left foot loses contact and all the weight is held by the right leg. The ankles also seem to show higher torques, in the right ankle there is a spike starting from $t = 0.65s$ which is at the point the right heel makes contact with the ground. The negative spikes in all torques are a result of an implemented over-extension prevention torque that is activated when the angle limits for the specific joints are reached.

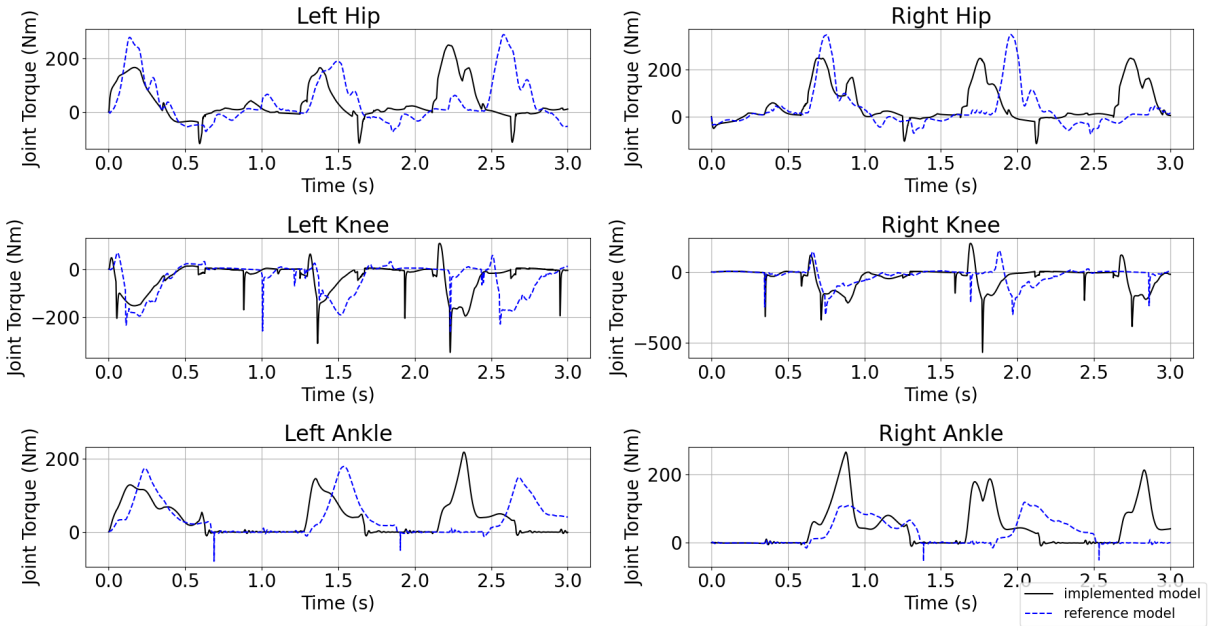

Figure 3.14: Comparison of joint torques of reference model [1] against the implemented model for 3 seconds

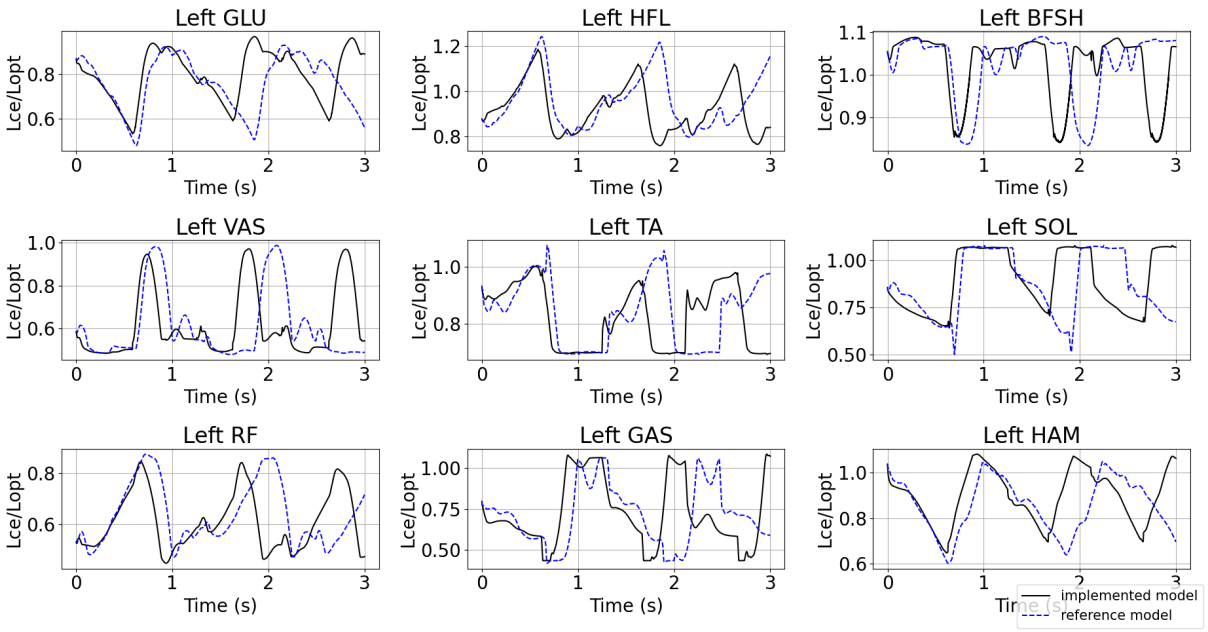

Figure 3.15: Left leg muscle contractile element lengths L_{ce} normalized against muscle optimum length L_{opt} which is when the muscle produces its maximum force, comparing the reference model [1] against the implemented model for 3 seconds.

3.3.4 Muscle length data

Another level of comparison was done on a lower level of the system, in the muscle subsystem. The main state of concern here was the muscle contractile length because it directly affects the muscle forces and consequently the behaviour of the entire system.

It can be seen in Fig 3.15 that the implemented model muscle lengths L_{ce} follow those of the referenced model closely although slightly delayed later. It should be noted that the Soleus muscle (SOL) seems to have significantly less drastic changes or spikes in the implemented model when compared to the referenced one. It is also evident in the graphs that the Tibalius Anterior muscle (TA) has smaller spikes as well. Overall, the graphs show that most of the muscle lengths are lower in the implemented model. And any clear difference between the models happens on the rigid body dynamics level such as the joint torques and angles.

Chapter 4

Optimal Control Problem

This chapter explains the walking problem from an optimal control point of view, the aim of this is to create a setup for use with the reflex model explained in chapter 3. The method taken is starting from a simplified purely mechanical model and then adds complexity in the form of muscles and at the end adds the reflex layer from [1] with the goal of using minimum control variables to affect the way the motion is executed, whether it be step length or speed.

4.1 Mechanical Walking Formulation

Walking is considered a multi-phase motion, which means the dynamics of the system change in each phase based on the contact points. The phases are shown in Fig 4.1, in the current implementation there are two contact points at each foot, one at the heel and the other at the toe. The phase transition occurring between the phases is marked by arrows that indicate either a takeoff or a strike. In the case of a strike or impact motion, this causes a discontinuity between the phases and results in the addition of transition phases to handle the discontinuities. The dynamics of the system are represented in the seven-segment model described in the previous chapter, the model contains seven segments: combined head, torso and arms (HAT), thigh, shank and foot segment. The degrees of freedom of the model comes from the joints: hip, knee and ankle rotations about the x-axis as seen in Fig 4.2.

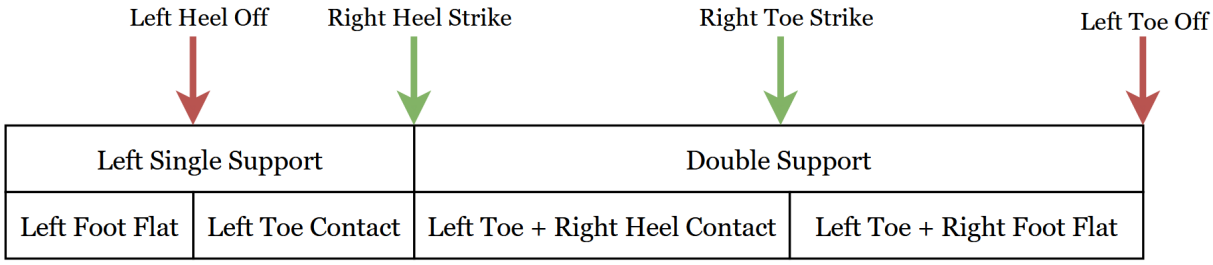

Figure 4.1: Single-step phases of motion, starting from the left foot flat on the ground

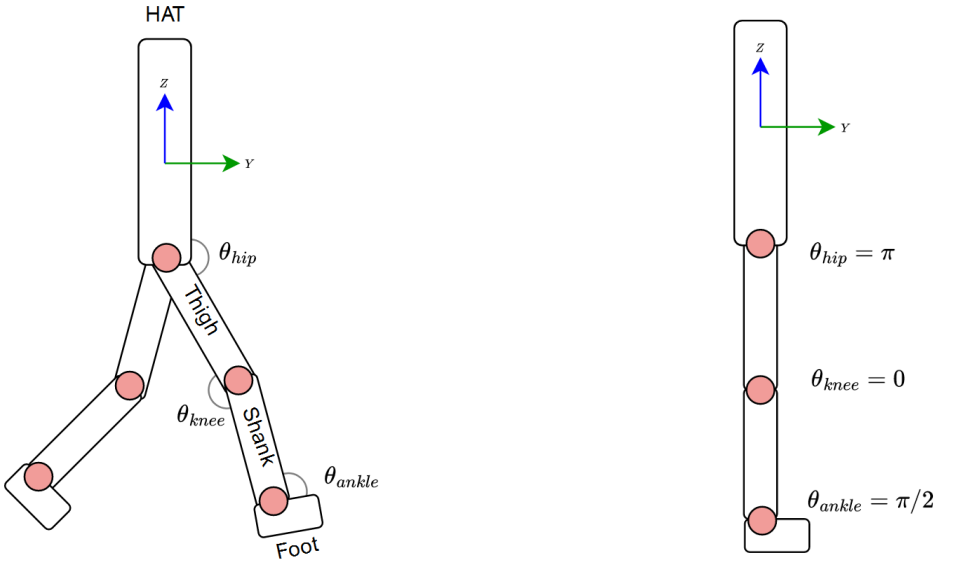

(a) Model degrees of freedom

(b) Standing straight configuration

Figure 4.2: Seven-segment model

$$x(t) = [q(t), \dot{q}(t)] \tag{4.1}$$

In the case of the simplified model, the reflexes and muscles are not considered. Instead, the model is purely mechanical walking with the states being the generalized angles q which include the base degrees of freedom along with the joints' degree of freedom, velocities $\dot{q}$.

The states are bounded by the bounds in Table 4.1 and the problem is subject to the objective function in Eq 4.2 which minimizes torque squared through the motion.

Minimum	Variable	Maximum
0	q_{hip}	2π
0	q_{knee}	π
-2.22	q_{ankle}	-1.22
-30	$\dot{q_{hip}}$	30
-30	$\dot{q_{knee}}$	30
-30	$\dot{q_{ankle}}$	30
-200	τ	200

Table 4.1: States and controls bounds for mechanical walking

$$\min \int_{t_o}^{T} \sum_{j=0}^{nDof} W_j \tau_j^2 \quad dt \tag{4.2}$$

The problem starts from a fixed initial global position in the forward-backward (Y) direction and free angles q and $\dot{q}$ with an initial constraint of the left foot in the foot-flat phase; with both heel and toe in contact and constrained to a linear velocity of zero. The contact constraints in the system maintain the position of both heel and toe contact points by constraining the acceleration at the contact points to zero.

The constraints on the system along with the phases are shown in Fig 4.3. The arrows represent the points where switching occurs.

The first phase of motion is the foot-flat phase of the left foot, the constraints maintain the starting point to have zero height and velocity at both contact points of the left foot. The first phase ends when the ground reaction force (GRF) at the left heel reaches zero ($Fz_{heel} = 0$), then the contact constraint releases and we enter the second phase which only constrains the left toe to the ground. The third phase starts once the right heel touches the ground, reaching a height of zero ($Hz_{heel} = 0$) and activating the right heel contact constraint for the following phase. The fourth phase ends with the transition of the right foot from heel contact to a foot-flat with the height of the right toe going to zero ($Hz_{toe} = 0$) and activating the right toe constraint. The final phase ends when the left foot toe GRF reaches a zero value resulting in the loss of contact ($Fz_{toe} = 0$). The motion is considered cyclic for both legs and thus only modelled for a single step taken by the right foot, with a periodicity constraint that flips the leg joint angles at the endpoint.

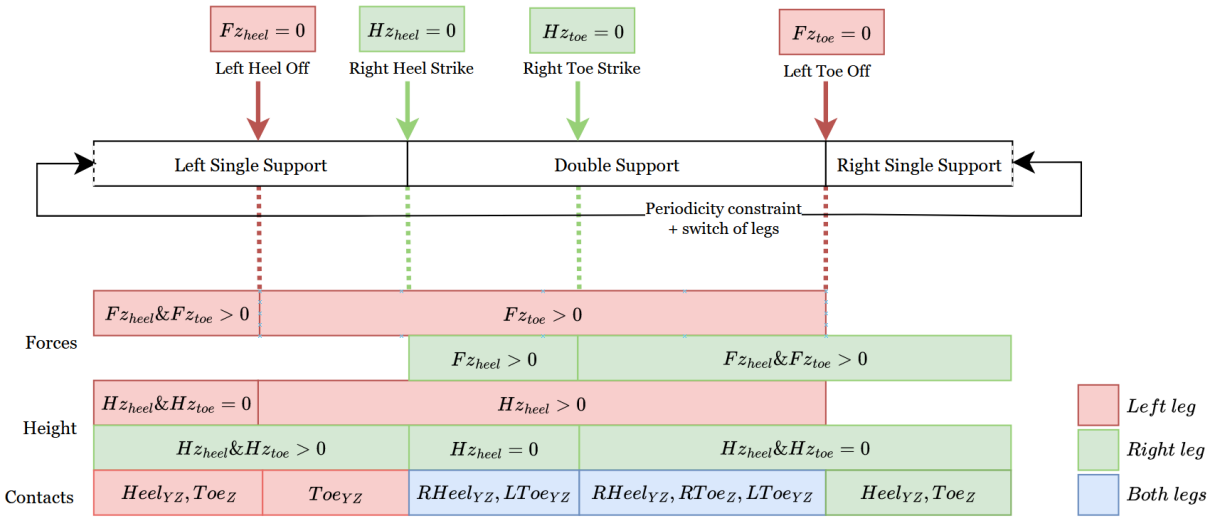

Figure 4.3: Optimal control phases for a single step. The arrows represent the switching points, with the required condition. The final switch occurs at the end of the step and guarantees periodicity in the states between the end and start points of the motion

4.2 Muscle-Based Walking Formulation

The problem considers the states in Eq 4.3 to be the generalized angles q which include the base degrees of freedom along with the joints' degrees of freedom, velocities $\dot{q}$ and muscle contractile element lengths l_{ce}

$$x(t) = [q(t), \dot{q}(t), l_{ce}(t)] \tag{4.3}$$

$$u(t) = Act(t) \tag{4.4}$$

Additional constraints are imposed on the states, specifically the contractile element length L_{ce} they are implemented as equality constraints at the starting node, the constraints can be expanded into the two equations 4.5 for the hip joint and 4.6 for the knee and ankle joints.

$$l_{ce} - l_{opt} - \rho r(q - q_{ref}) = 0 \tag{4.5}$$

$$l_{ce} - l_{opt} - \rho r[sin(q - q_{max}) - sin(q_{ref} - q_{max})] = 0 \tag{4.6}$$

The optimal control problem is further constrained by the inequality constraints imposed by the bounds on the states found in table 4.2

Minimum	Variable	Maximum
0	q_{hip}	2π
0	q_{knee}	π
-2.22	q_{ankle}	-1.22
-30	$\dot{q_{hip}}$	30
-30	$\dot{q_{knee}}$	30
-30	$\dot{q_{ankle}}$	30
0.001	lce	0.2
0.01	act	1

Table 4.2: States and controls bounds for muscle based walking

The cost function Eq 4.7 was implemented in the optimal control program to minimize the individual muscle activation to minimize the overall effort of the human through the walking task.

$$min \int_{t_o}^{T} \sum_{m=0}^{n} Act_m^2 \tag{4.7}$$

4.3 Neuro-muscular Based Walking Formulation

This section follows the additions of the reflex modules M_1 to M_{10} previously explained in subsection 3.1.3, The muscle stimulations are calculated based on equations 4.9 that were explained in more detail in the previous chapter, where the inputs were the muscle lengths l_{ce}, muscle velocities $\dot{l_{ce}}$, joint angles q, joint velocities $\dot{q}$ and activations Act. The stimulations are in turn used to calculate $\dot{Act}$ through Eq 4.10 where $Act(t)$ is the input activation and τ_d is a time constant representing a chosen delay in milliseconds.

$$x(t) = [q(t), \dot{q}(t), l_{ce}(t)] \tag{4.8}$$

$$Stim = f(L_{ce}, \dot{L_{ce}}, q, \dot{q}, Act) \tag{4.9}$$

$$\dot{Act}(t) = \frac{Stim(t) - Act(t)}{\tau_d} \tag{4.10}$$

$$u(t) = [\alpha_{tgt}^{right}, \alpha_{tgt}^{left}] \tag{4.11}$$

The controls Eq 4.11 in this implementation would replace the higher level control level in 3.1.4, changing the system proposed to look like Fig 4.4. The controls are the sagittal target leg angles, which is the angle the hip-knee-ankle line makes with the horizontal plane upon ground contact.

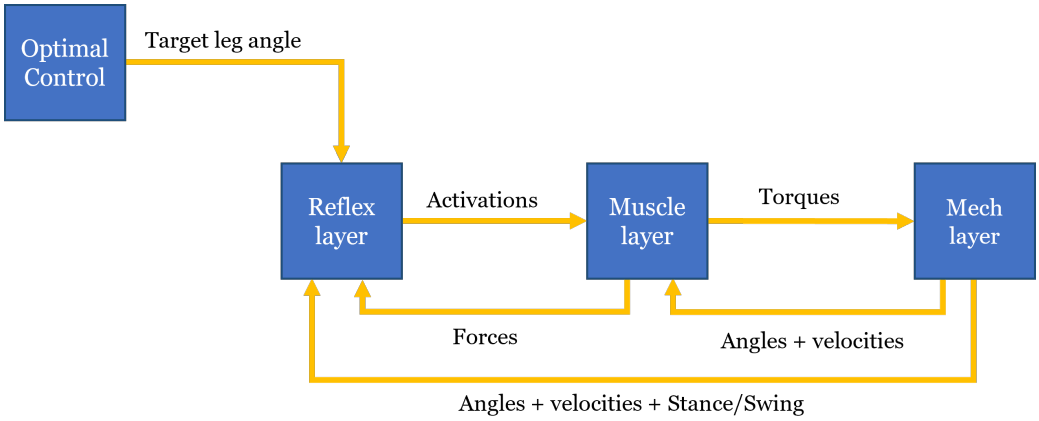

Figure 4.4: The neuro-muscular system with optimal control

Based on the input activations Act and the current angles q, the forces F_{mtu} and moment arms R of each muscle are calculated. Using Eq 4.12 the total torque τ at each joint is subsequently calculated.

$$\tau_{joint} = \sum F_{mtu} R \tag{4.12}$$

The torque is used by the forward dynamics to calculate the generalized accelerations according to the system dynamics at that phase.

Lastly, the $\dot{L_{ce}}$ which represents the velocity of the contractile element is calculated from the states and is used in the next time step to calculate l_{ce}.

$$\dot{L_{ce}} = f(L_{ce}, Act) \tag{4.13}$$

4.4 Implementation

The optimization was performed on the problems described in the previous sections through the software package MUSCOD-II [12]. Initially, the optimization problem was tested with several other software packages, RBDL-Casadi, Biorbd-Casadi and Bioptim. Each library

used had a few limitations, but the critical limitation would appear in the addition of the muscle system complexity that resulted in incompatibility errors. All the previous libraries were based on symbolic variables and used automatic differentiation, however, MUSCOD-II uses solves numerically so it was chosen to reduce the errors seen with the other libraries. Only the mechanical walking problem was able to generate results. Run-time problems were faced with the muscle-based walking problem. The reflex-based walking problem was never attempted.

4.5 Mechanical Walking Results

The mechanical walking implemented used the dynamics of the mechanical model explained in 3.2.1 and the constraints and phases described in 4.1. This was tested with two objective functions and the results will be discussed in the following section. The problem was divided into seven phases, two of which were instantaneous transition phases. The first phase started with left foot-flat (2-point contact), the second phase was left heel-only contact, the third phase was a transition phase that introduced right heel contact, and the fourth phase was left-toe contact and right heel contact. The fifth phase was a transition phase to introduce right-toe contact. The sixth phase was left-toe contact and right foot-flat. The last phase was only right foot-flat contact.

Each phase was given 20 shooting nodes with the exception of the transition phases and the time was left free for all the phases.

Minimization of torque

The optimization converged after about 260 iterations, taking approximately 4.5 hours to solve. The motion steps/phases can be seen in Fig 4.5. The time taken to execute the motion is 0.73 seconds. The resulting time for each step can be seen in Table 4.3.

Phase	Time (s)
Left foot flat	0.5
Left toe only contact	0.100084
Right heel contact + left toe contact	0.01
Right foot flat + left toe contact	0.1192
Right foot flat	0.02468

Table 4.3: Selected time for each phase of motion

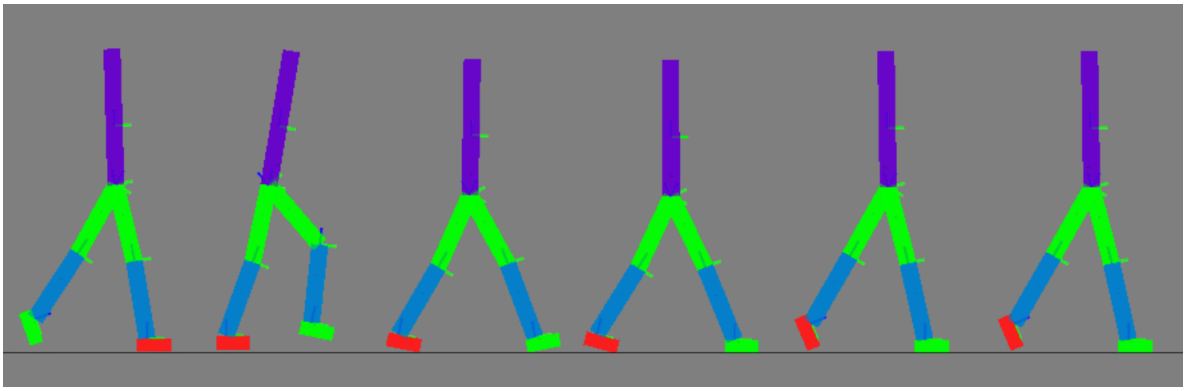

Figure 4.5: Steps of motion for torque minimization objective function

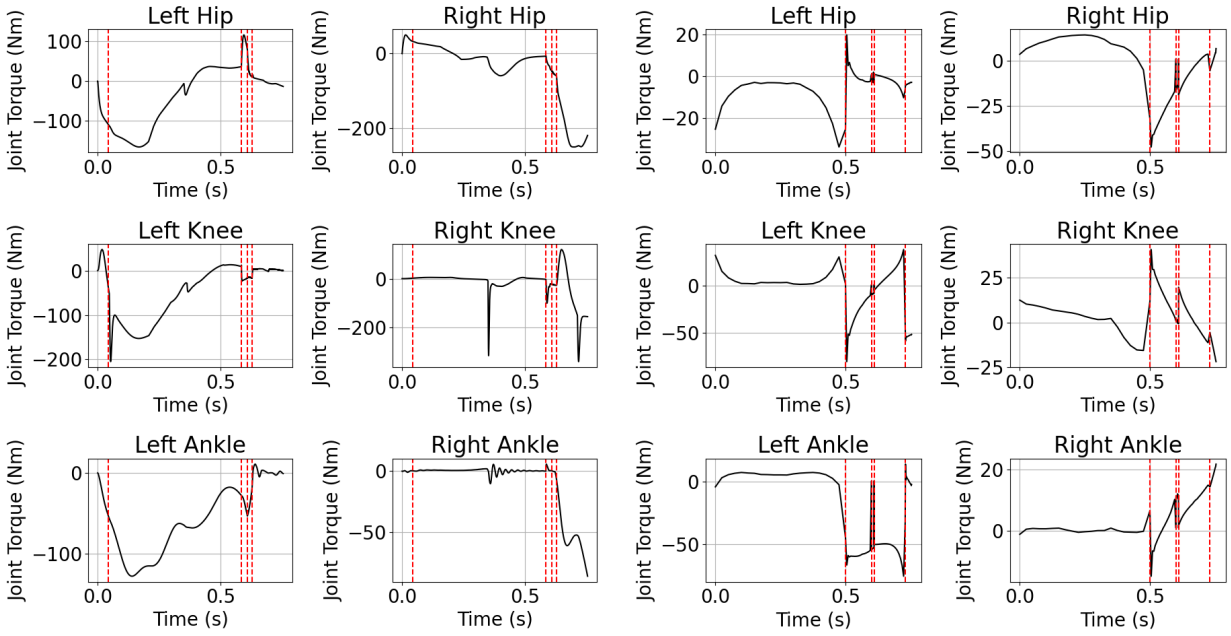

(a) Torques from chapter 3

(b) OCP resulting torque profile

Figure 4.6: Comparison of torque profiles of a single step from the implemented model shown in (a) and the optimal control formulation of torque minimization (b). The dashed lines separate the different phases of the motion. The first dashed line represents the heel-off of the left foot. The second dashed line represents the heel strike of the right foot. The third dashed line represents the toe strike of the right foot. The last dashed line represents the toe-off of the left foot.

The resulting torque profile is seen in Fig 4.6b, the overall torques were significantly lower than the torques seen in the implemented model from the previous chapter in Fig 4.6a. The maximum torque seen in the motion is in the left knee at the point of the contact switch from a foot flat to only toe contact [t = 0.5]. The other higher torque seen in the motion is at the left ankle also at transition points of foot-flat to toe-contact and then near the end when toe-off happens [t=0.73].

The resulting joint angles are seen in Fig 4.7, the motions generated satisfy the objective function and constraints given although some jumps exist in the left knee and right ankle joints. These jumps occur at the point of heel-strike of the right foot which is expected since that is an impact. When compared to the results from the earlier implemented model in chapter 3, a big difference can be noted in the right ankle motion, where in the optimal control solution the ankle oscillates more, presumably to create the driving force to swing forwards. The starting point for both models is not the same since in the optimal control solution the optimizer was left to decide its own preferred starting position to ensure cyclic motion.

The motion starts with the left foot fully in contact and the right hip swings to propel the leg forward as seen in the right hip graph, after reaching maximum flexion the hip extends to allow the right foot to strike the ground at the third phase. The motion is quite smooth up to this point in all the other joints as well. The hip and knee motions are close to the regular human gait referenced in Chapter 2

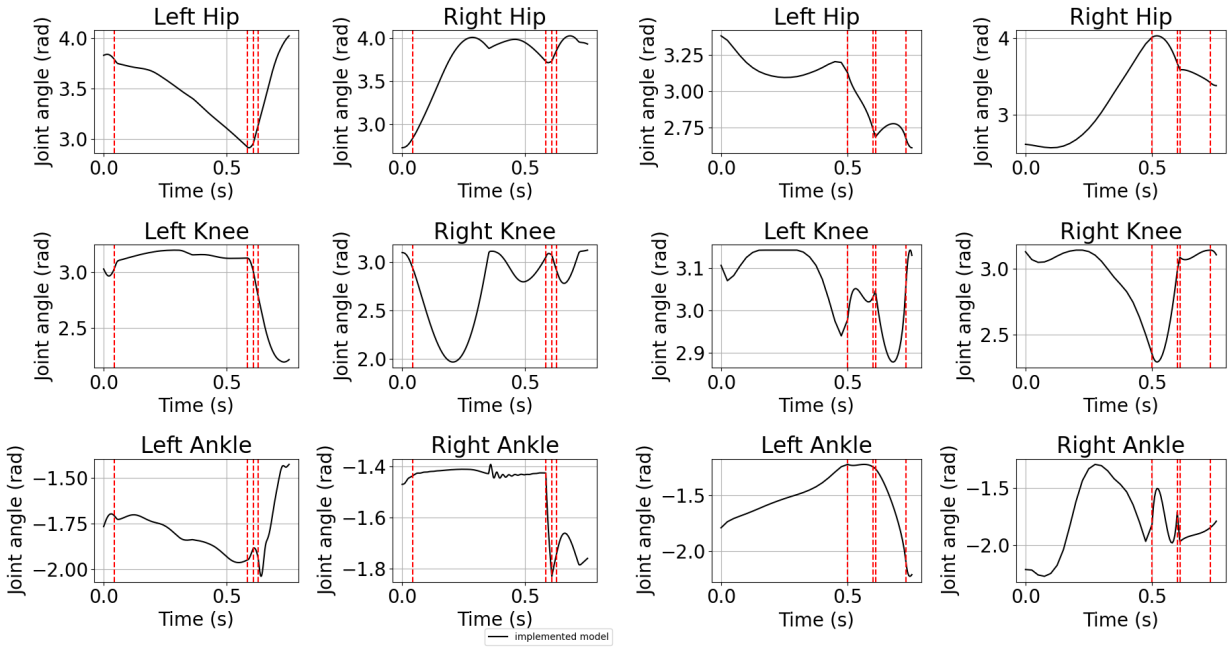

(a) Joint angles from chapter 3

(b) Joint angles based on torque minimization

Figure 4.7: Resulting angles of a single step from the implemented model shown in (a) and the optimal control formulation of torque minimization (b)

Overall, the results of the torque minimization objective function show greater promise since they are closer to normal human motion during gait. The objective function of torque minimization was just used to test the formulation and explore the results. The next steps would be to make the muscle-based walking formulation work with the objective function of muscle activation minimization.

Part II

Experimental Work

Chapter 5

Lower Limb Exoskeletons to Assist Walking

5.1 Overview of Current Technology

An exoskeleton is a robotic device that is worn by the user and acts on the user's joints to control/move them in a human-like manner. In this thesis we will be looking more closely at full lower-limb exoskeletons, acting mainly on the hip, knee and ankle joints.

Summarized in table 5.1, a review of the currently available technology in lower-limb exoskeletons was performed based on [35][36] and specific papers for the design of the exoskeletons [37] [38] [39] [40] . The key points looked at were the degrees of freedom and the use of crutches. Many of the common exoskeletons used to date have actuation in the sagittal plane which is represented by the hip flexion/extension **HFE**, knee flexion/extension **KFE** and ankle dorsi and plantar flexion **ADP**. Additional degrees of freedom added depend on the exoskeleton design and are represented as follows: hip adduction/abduction **HAA**, hip inversion/eversion **HIE** and ankle inversion/eversion.

The most commonly used lower-limb exoskeletons, which are also Food and drug administration (FDA) approved are the ReWalk™, Ekso™ and Indego®.

The ReWalk™ [41] exoskeleton is a lower-limb wearable device created to provide powered assistance to the hip and knee joints to help spinal cord injury patients walk, sit and stand. It was intended to provide improved mobility and posture support to decrease detrimental health effects such as muscular atrophy, etc. The device provided the hip range of motion: 34°of extension and 104°of flexion, for the knee joint it was 110°of flexion and

Exoskeleton name	Actuated DOFs	Weight (kg)	Crutches
TWIN	HFE, KFE	25	Yes
UGO	HFE, KFE	-	Yes
HEXO	HFE, KFE	25	No
MindWalker	HAA, HFE, KFE	30	Yes
ATLAS (children)	HFE, KFE	14	-
Vanderbilt Indego	HFE, KFE	12	Yes
ReWalk	HFE, KFE	23.1	Yes
Ekso	HFE, KFE	23	Yes
REX	HFE, HAA, KFE, ADP, AIE	38.1	No
HAL	HFE, KFE	23	No
Robin	HFE, KFE	-	Yes
Mina V2	HFE, KFE, ADP	32	Yes
WPAL	HAA, HFE, HEE	13	No
Symbitron	HAA, HFE, KFE, ADP	37.2	-
Atalante	HFE, HAA, HIE, KFE, ADP, AIE	59	Yes
Phoenix	HFE, HAA	12.25	Yes
H3	HFE, KFE, ADP	17	Yes

Table 5.1: Overview of lower-limb exoskeletons with their degrees of freedom

2°of extension. The device was intended for use in the home or healthcare facility settings and required to be used with crutches.

Ekso™ [42] exoskeleton is designed to provide powered hip and knee support to individuals with lower extremity weakness or paralysis caused by SCI, stroke etc. It is intended for use under the supervision of a physical therapist. Like the ReWalk™, it is able to sit, stand, walk and turn with the help of crutches. The device actuated the hip and knee joints with 20°of extension and 135°of flexion, for the knee joint it was 130°of flexion and 0°of extension and passive ankle joint 10°flexion and 10°extension.

The Indego®[43] exoskeleton was also designed to help individuals with SCI, powered in the hip and knee joints with range of motion of 110°flexion to 30°extension in the hip and 110°flexion to 10°extension in the knee joint. Similarly, it is used with crutches, walkers or canes.

An exoskeleton worth mentioning is the REX exoskeleton created by REX Bionics, it is the world's first self-balancing exoskeleton containing 5 degrees of freedom per leg, two in the hip, two in the ankle and one in the knee. It does not require any crutches for the

usage however it is bulky and weighs around 38 kg [44]

The UGO exoskeleton was developed by RoboCT for SCI, stroke patients or people with other nervous system diseases. The newest version UGO 220 comes with two actuated degrees of freedom hip and knee extension and flexion and passive ankle dorsi/plantar flexion and is used with crutches. It estimates the intent of the user based on the combined center of pressure measured [45].

The Mindwalker exoskeleton [46] has 3 degrees of freedom per leg consisting of hip adduction/abduction, flexion/extension and knee flexion/extension. The hip internal/external rotation and ankle plantar/dorsi flexion are passive degrees of freedom and are spring-loaded. It does not require crutches for usage with healthy individuals but crutches or walking rails have to be used for paraplegic people. The control of the exoskeleton is implemented through the use of a finite-state machine consisting of 9 states: S1: stand, S2: assisted weight shift to left, S3: half step right swing, S4: full step right swing, S5: double stance right foot leading, S6: assisted weight shift to right, S7: half step left swing, S8: full step left swing, S9: double stance left foot leading. For the standing states (S1, S5, S9) a reference trajectory is used such that the person is standing straight. For the weight shifting phases (S2, S6) the joint angles are generated by interpolation between the double stance phases and the beginning of swing phases. For swing phases (S3, S4, S7) the joint angles are based on the gait of a healthy individual wearing the exoskeleton in zero-torque mode.

The Mina V2 Exoskeleton [47] built by Florida Institute for Human and Machine Cognition works with three degrees of freedom that act on the hip, knee and ankle in the sagittal plane. Like many other sagittal exoskeletons, it relies on the user to balance themselves using the crutches. For the original Mina [48] exoskeleton the walking trajectories used were based on recording the walk of a healthy person wearing the exoskeleton and the trajectories were modified and played back in assistive mode.

The Symbitron exoskeleton [49] has 4 degrees of freedom per leg: hip abduction/adduction, hip flexion/extension, knee flexion/extension and ankle plantar/dorsi flexion . All the actuated joints are powered with a rotary series elastic actuator. For incomplete SCI pilots, the exoskeleton uses a neuro-muscular controller (NMC) based on the 2D model of reflex-based walking developed in [8] and its 3D extension in [1]. The controller uses joint angles and foot contacts to drive the device using joint torques. For complete SCI pilots, the NMC was combined with a trajectory controller based on the algorithm in the speed-dependent trajectory generation method in [50].

5.2 Overview of Exoskeleton Control

The general control of lower limb exoskeletons involves several layers, ranging from user intent estimation in the highest layer to direct low-level motor control in the lowest one. Our main concern in this thesis is a mid-level layer that determines the gait phase and the needed trajectory that the exoskeleton will follow to perform the next move.

In [51], the mid-level controller is defined as the layer determining the continuous behaviour of the robot by computing joint angles or torques with each time step of the motion. The proposed classification in [51] divides the mid-level controller into two levels as shown in [51, Fig 5.1]. The first is responsible for determining the gait phase(detect/sync level) and the second (action level) is responsible for the action triggered by the gait phase and producing the resulting torque or joint angles depending on the method of control.

The second level that decides the resulting gait motion can be one of many methods. Several exoskeleton controls involve the usage of pre-recorded gait database as a reference for the joint angles, in other cases, the recorded data came from a healthy user wearing the exoskeleton passively like in the Mina exoskeleton [48]. Another method of generating the required motion comes from the formulation of a model.

Based on [51] methods of controlling the motion could be summarized as follows: *Position profile* which moves the exoskeleton joints through a predefined trajectory. In some cases the trajectory does not have to be fixed and can be modified online. Online reference trajectory adaptation proposed by [52] uses a cost function to modify/adapt the trajectory to the user. The cost function penalises interaction forces and trajectory modification. *Torque profile* that uses direct torque control on the joints in case of partial assistance. Another recent method in torque control can be seen in [53], where a novel method is proposed as a virtual energy regulator. The controller imposes a constraint on the state-space by creating a limit cycle for each joint to control its mechanical energy. *Impedance controllers* for the use in rehabilitation where assistance is only needed when the user deviates greatly from the required motion such as in [54]. Impedance control is implemented in one of three ways, the use of an inertia/stiffness/damping dynamic system that can relate the joint angles to torques, using a force field with joint states or by attracting the joint to the position with a virtual stiffness field. A variation of the force field method is seen as flow field controller in [55], where the controller is forgiving in big deviations of motion that could be required to maintain balance.

Muscle activity amplification where the joint torques directly depend on measured muscle activities of the user. *Direct joint torque estimation* by using a simplified mathematical model of the human body with the exoskeleton to estimate the required torques for the

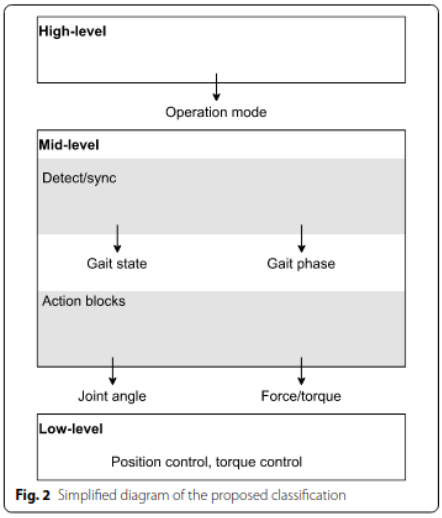

Figure 5.1: Simplified classification diagram from [51]

motion. *Model computed action to keep balance (BAL)* where action is taken to correct imbalances in walking, usually implemented with fully actuated exoskeletons and using similar walking controllers to humanoid robotics.

Body weight support (BWS) this method is similar to gravity compensation in the sense that it takes off some of the weight of the user during motion instead of acting on the joints to force the motion.

Neuromuscular model (NMM) describes a class of models that are bio-inspired attempting to simulate the human neuromuscular system consisting of neurons and muscles. The muscles are based on hill-type muscle model that end up generating muscle forces based on muscle lengths and activation. That force is then converted to torques that act on the specific joints. The advantage of this model is that it does not use predefined trajectories so it does not force the motion on the user, instead it adapts to the movements and is able to reject perturbations. The drawbacks of this model are that it requires many muscle specific parameters and these would change based on the user and requires the user to start the walking motion which means it cannot be directly used with complete SCI patients. Some early work done with NMM as a controller for an ankle exoskeleton in [56] shows promising results in the reduction of muscle activity when using this type of controller.

Figure 5.2: IIT-TWIN exoskeleton

5.3 TWIN lower limb exoskeleton

The TWIN lower-limb exoskeleton was created by the Italian Institute of Technology (Istituto Italiano di Tecnologia - IIT) at the INAIL Rehab Technologies Lab and features a modular design [57] that allows the exoskeleton to be easily fitted to the user height and segment length. The exoskeleton has two degrees of freedom (DOF) in each leg for the hip and knee, connected to five rigid segments; the pelvis and two femurs and two shanks actuating them in the sagittal plane to allow for flexion and extension of the joints. The TWIN comes with a predefined walking trajectory as its main mode of operation, the trajectories were created based on the human walking trajectory with an emphasis on safety and an addition of higher foot clearance [58] and requires crutches or rails to be used safely.

The TWIN exoskeleton comes with a tablet to control it and four modes of operation: Gravity compensation mode, Assistance mode, Manual and automatic walk modes. All the modes rely on the tablet to control the TWIN and modify any settings, especially the manual walk more that requires triggers from the tablet. The manual walking mode uses the predefined trajectories to cause the TWIN to take a step, it waits for the manual trigger signal from the tablet. The automatic mode follows the same trajectories but waits

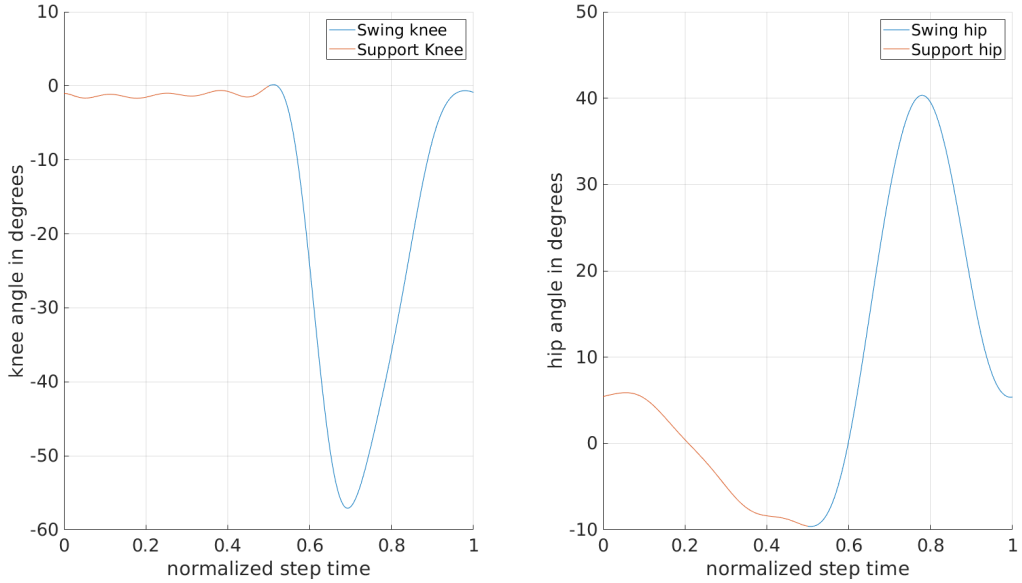

Figure 5.3: TWIN sample step

for the user to give the signal by bending their trunk forward.

A sample step of the TWIN joint angles can be seen in Fig 5.3, based on the personal experience in our lab, the motion feels jerky and unnatural, which we can attribute to the execution of motion as seen by consecutive steps in Fig 5.4. The timing is not consistent and the user has to come to a complete stop before starting the next step as indicated by an orange highlight in the figure. Aside from the abrupt stops the trajectories follow the human walking seen in chapter 2. A big part of this thesis aims to modify this motion in order to make it feel more natural. A few assumptions can be made on why this motion feels odd, one factor could be the lack of continuity in the motion where the user has to come to a complete stop before taking the next step and then wait for the manual trigger of the next step. This part can be seen in Fig 5.4 where the time between each step is varying. A big part of what makes human walking an efficient motion is the continuity of it, several steps are taken sequentially before coming to a complete stop.

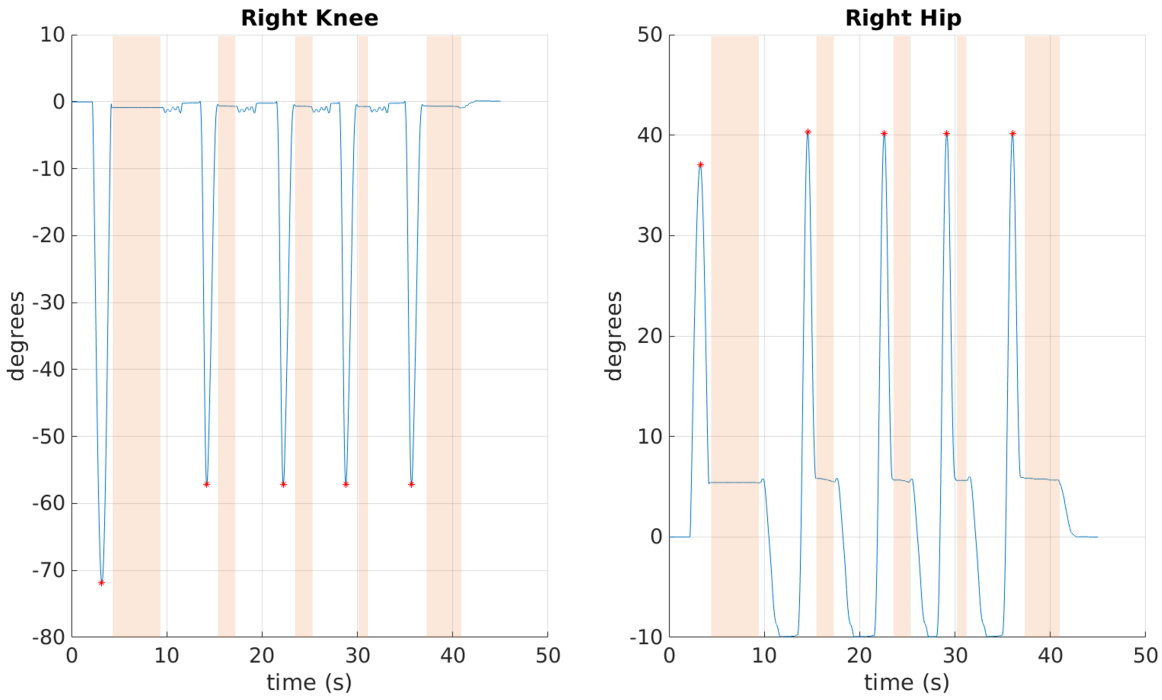

Figure 5.4: TWIN trajectories during manual walking mode, highlighted are the stops between each step

Chapter 6

Testing frame

This chapter deals with the design and creation of the exoskeleton test bench that was created to hold the exoskeleton stably for any tests. The requirements were first identified then a suitable design was chosen to hold the exoskeleton for testing. The design was then manufactured and tested with the exoskeleton attachment.

Since this project deals with a lower-limb exoskeleton that comes in direct contact with the human joints and may damage them if used incorrectly, it was essential to create a test bench where any modifications can be tested on the exoskeleton without any risk to human participants. The previous methods used had some drawbacks that prevented correct testing.

The goal of the frame was to be allow the use of the exoskeleton in the air (without ground contact) and in contact with the ground with the dummy or on its own. Being contained in a test-bench allows us to minimize the amount of people involved in testing since the entire test can be performed by a single person. The frame needed to be sturdy enough to hold the exoskeleton without twisting under the torques generated by the motors, or buckling under its weight. We also wanted the additional option of having the exoskeleton walk on the ground and move the entire frame or be raised to walk without any contact.

6.1 Previous solutions

Previous solutions used to test trajectories on the exoskeleton included hanging it in the lift, but due to the ground being slippery and it being empty, the exoskeleton feet would

Figure 6.1: TWIN exoskeleton with Jujitsu dummy

slide on the floor and this would result in the exoskeleton rotating about itself instead of taking forward steps.

Another solution proposed was using a Jujitsu dummy in place of the human wearer with the exoskeleton attached to the lift Fig 6.1, this decreased the previous problem but the dummy was not heavy enough to solve the sliding problem. Furthermore, the exoskeleton required crutches in order to operate normally so additional restrictions on the rotation of the exoskeleton unit were needed.

6.2 Mechanical design

The design chosen for the frame was a simple one, 30x30 Aluminum T-slot bars were chosen as the main material for sturdiness, ease of assembly and versatility. The exoskeleton

design was exploited when designing this metal frame, the connection point between the exoskeleton and the frame was specifically designed to fit with the geometry of the TWIN exoskeleton by attaching to the pelvis/trunk.

The exoskeleton was contained in a frame from all sides Fig 6.2. The dimensions of the frame Fig 6.5 were designed to give enough space for the exoskeleton to take the big steps forward while being contained in the frame by giving it over 1.2 meters of horizontal space. The width of the frame was selected such that it is able to pass through the standard doors of width 0.8+ meters while also holding the exoskeleton with enough clearance for ease of assembly and disassembly.

The attachment of the exoskeleton to the frame happens by fixing the metal trunk of the exoskeleton flush against 30x60 aluminum bars from both sides using 2 metal plates and 4 M8 bolts. This attachment is snug and guarantees that the exoskeleton does not disengage from the frame during motion. Since T-slots are used, this adds the advantage of flexibility in the design, and most of the frame can be easily disassembled and moved vertically or horizontally. The main usage of the vertical displacement ability that can be seen in Fig 6.5a is to make the TWIN feet come in contact with the ground and actually see the overall displacement caused by the motion as if someone was wearing it, that is the same reason wheels were added. In other cases where that was not needed, the TWIN could be lifted upwards and the motion could be performed without any ground contact and thus no resulting displacement.

The design was created on Autodesk Inventor and forces were added to the connection point between the frame and the exoskeleton to guarantee that it is capable of carrying the load.

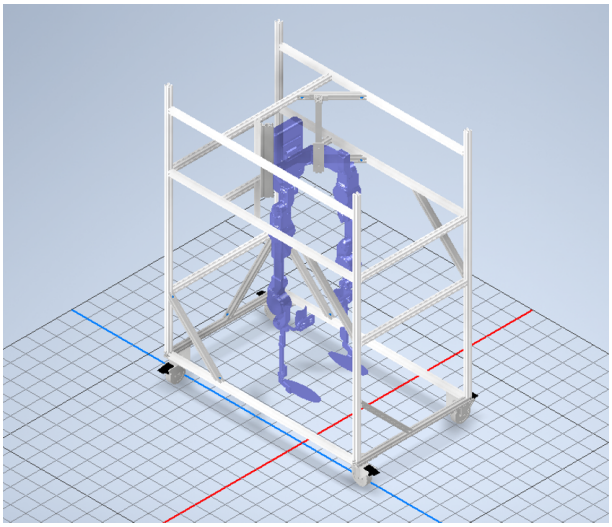

Figure 6.2: Isometric view of frame

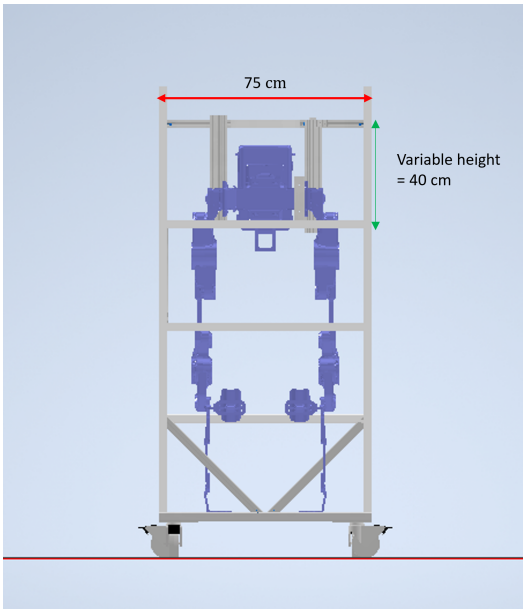

(a) Front view

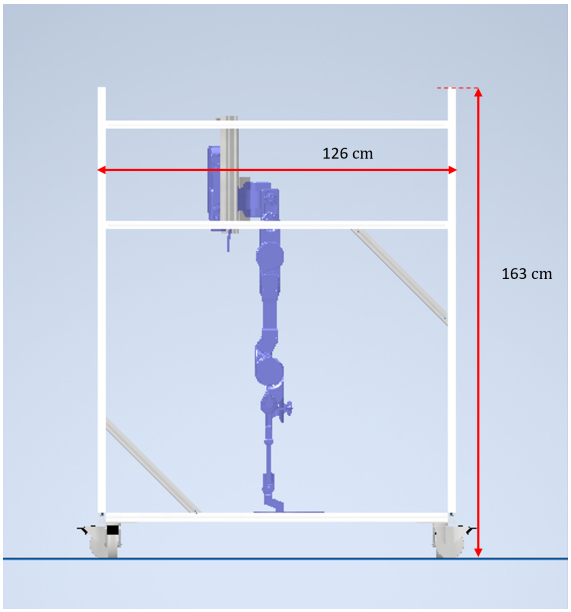

(b) Side view

Figure 6.3: Front and side views of the frame

Figure 6.4: Plate positioning for attachment to frame

6.3 Implementation

Aluminum T-slot bars were bought and cut to fit the specific lengths in the design, the entire frame was then assembled using the brackets for support and the exoskeleton was attached through the attachment clamping mechanism between the plate and the 30x60 bar Fig 6.4.

The frame was tested with the exoskeleton attached. The steps were taken while the exoskeleton was raised above the ground and without contact with the floor. Then the exoskeleton was lowered to touch the ground and move the entire frame with it. The frame was able to stably hold the exoskeleton in both scenarios and only a single person was needed to perform any test motion.

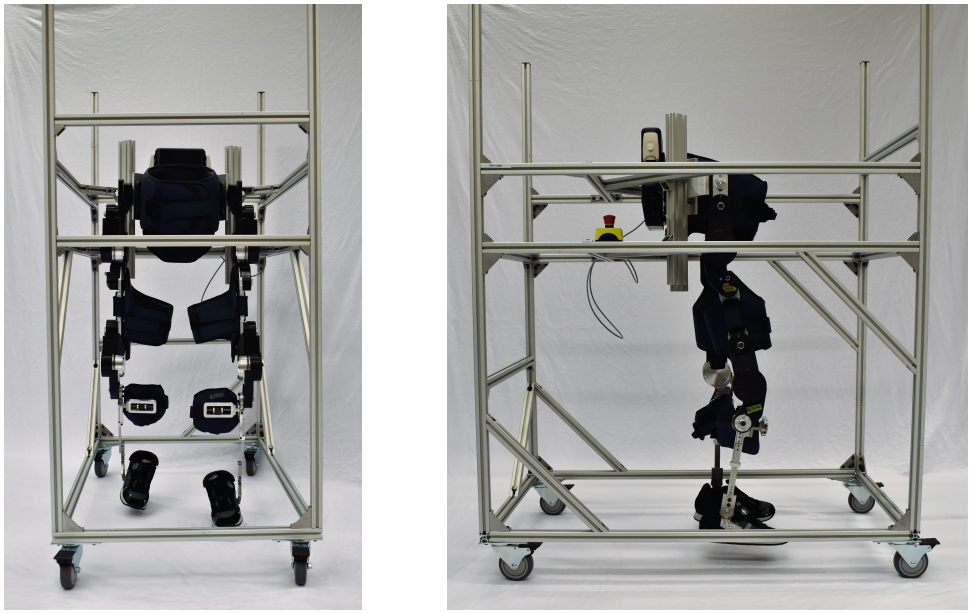

(a) Front view (b) Side view

Figure 6.5: Front and side views of the manufactured frame

Chapter 7

Human exoskeleton experience analysis

In this chapter, we will discuss the steps taken to provide a suitable test for the trajectories, as well as a proposed method to identify if any generated trajectories can objectively be considered better or worse than the original trajectories or any future trajectories. As a simplified test case, this experiment only uses the different modes of the exoskeleton as a comparison.

7.1 Introduction

In [59], the authors conducted a comprehensive review of existing literature to summarize the current performance indicators for lower limb exoskeletons. They focused on two main questions, the first concerning the motor skills considered in the performance evaluation. The second looks at which metrics and variables are used.

The result showed that the main concern in these studies was straight walking, which is insufficient to determine the full performance of the exoskeleton since the daily activities of humans include so much more than walking. Regarding the metrics used in the studies they reviewed, it showed a bigger focus on the kinematic and kinetic side of things, meaning they focused on things like joint torques, angular velocities and trajectories.

Some of the performance indicators listed in this review were covered by three main umbrellas; Goal-level: included the robot's maximum speed or minimum time, the distance it can travel, as well as its reliability, stability, and endurance. Kinematics/Kinetics:

included spatiotemporal parameters, joint/limb kinematics and kinetics, symmetry, coordination and human likeness. Human-robot interaction: included ergonomics, comfort, metabolic cost, muscle effort, interaction forces, cognitive effort and safety.

The performance indicator of interest in this thesis is comfort, which according to the review [59] was through the perception of the user. An alternative method proposed in this thesis to identify comfort here is through the use of a combination of readings; Electromyography (EMG), Tekscan grip sensors alongside kinematic data from trajectories and comparing it against the comfort reported by the user.

The hypothesis is that using this combination of sensors can help identify the user comfort. The human comfort is assumed to be higher with the decrease of lower-limb muscle activations which means the user is not resisting the motion of the exoskeleton and is following it smoothly. This can be seen in the EMG readings. The other part is based on the gripping force, we assume the user will grip the crutches harder when they feel unstable/uncomfortable or about to lose, in this case a decrease in grip forces on crutches seen through the Tekscan gloves can mean higher comfort as well.

7.2 Methods

In order to test our hypothesis, Electromyography (EMG) and Tekscan Grip sensors were used. These sensors and their setup will be discussed in this section. An intial pre-experiment was set up and data was collected to justify the use of the Tekscan Grip sensors as a measure of stability when gripping the crutches.

7.2.1 Electromyography

Electromyography is a technique to measure the muscle's electrical activation. In the case of surface EMG (sEMG) it involves placing electrodes on the skin surface at specific muscle locations to detect the electrical signals generated by the muscle fibres as they contract. These measurements are then amplified, filtered and processed to produce a visual representation of the muscle activity.

EMG signals can be used to determine the level of effort or force that a muscle is producing during a particular activity, such as walking or lifting a weight. The amplitude of the EMG signal is proportional to the level of muscle activation, and hence the effort that the muscle is producing.

Although EMG is a measure of effort and has been used as such in many of the studies explored in the review, it is believed that it can also represent human comfort with the assumption that our gait is optimized to our geometry [60] and hence any exoskeleton that seems to reduce our overall effort in gait by extension indicates higher comfort. A preliminary study was created using the TWIN exoskeleton and will be described in more detail in the following section.

7.2.2 Tekscan grip sensors

The Tekscan Grip system [61] is a portable pressure measuring system that can measure both the static and dynamic pressure when the user is grasping an object, it consists of thin flexible sensors that can be attached to the user's hand or stuck on gloves that the user wears. The sensor system is able to provide a detailed real-time pressure map to study grip force and pressure distribution, which is why it is used in various applications to evaluate comfort and ergonomics.

Figure 7.1: Tekscan sensor attachment

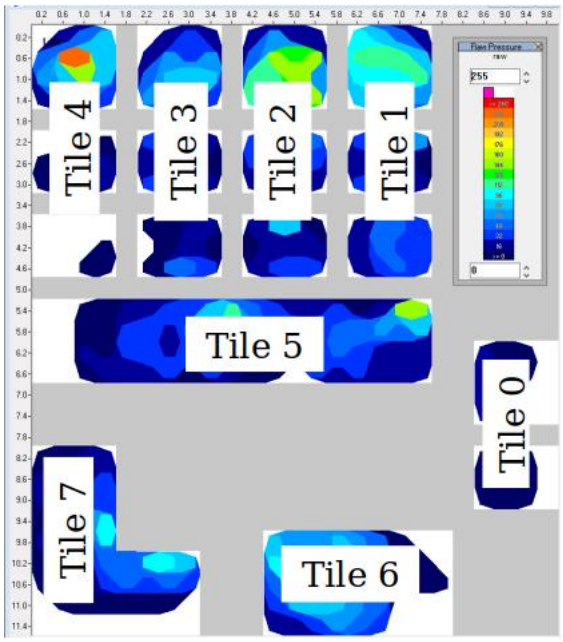

Figure 7.2: Tiles in the Tekscan grip sensors

The sensors were attached to golf gloves as seen in Fig 7.1 , and the sensors are divided into eight tiles Fig 7.2. For the use with the TWIN exoskeleton, the user has to use crutches as mentioned before in Chapter 5. Based on how the user holds the crutches we can divide the 8 tiles into two groups "Grip" which refers to tiles 0-5 and "Load" which refers to tiles 6 & 7.

7.2.3 Pre-experiment

To prove that the difference between the load and the grip is what we assumed, a set of tests was created. First the participant was asked to grip the crutches as hard as they could, the results shown in Fig 7.3 show the difference between the load and grip grouping as expected. The second, the participant was asked to put their entire load on the crutches and remove their feet off the ground shown in Fig 7.4, the first peak represents the participant starting to load the crutch with their entire weight and the second peak was when they lifted their feet off the ground and represents the maximum instantaneous weight.

Another test was where a participant was told to walk with their load on the crutches as they would with the TWIN exoskeleton and this can be seen in Fig 7.5 which shows

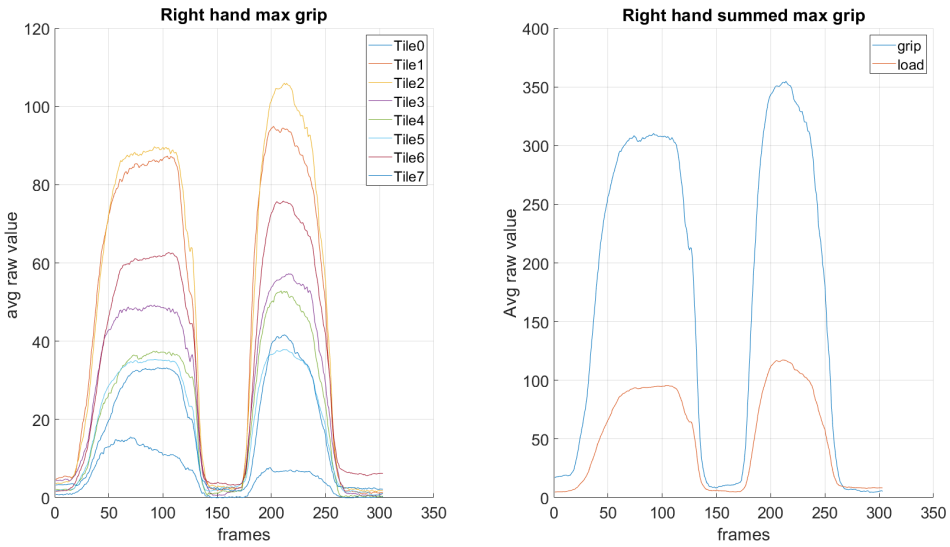

Figure 7.3: Maximum gripping by participant on crutches

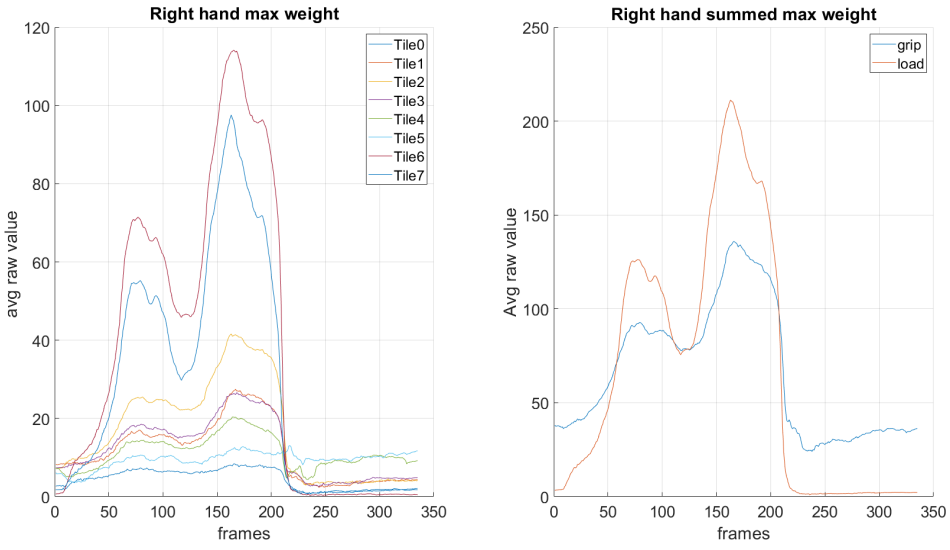

Figure 7.4: Maximum loading by participant weight on crutches

the values for the left hand during the experiment. As expected, the values for the load increased significantly more than the values for the grip with each step as the user leaned on their left crutch more.

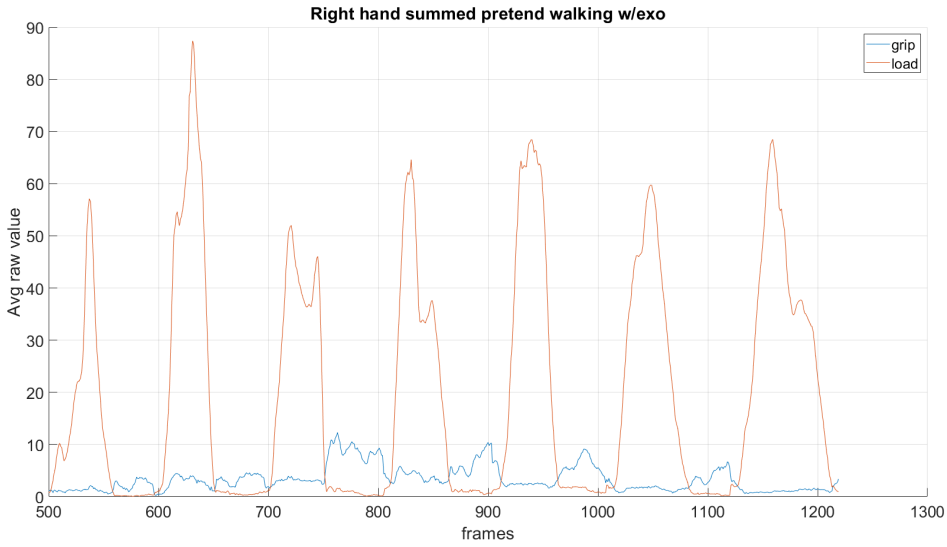

Figure 7.5: Pretend walking with exoskeleton

For the last test case the user was asked to walk like the previous test with the addition of random pushes that caused small instability being introduced. The purpose of this part was to show that instability or panic in the user would cause a higher grip force to appear as seen in Fig 7.6. The user was pushed 3 times, the 3 pushes can be seen in Fig 7.6 distinctly in the grip force.

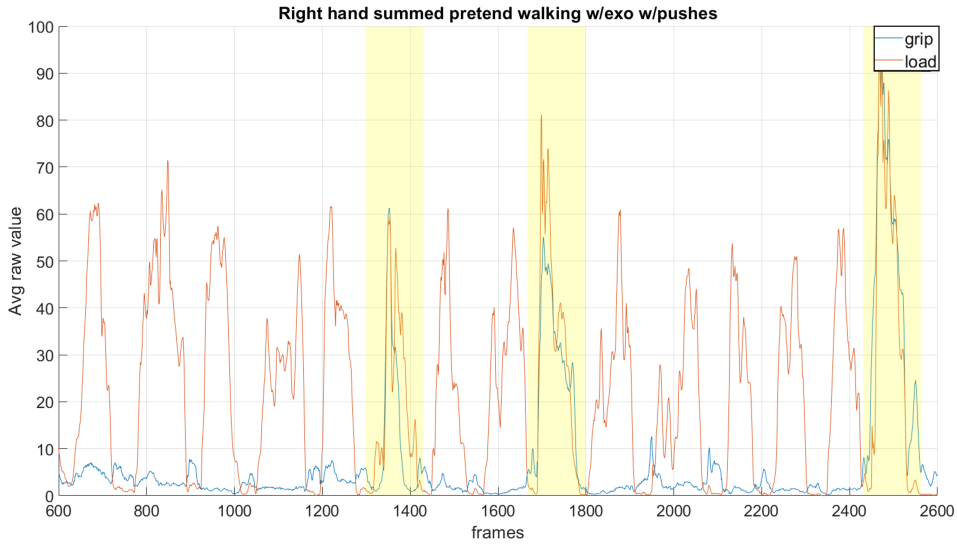

Figure 7.6: Pretend walking with exoskeleton with 3 pushes indicated by the yellow highlights

7.2.4 Experimental procedure

This experiment was performed on a user who was most familiar with the TWIN exoskeleton and has used it several times before. The purpose of that was to eliminate any changes in the data that would come from first-time or new users. A quick view of the experiment steps can be seen in Fig 7.7

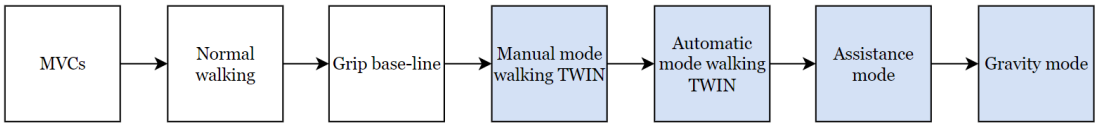

Figure 7.7: Flow of experiment

A set of EMG sensors were attached to the user with locations across the lower limb and upper limb. A round of collection was done to collect the maximum voluntary contractions (MVCs) for the specified muscles. Due to previous experiences with MVCs, we were aware

of limitations in previous trials where we faced the problem where normal walking resulted in higher muscle activation than the MVC collections. Thus, a set of exercise moves involving the use of a weight of $5kg$ was created to ensure the maximum activation of each muscle.

The participant was asked to do the following moves: dead-lift with weights, row with weights, deep squat, biceps curl with weights, triceps kick back with weights, arm lateral raise with weights, push-up and knee flexion with resistance. The next step of the collection involved getting a base-line for the participant's EMGs during normal walking, they were asked to walk a set number of steps.

The walking trials consisted of the user walking for 5 steps in each mode on a level ground. In normal walking the user was asked to walk without the exoskeleton and at their self selected speed for 5 steps, this part was repeated twice. In the next trials colored blue in Fig 7.7 where the user was wearing the exoskeleton, the user was instructed to walk 5 steps as well.

After the setup with EMGs was done, the Tekscan sensor system was added. The participant was then asked to perform a series of motions to get the maximum forces while holding the crutches; they were asked to grip the crutch as hard as they could, then asked to place as much weight as possible on the crutches and that was compared against their normal grip style. It should be noted that the grip sensors were not calibrated to a specific max weight and instead the raw data was extracted and compared relatively.

7.3 Results and discussion

The EMG signals were collected for the different experimental setups, the signals were normalized against the MVCs collected at the beginning of the experiment. Then each step was isolated and the average EMG signal across the step was calculated. The results can be seen in the following figures.

7.3.1 Lower Limb muscles EMG

First, we will talk about the results of the lower limb mean muscle activations in Fig 7.8. The muscles selected were: Tibalis Anterior, Soleus, Gastrocnemius, Vastus, Biceps Femoris, Rectus Femoris. The Tibalis Anterior muscle activations were the highest in the assistive mode, where the user was required to initiate the motion and move the exoskeleton

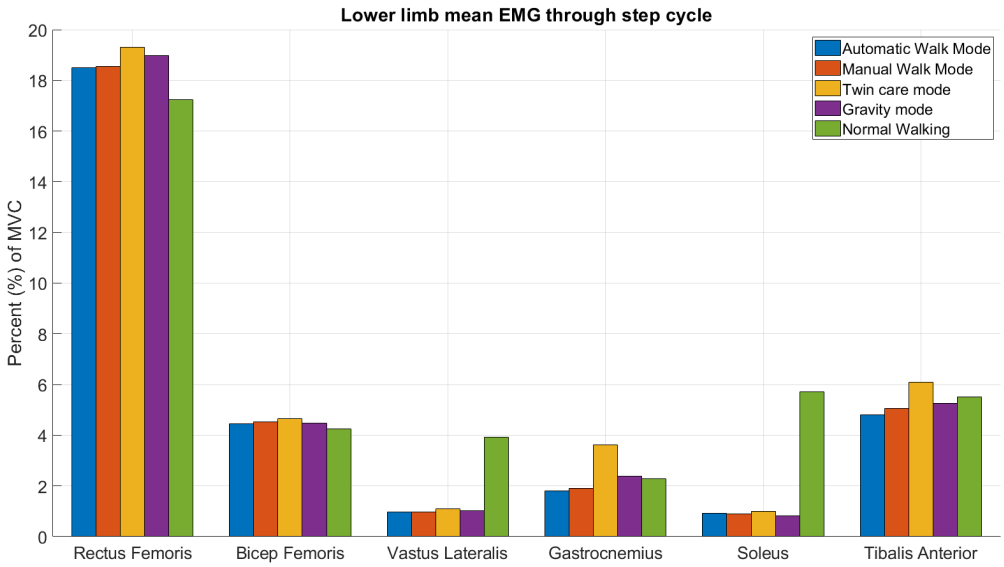

Figure 7.8: Lower limb mean EMG signals

along.Following closely behind is the normal walking collection, which we can use to set the baseline for the activation. If the activation of the muscle is lower in the exoskeleton modes than normal walking then we consider this a successful motion without any extra resistance from the user, which is the case for the remaining modes with the minimum being the automatic walk mode.

The Soleus and Vastus lateralis muscles show the greatest difference here, with the highest activation occurring in normal walking without the exoskeleton and all the modes of the exoskeleton overlapping at a lower point at less than 2% of the MVC. For the Gastrocnemius, the highest activation happened in the assistive mode and the lowest was in the automatic walk mode. Bicep Femoris and Rectus Femoris both had the highest activation in the assistive walking mode followed by the other three modes of the exoskeleton and lastly normal walking. The maximum activations shown in Fig 7.9 show the highest max activation per step for normal walking occurring in the Vastus lateralis and Soleus muscles. And in Rectus Femoris, Bicep Femoris, Gastrocnemius and Tibalis Anterior the max occurs in the Twin care mode. Although most modes are close together, the overall trend shows that there is lower activation in the automatic and manual walk modes except for the Soleus muscle where the minimum occurs in gravity mode.

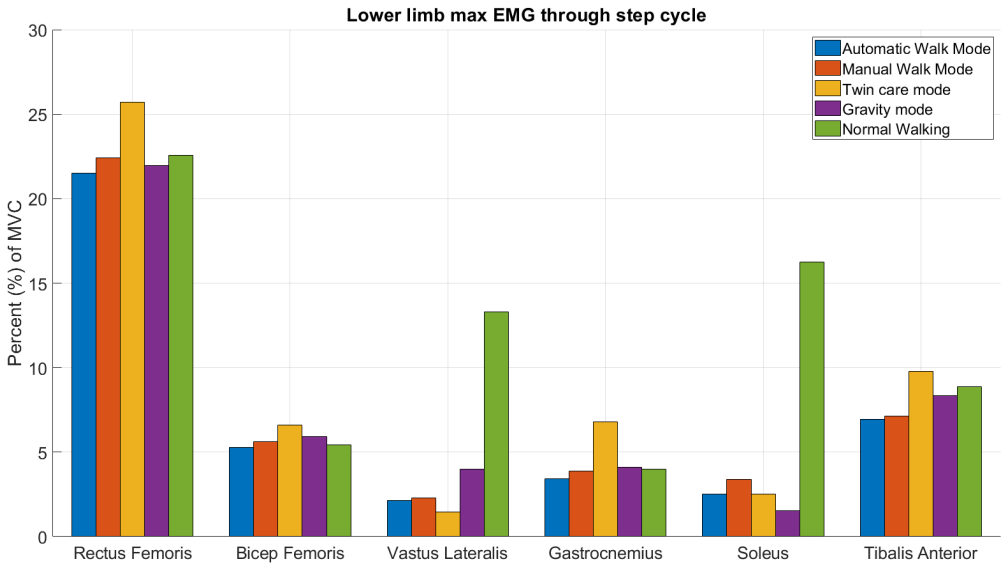

Figure 7.9: Lower limb max EMG signals

7.3.2 Back, Abdomen and upper limb muscles EMG

The back and abdomen muscles mean activations are shown in Fig 7.10: Rectus Ab, Ab Oblique and L3 paraspinals. The lowest activation in all of these muscles is in normal walking conditions where no crutches are used and it is only there for reference. The highest activation seen in the Ab Oblique and L3 paraspinals occurs in the automatic and manual walk modes. The other assistive modes follow behind. The results of all modes overlap in Rectus Ab. Given the max activations in Fig 7.11, the trend is quite similar to that seen in the mean activations figure. The only difference exists in the Ab oblique muscle, where here it shows higher peak activations in the assistive and gravity mode. This can be contributed to the user having to initiate the movement by pulling their leg forward.

The upper limb mean activations in Fig 7.12: Mid interscapular, Lateral deltoid, Serratus Anterior, Triceps, Biceps, Upper Trapezius and Lattisimus dorsi. Again, the lowest activation occurs in normal walking conditions that does not include the use of crutches. The Mid interscapular, Lateral deltoid and Upper Trapezius show similar trends where the manual walk mode is the highest activation followed by the automatic walk mode. The Serratus Anterior, Triceps and Biceps show the opposite trend where the highest activation

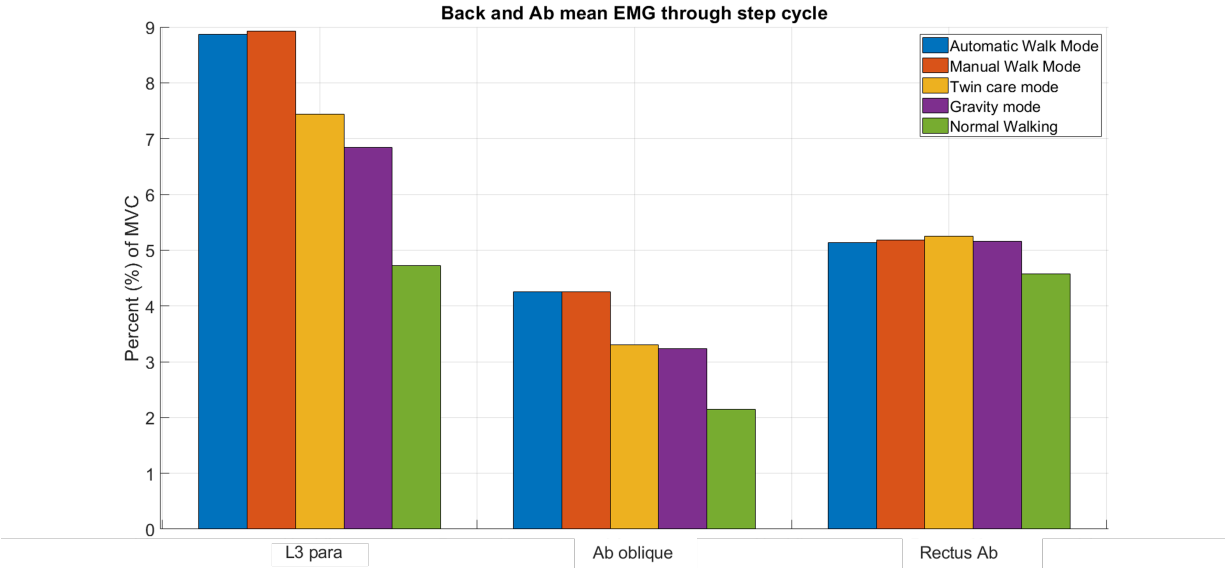

Figure 7.10: Back and Ab mean EMG signals

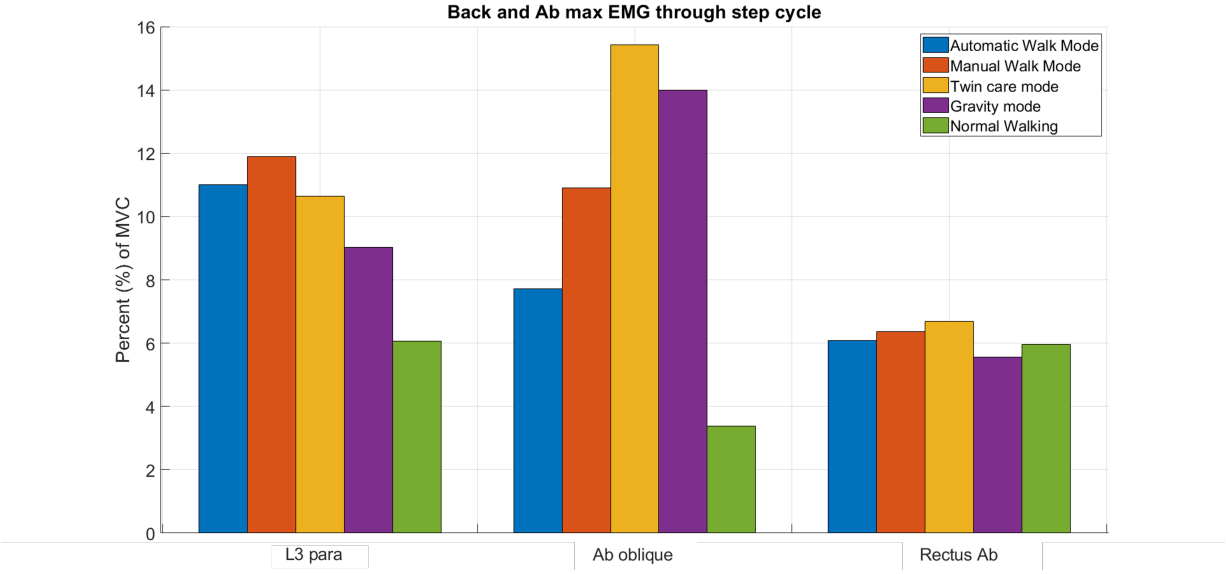

Figure 7.11: Back and Ab max EMG signals

is in the automatic walk mode followed by the manual walk mode. The results of all modes overlap in Lat dorsi. For the maximum activations 7.13, the Lateral deltoid has the highest peak in the manual walk mode followed by the Triceps in the automatic walk mode. The Lat dorsi, Serratus Anterior, Mid interscapular and Biceps show the same trend as in the mean muscle activations. All the upper limb muscles show a higher peak was reached in the active walk modes (automatic and manual walk modes) than the assistive modes (gravity and twin care).

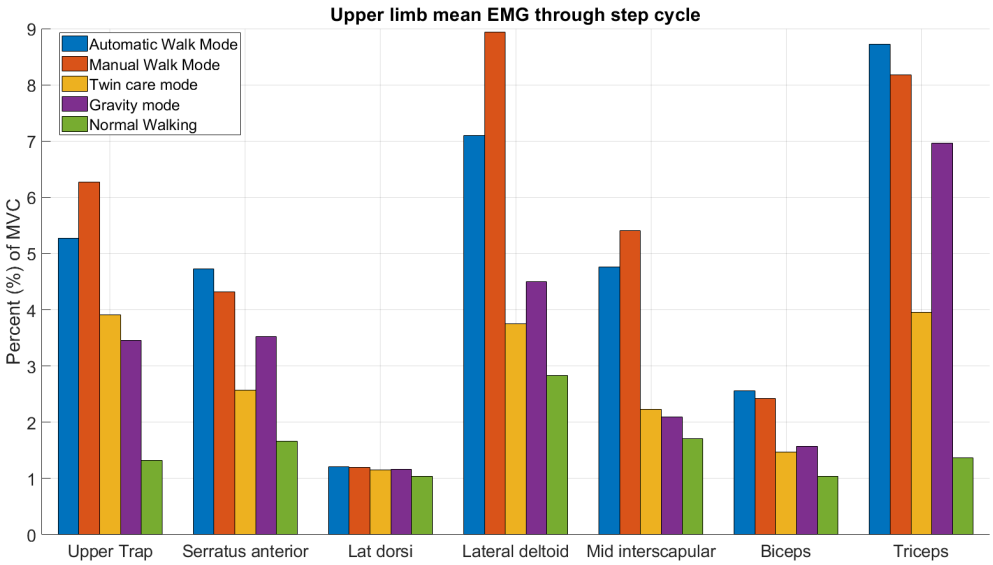

Figure 7.12: Upper limb mean EMG signals

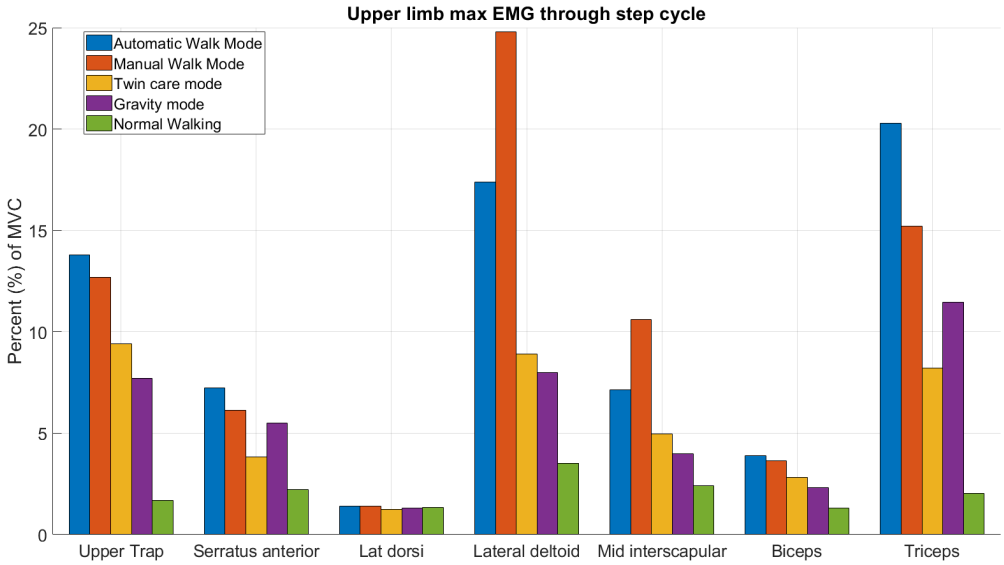

Figure 7.13: Upper limb max EMG signals

7.3.3 Tekscan sensor readings

The Tekscan grip reading from the experiments were collected for 5 steps with each mode of walking. The results collected were averaged to represent each mode with 2 points: grip and load force. The results were normalized against the maximum grip and load collected at the beginning of the experiment. Fig 7.14 shows the results for the four modes. The lowest grip forces seen were in the assistive and gravity mode, the highest was the automatic walk mode followed by the manual walk mode. The load forces show a similar trend where the highest were also the active modes. Although it was assumed that a higher grip force would indicate that the user was uncomfortable or felt unstable in the motion, the results do not show a clear distinction between the active modes. The user mentioned they felt more comfortable in the active mode because they were in control to initiate the motion. The reason that the automatic walk mode has the highest value would be because the user had to lean themselves forward on the crutches to trigger the IMU sensor in the exoskeleton trunk to take a step forward. While in the assistive and gravity modes the user could depend on their legs to initiate the motion without relying on the crutches too much.

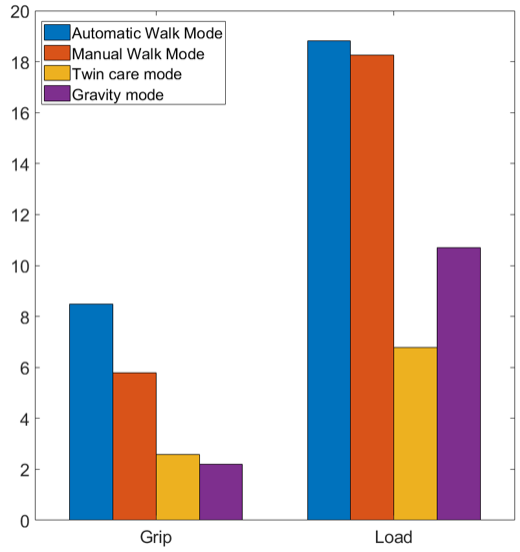

Figure 7.14: Grip force results

7.3.4 Conclusion

Overall for the lower-limb muscles, we can see a decrease in activations in three main muscles; the Tibalis Anterior, Soleus and Vastus Lateralis. This indicates that the exoskeleton relieved the work of these muscles the most. However, it increased the work slightly for the Rectus Femoris and Bicep Femoris muscles, this could be due to the increased weight of the exoskeleton and the user not being in sync with the motion i.e: that the user tries to expect and move with the exoskeleton before the exoskeleton actually moves. It could also be due to the weight-shifting phase occurring before each step, where the user shifts their entire weight to one leg in order to free the other one to take a step forward.

The back muscles show no distinct difference between the automatic and manual walking modes, however, they show that these automated modes increased the overall activation of the Ab Oblique and the L3 Paraspinals. This would be due to the fact that the user needed to use these muscles to maintain their stability while walking under the imposed motion of the exoskeleton. We can see that the activations are lower when the user completely controls the motion in the gravity and assistive modes.

The upper limb muscles show a similar trend to the back muscles, where the automatic and manual walk modes produce significantly higher activations than the assistive and

gravity modes.

Although the EMG results cannot help us identify which mode the user felt more comfortable in right now, they can be used to infer information regarding how much the activations change between the active modes (automatic and manual walk modes) and the assistive and gravity modes. We can use this information to compare different trajectories in the active mode to see if they cause the user to have higher activations in the stabilizing muscles and arms on crutches or not. The results also show that at least to some extent, the exoskeleton helps decrease the activation of certain lower-limb muscles, therefore, reducing the overall effort in walking.

Overall, this experiment shows promise to understand the user behaviour when wearing an exoskeleton. A true test would be to remain in one active control mode and change the trajectories then compare the user responses.

Part III

Conclusion

Chapter 8

Conclusion & Future Work

This chapter will summarize the results of the attempted work in this thesis, mention some of the challenges and limitations, and discuss relevant future developments on this work.

8.1 Summary

In this work, a neuromuscular model was implemented in C++ based on the paper [1]. The individual model variables and states were compared against the referenced model to proof the validity of the implementation. Although there were some differences in the implementation such as different switching methods between walking phases and different ground contact modelling and some extra simplification of the model in terms of the neural delays implemented the model was able to closely follow the results of the referenced model in terms of the main motion metrics which were the joint kinematics and overall translation of the body.

Optimal control methods were then used on the simplified mechanical model of the human to solve the multi-phase walking problem with two objective functions: minimizing the torque to minimizing the angular momentum. The problem converged in both cases and the solution found was cyclic and satisfied all the constraints on the system. The torque minimization objective function resulted in a smoother torque profile and motion. The next step of work was the addition of the same muscle models from the previous attempt and gradually increasing complexity until the reflex modules from [1] were also added. However, the problem with only muscle models resulted in run-time errors and thus the reflex module was never added.

The other part of this thesis was concerned with how humans perceive the motions of the exoskeleton and whether they are resisting it or feel comfortable enough to relax and follow along. Using EMG and Grip sensors in an attempt to measure human response by comparing the muscle activations from the EMG sensors between normal walking and walking while wearing the exoskeleton. Another test devised was the comparison of gripping forces between different modes or trajectories of the exoskeleton walking to determine which of them feels less scary. The first hypothesis was that the EMGs measured on the leg muscles would be lower in the exoskeleton than in normal walking and the second hypothesis was that if the person was uncomfortable while using the exoskeleton that they would rely on the crutches more and grip it harder for balance. The results of the experiment showed decreased mean muscle activations in most of the lower limbs while in the active modes throughout the step except for Bicep Femoris and Rectus Femoris. The reaction of those two muscles can be attributed to the weight-shifting phase where the user had to manually shift their entire weight to the stance leg. For the upper limb and back muscles, the results showed higher activations in the active walking modes, which means the user relied on those muscles to balance themselves with the help of the crutches.

8.2 Limitations

The limitations of the implemented model carry the same limitations of the referenced model, since it is a reflex-based model it is unable to start from standing straight and needs to start at specific configurations and velocities in the gait cycle to maintain the walking motion without failure. For specific limitations, the suggested solution was to use optimal control to fill the gap by providing a trajectory that goes from the standing straight phase to the first step in the gait cycle that the model can start from.

The optimal control part that required the addition of the muscle model faced many challenges with symbolic-based libraries like casADI and Bioptim, the entire muscle system was written in symbolics yet it would not run and cause compatibility issues with the code. The last resort used was numerically based and showed some promise however given the limited time we were unable to reach an optimal solution.

Hardware problems were faced when it came to the connection of the TWIN exoskeleton and the sensors in the experimental part. Due to the TWIN relying on Bluetooth to connect, some instability in the connections was faced and a lot of time was spent on restoring the connections. Another limitation of the exoskeleton was when attempting to add new trajectories to the system, since the system is entirely based on a compiled executable, the entire source code had to be changed to update any trajectories.

8.3 Future developments

The reflex model created in Chapter 3 can be optimized to allow for the cyclic motion seen in the referenced model from [1]. This can be implemented by using optimization to solve for the parameters as done in [1] to maintain the cyclic motion and follow ground reaction profiles.

Given sufficient time, the reflex model can be combined with the optimal control formulation and we believe it will be able to overcome the limitations on the starting point and will be able to walk and reject some level of perturbation. To be eventually used with the exoskeleton, we can lump the models together and re-run the optimal control problem with updated parameters. Another method of implementing this on the exoskeleton would be to use the trajectories generated directly. A comparison has to be done between the two methods to determine which is more suitable and which would be closer to how the user wearing the exoskeleton would walk with that added weight.

Furthermore, the model needs to be tested with different objective functions and compared in depth against human walking data and against other models, the aspects of comparison of interest would be the joint angles, torques and ground reaction forces. Then the trajectory can be tested in the experimental set-up explained in Chapter 6 to evaluate it relative to the existing pre-defined trajectories without the involvement of humans.

After the trajectory has been deemed safe, we can test it with participants according to the experimental setup proposed in chapter 7. A more in-depth analysis of the experimental results obtained is needed to further understand how the user reacts to certain motions done by the exoskeleton. Additional trajectories should be added to the exoskeleton and used through the same mode of operation to explore the difference in behaviour when the user experiences them. By applying the trajectories in the same mode of control in the exoskeleton we would get a better idea of which trajectory the participant deems "comfortable".

An automated method of debugging needs to be developed to save the time spent locating errors, the current method involves a lot of manual work, and automating parts of the testing and debugging would be beneficial.

References

[1] S. Song and H. Geyer, "A neural circuitry that emphasizes spinal feedback generates diverse behaviours of human locomotion," *The Journal of Physiology*, vol. 593, no. 16, pp. 3493–3511, 2015.

[2] Makinson, B. J., General Electric Co Schenectady Ny Specialty Materials Handling Products Operation, "Hardiman i prototype for machine augmentation of human strength and endurance," 1971.

[3] World Health Organization, "Spinal cord injury," 2013.

[4] V. K. Noonan, M. Fingas, A. Farry, D. Baxter, A. Singh, M. G. Fehlings, and M. F. Dvorak, "Incidence and prevalence of spinal cord injury in canada: A national perspective," *Neuroepidemiology*, vol. 38, no. 4, pp. 219–226, 2012.

[5] SCI. Canada, "About sci."

[6] Mayo Clinic, "Spinal cord injury."

[7] R. B. van Dijsseldonk, J. E. Vriezekolk, N. L. W. Keijsers, A. C. H. Geurts, and I. J. W. van Nes, "Needs and wishes for the future lower limb exoskeleton: an interview study among people with spinal cord injury with community-based exoskeleton experience," *Disability and Rehabilitation*, vol. 0, no. 0, pp. 1–8, 2022. PMID: 35332808.

[8] H. Geyer and H. Herr, "A muscle-reflex model that encodes principles of legged mechanics produces human walking dynamics and muscle activities," *IEEE Transactions on Neural Systems and Rehabilitation Engineering*, vol. 18, no. 3, pp. 263–273, 2010.

[9] M. L. Felis, "Rbdl: an efficient rigid-body dynamics library using recursive algorithms," *Autonomous Robots*, vol. 41, pp. 495–511, Feb 2017.

[10] J. A. E. Andersson, J. Gillis, G. Horn, J. B. Rawlings, and M. Diehl, "CasADi – A software framework for nonlinear optimization and optimal control," *Mathematical Programming Computation*, vol. 11, no. 1, pp. 1–36, 2019.

[11] B. Michaud, F. Bailly, E. Charbonneau, A. Ceglia, L. Sanchez, and M. Begon, "Bioptim, a python framework for musculoskeletal optimal control in biomechanics," *IEEE Transactions on Systems, Man, and Cybernetics: Systems*, vol. 53, no. 1, pp. 321–332, 2023.

[12] D. B. Leineweber, I. Bauer, H. G. Bock, and J. P. Schlöder, "An efficient multiple shooting based reduced sqp strategy for large-scale dynamic process optimization. part 1: theoretical aspects," *Computers Chemical Engineering*, vol. 27, no. 2, pp. 157–166, 2003.

[13] P. M. McGinnis, *Front cover image for Biomechanics of sport and exercise Biomechanics of sport and exercise*. Human Kinetics, Champaign, IL, ©1999, 1999.

[14] S. T. PHEASANT, "A review of: "human walking". by v. t. inman, h.j. ralston and f. todd. (baltimore, london: Williams & wilkins, 1981.) [pp.154.]," *Ergonomics*, vol. 24, no. 12, pp. 969–976, 1981.

[15] V. Racic, A. Pavic, and J. Brownjohn, "Experimental identification and analytical modelling of human walking forces: Literature review," *Journal of Sound and Vibration*, vol. 326, no. 1, pp. 1–49, 2009.

[16] M. W. Whittle, "Clinical gait analysis: A review," *Human Movement Science*, vol. 15, no. 3, pp. 369–387, 1996.

[17] A. Bonnefoy-Mazure and S. Armand, *Normal gait*, pp. 199–214. 01 2015.

[18] D. A. Rosenbaum, "Chapter 3 - physiological foundations," in *Human Motor Control (Second Edition)* (D. A. Rosenbaum, ed.), pp. 43–91, San Diego: Academic Press, second edition ed., 2010.

[19] R. H. Miller, *Hill-Based Muscle Modeling*, pp. 1–22. Cham: Springer International Publishing, 2018.

[20] S. P. Sethi, *What Is Optimal Control Theory?*, pp. 1–23. Cham: Springer International Publishing, 2021.

[21] K. Mombaur, "Lecture on boundary value problems and inital value problems," February 2021.

[22] H. Bock and K. Plitt, "A multiple shooting algorithm for direct solution of optimal control problems*," *IFAC Proceedings Volumes*, vol. 17, no. 2, pp. 1603–1608, 1984. 9th IFAC World Congress: A Bridge Between Control Science and Technology, Budapest, Hungary, 2-6 July 1984.

[23] M. A. Sharbafi and S. Andre, *Bioinspired Legged locomotion: Models, concepts, control and applications*. Elsevier, 2017.

[24] M. Garcia, A. Chatterjee, A. Ruina, and M. Coleman, "The Simplest Walking Model: Stability, Complexity, and Scaling," *Journal of Biomechanical Engineering*, vol. 120, pp. 281–288, 04 1998.

[25] M. Wojtyra, "Multibody simulation model of human walking," *Mechanics Based Design of Structures and Machines*, vol. 31, no. 3, pp. 357–379, 2003.

[26] M. Felis and K. Mombaur, *Modeling and Optimization of Human Walking*, vol. 18, pp. 31–42. 01 2013.

[27] S. L. Delp, F. C. Anderson, A. S. Arnold, P. Loan, A. Habib, C. T. John, E. Guendelman, and D. G. Thelen, "Opensim: Open-source software to create and analyze dynamic simulations of movement," *IEEE Transactions on Biomedical Engineering*, vol. 54, no. 11, pp. 1940–1950, 2007.

[28] M. G. Hoy, F. E. Zajac, and M. E. Gordon, "A musculoskeletal model of the human lower extremity: The effect of muscle, tendon, and moment arm on the moment-angle relationship of musculotendon actuators at the hip, knee, and ankle," *Journal of Biomechanics*, vol. 23, no. 2, pp. 157–169, 1990.

[29] S. Delp, J. Loan, M. Hoy, F. Zajac, E. Topp, and J. Rosen, "An interactive graphics-based model of the lower extremity to study orthopaedic surgical procedures," *IEEE Transactions on Biomedical Engineering*, vol. 37, no. 8, pp. 757–767, 1990.

[30] A. Rajagopal, C. L. Dembia, M. S. DeMers, D. D. Delp, J. L. Hicks, and S. L. Delp, "Full-body musculoskeletal model for muscle-driven simulation of human gait," *IEEE Transactions on Biomedical Engineering*, vol. 63, no. 10, pp. 2068–2079, 2016.

[31] H. Geyer, A. Seyfarth, and R. Blickhan, "Positive force feedback in bouncing gaits?," *Proceedings: Biological Sciences*, vol. 270, no. 1529, pp. 2173–2183, 2003.

[32] K. Yin, K. Loken, and M. Panne, "Simbicon: simple biped locomotion control," *ACM Trans. Graph.*, vol. 26, p. 105, 07 2007.

[33] B. Michaud and M. Begon, "biorbd: A c++, python and matlab library to analyze and simulate the human body biomechanics," *Journal of Open Source Software*, vol. 6, no. 57, p. 2562, 2021.

[34] B. Michaud and M. Begon, "bioviz: A vizualization python toolbox for biorbd." Web page, 2018.

[35] A. Esquenazi, M. Talaty, and A. Jayaraman, "Powered exoskeletons for walking assistance in persons with central nervous system injuries: A narrative review," *PM&R*, vol. 9, no. 1, pp. 46–62, 2017.

[36] B. Kalita, J. Narayan, and S. K. Dwivedy, "Development of active lower limb robotic-based orthosis and exoskeleton devices: A systematic review," *International Journal of Social Robotics*, vol. 13, pp. 775–793, Jul 2021.

[37] F. Chen, Y. Yu, Y. Ge, J. Sun, and X. Deng, "Wpal for enhancing human strength and endurance during walking," in *2007 International Conference on Information Acquisition*, pp. 487–491, 2007.

[38] K. Suzuki, Y. Kawamura, T. Hayashi, T. Sakurai, Y. Hasegawa, and Y. Sankai, "Intention-based walking support for paraplegia patient," in *2005 IEEE International Conference on Systems, Man and Cybernetics*, vol. 3, pp. 2707–2713 Vol. 3, 2005.

[39] J. Jung, I. Jang, R. Riener, and H. Park, "Walking intent detection algorithm for paraplegic patients using a robotic exoskeleton walking assistant with crutches," *International Journal of Control, Automation and Systems*, vol. 10, pp. 954–962, Oct 2012.

[40] "Phoenix."

[41] Food and Drug Administration, "Rewalk™ P6.0 - K200032," 2020.

[42] Food and Drug Administration, "Ekso™ and Ekso GT™ - K143690," 2020.

[43] Food and Drug Administration, "Indego® - K173530," 2018.

[44] G. Barbareschi, R. Richards, M. Thornton, T. Carlson, and C. Holloway, "Statically vs dynamically balanced gait: Analysis of a robotic exoskeleton compared with a human," in *2015 37th Annual International Conference of the IEEE Engineering in Medicine and Biology Society (EMBC)*, pp. 6728–6731, 2015.

[45] W. Yang, J. Zhang, S. Zhang, and C. Yang, "Lower limb exoskeleton gait planning based on crutch and human-machine foot combined center of pressure," *Sensors*, vol. 20, no. 24, 2020.

[46] S. Wang, L. Wang, C. Meijneke, E. van Asseldonk, T. Hoellinger, G. Cheron, Y. Ivanenko, V. La Scaleia, F. Sylos-Labini, M. Molinari, F. Tamburella, I. Pisotta, F. Thorsteinsson, M. Ilzkovitz, J. Gancet, Y. Nevatia, R. Hauffe, F. Zanow, and H. van der Kooij, "Design and control of the mindwalker exoskeleton," *IEEE Transactions on Neural Systems and Rehabilitation Engineering*, vol. 23, no. 2, pp. 277–286, 2015.

[47] C. Mummolo, W. Peng, S. Agarwal, R. Griffin, P. Neuhaus, and J. Kim, "Stability of mina v2 for robot-assisted balance and locomotion," *Frontiers in Neurorobotics*, vol. 12, 10 2018.

[48] P. D. Neuhaus, J. H. Noorden, T. J. Craig, T. Torres, J. Kirschbaum, and J. E. Pratt, "Design and evaluation of mina: A robotic orthosis for paraplegics," in *2011 IEEE International Conference on Rehabilitation Robotics*, pp. 1–8, 2011.

[49] C. Meijneke, G. van Oort, V. Sluiter, E. van Asseldonk, N. L. Tagliamonte, F. Tamburella, I. Pisotta, M. Masciullo, M. Arquilla, M. Molinari, A. R. Wu, F. Dzeladini, A. J. Ijspeert, and H. van der Kooij, "Symbitron exoskeleton: Design, control, and evaluation of a modular exoskeleton for incomplete and complete spinal cord injured individuals," *IEEE Transactions on Neural Systems and Rehabilitation Engineering*, vol. 29, pp. 330–339, 2021.

[50] B. Koopman, E. van Asseldonk, and H. van der Kooij, "Speed-dependent reference joint trajectory generation for robotic gait support," *Journal of Biomechanics*, vol. 47, no. 6, pp. 1447–1458, 2014.

[51] R. Baud, A. R. Manzoori, A. Ijspeert, and M. Bouri, "Review of control strategies for lower-limb exoskeletons to assist gait," *Journal of NeuroEngineering and Rehabilitation*, vol. 18, p. 119, Jul 2021.

[52] M. Shushtari, R. Nasiri, and A. Arami, "Online reference trajectory adaptation: A personalized control strategy for lower limb exoskeletons," *IEEE Robotics and Automation Letters*, vol. 7, no. 1, pp. 128–134, 2022.

[53] R. Nasiri, M. Shushtari, H. Rouhani, and A. Arami, "Virtual energy regulator: A time-independent solution for control of lower limb exoskeletons," *IEEE Robotics and Automation Letters*, vol. 6, no. 4, pp. 7699–7705, 2021.

[54] A. Duschau-Wicke, J. von Zitzewitz, A. Caprez, L. Lunenburger, and R. Riener, "Path control: A method for patient-cooperative robot-aided gait rehabilitation," *IEEE Transactions on Neural Systems and Rehabilitation Engineering*, vol. 18, no. 1, pp. 38–48, 2010.

[55] A. Martínez, B. Lawson, C. Durrough, and M. Goldfarb, "A velocity-field-based controller for assisting leg movement during walking with a bilateral hip and knee lower limb exoskeleton," *IEEE Transactions on Robotics*, vol. 35, no. 2, pp. 307–316, 2019.

[56] F. Dzeladini, A. R. Wu, D. Renjewski, A. Arami, E. Burdet, E. van Asseldonk, H. van der Kooij, and A. J. Ijspeert, "Effects of a neuromuscular controller on a powered ankle exoskeleton during human walking," in *2016 6th IEEE International Conference on Biomedical Robotics and Biomechatronics (BioRob)*, pp. 617–622, 2016.

[57] M. Laffranchi, S. D'Angella, C. Vassallo, C. Piezzo, M. Canepa, S. De Giuseppe, M. Di Salvo, A. Succi, S. Cappa, G. Cerruti, S. Scarpetta, L. Cavallaro, N. Boccardo, M. D'Angelo, C. Marchese, J. A. Saglia, E. Guanziroli, G. Barresi, M. Semprini, S. Traverso, S. Maludrottu, F. Molteni, R. Sacchetti, E. Gruppioni, and L. De Michieli, "User-centered design and development of the modular twin lower limb exoskeleton," *Frontiers in Neurorobotics*, vol. 15, 2021.

[58] C. Vassallo, S. De Giuseppe, C. Piezzo, S. Maludrottu, G. Cerruti, M. L. D'Angelo, E. Gruppioni, C. Marchese, S. Castellano, E. Guanziroli, F. Molteni, M. Laffranchi, and L. De Michieli, "Gait patterns generation based on basis functions interpolation for the twin lower-limb exoskeleton," in *2020 IEEE International Conference on Robotics and Automation (ICRA)*, pp. 1778–1784, 2020.

[59] D. Pinto-Fernandez, D. Torricelli, M. d. C. Sanchez-Villamanan, F. Aller, K. Mombaur, R. Conti, N. Vitiello, J. C. Moreno, and J. L. Pons, "Performance evaluation of lower limb exoskeletons: A systematic review," *IEEE Transactions on Neural Systems and Rehabilitation Engineering*, vol. 28, no. 7, pp. 1573–1583, 2020.

[60] R. M. Alexander, "The gaits of bipedal and quadrupedal animals," *The International Journal of Robotics Research*, vol. 3, no. 2, pp. 49–59, 1984.

[61] Tekscan, "Grip system."

[62] A. D. Gardner, J. Potgieter, and F. K. Noble, "A review of commercially available exoskeletons' capabilities," in *2017 24th International Conference on Mechatronics and Machine Vision in Practice (M2VIP)*, pp. 1–5, 2017.

[63] L. H. Sloot and M. M. van der Krogt, *Interpreting Joint Moments and Powers in Gait*, pp. 625–643. Cham: Springer International Publishing, 2018.